

TRABAJO ESPECIAL DE GRADO

**TÉCNICAS DE MEDICIÓN A MICROONDAS PARA LA  
CARACTERIZACIÓN DE DISPOSITIVOS ACTIVOS EN EL DOMINIO DEL  
TIEMPO**

Presentado ante la Ilustre  
Universidad Central de Venezuela  
Por el T.S.U Pedro A. Ruiz B.  
para optar al Título de  
Ingeniero Electricista

Caracas, 2008

TRABAJO ESPECIAL DE GRADO

**TÉCNICAS DE MEDICIÓN A MICROONDAS PARA LA  
CARACTERIZACIÓN DE DISPOSITIVOS ACTIVOS EN EL DOMINIO DEL  
TIEMPO**

Tutor Académico:  
Prof., Dr. Valeria Teppati

Presentado ante la Ilustre  
Universidad Central de Venezuela  
Por el T.S.U Pedro A. Ruiz B.  
para optar al Título de  
Ingeniero Electricista

Caracas, 2008

Pedro A. Ruiz B.

**TÉCNICAS DE MEDICIÓN A MICROONDAS PARA LA  
CARACTERIZACIÓN DE DISPOSITIVOS ACTIVOS EN EL DOMINIO DEL  
TIEMPO**

**Tutor Académico: Prof., Dr. Valeria Teppati. Opción: Electrónica. Institución:  
Politécnico di Torino. 2008. N° pág. 182.**

**Palabras claves:** Modelos de Error, Calibración Scattering, Calibración de Potencia, Calibración de Fase, Formas de Onda en el Dominio del Tiempo (time domain waveforms), Analizador Vectorial de Red (VNA), Analizador de Transiciones a Microondas (MTA), Medidor de Potencia (Power Meter), Microwave Measurement Software (MMS-NT), Dispositivo Diferencial bajo Test (DDUT), Load- Pull Diferencial y Source- Pull Diferencial.

Esta tesis describe el procedimiento de montaje y calibración de un sistema de medición para la caracterización de dispositivos activos diferenciales en el dominio del tiempo y en el dominio de la frecuencia a altas frecuencias de trabajo (GHz). El setup de tal sistema se muestra en la figura 6.1. Los instrumentos de medición utilizados son: un VNA para las mediciones de las ondas de potencia incidentes y reflejadas en el DDUT, un power meter para la medida de potencia durante la calibración de potencia y un MTA para la medición de fase durante la calibración de fase. Adicionalmente el setup de la figura 6.1 permite la variación de los coeficientes de reflexión de entrada y salida del DDUT, para el modo común y para el modo diferencial a distintos armónicos ( $kf_0$ ). Esta última característica es conocida como Load-Pull y Source-Pull para dispositivos diferenciales.

Una vez montado y calibrado el sistema de medición, ha sido usado en la caracterización de dos amplificadores diferenciales trabajando a una frecuencia fundamental ( $f_0$ ) igual a 2GHz. Las formas de onda en el dominio del tiempo fueron medidas hasta el quinto armónico ( $5f_0=10\text{GHz}$ ). Las formas de onda obtenidas, corresponden a la tensión y corriente en la salida del dispositivo en modo común y en modo diferencial. Adicionalmente en ambos dispositivos se realizaron mapas de load y source pull, para el modo común y para el modo diferencial a distintos armónicos ( $kf_0$ ). Estas mapas permiten la optimización del performance del dispositivo trabajando en no linealidad, actuando en manera independiente, sea en el modo común sea en el modo diferencial. Finalmente, fueron obtenidas las curvas de ganancia operativa ( $G_{P@f_0}$ ) y la potencia de cada armónico en modo común y en modo diferencial ( $P_{OUTm@kf_0}$ ) respecto a un sweep en la potencia diferencial de entrada ( $P_{INd@f_0}$ ).



Polytechnic of Turin

Department of Electronic Engineering

Corso Duca degli Abruzzi, 24 - 10129 Torino, ITALY

Corso di Laurea Specialistica in Ingegneria Elettronica

# **Time Domain Measurements Techniques at Microwave Frequencies for Active Devices Characterization**


## **Academic Advisor:**

Prof, Dr: Valeria Teppati

Electronic Department

Polytechnic of Turin

By

Pedro A. Ruiz B. 

November 2008

# *Acknowledgments*

Above all I want to give thanks to God because he is continuously giving me health every day, wherever I go. Second, undoubtedly I would especially like to acknowledge the significant technical support of Valeria Teppati researcher and Professor, of the Department of Electronic Engineering of the Polytechnic of Turin in Turin-Italy also I would like to thank Professor, Dr Jan Erick Müller of Infineon Technologies AG in Munich-Germany who together with Valeria Teppati thought of and proposed to me a marvelous and wonderful thesis subject like this. Finally, I want to express my gratitude to FIDETEL for giving me a scholarship to study abroad.

# TABLE OF CONTENTS

Acknowledgments .....	v
CHAPTER I.....	1
1.1) Introduction .....	2
CHAPTER II .....	9
2.1) Differential Circuits.....	10
CHAPTER III.....	23
3.1) Introduction .....	24
3.2) Sources and Types of Errors on VNA Measurements Systems .....	25
3.2.1) Raw Errors: .....	26
3.2.1.1) Systematic Errors: .....	26
3.2.1.2 ) Random Errors: .....	26
3.2.2) Residual Errors: .....	29
3.3) Error Models .....	29
3.4) Error Model's Generation Process .....	30
3.5) Types of Multi-port VNA System Error Models .....	36
3.6) S-parameter Calibration .....	39
CHAPTER IV.....	49
4.1) Power Calibration.....	50
4.2) Phase Calibration .....	59
CHAPTER V .....	80
5.1) Active Differential Load and Source Pull System .....	81
5.1.1) Stimulus Section .....	82
5.1.2) Adder-Single-ended section.....	83
5.1.3) Single-ended-Coupler Section .....	84

5.1.4) $\Gamma$ s Measurement Section .....	85
5.1.5) Single-ended to Mixed-Mode De-coupler Section .....	85
5.1.6) Harmonic Mixed-Mode Path Section .....	86
5.1.6.1) Variable Attenuator .....	87
5.1.6.2) Phase Shifter.....	87
5.1.6.3) YIG-tuned filter.....	87
5.1.6.4) Amplifier .....	89
5.1.6.5) Isolator.....	89
5.1.7 Mixed-Mode to Single-ended Coupler Section.....	89
5.1.8) Four-port vector network analyzer system .....	91
5.1.8.1) Switch Unit.....	91
5.1.8.2) 8510C Network Analyzer System.....	92
5.1.8.3) Harmonic Phase Reference (HPR).....	92
5.1.8.4) R-Channel Phase-Locking considerations .....	92
5.2) Drift Errors .....	97
5.2.1) Frequency Drift.....	98
5.2.2) Phase Drift .....	99
5.2.2.1) Phase noise .....	99
5.2.2.2) Others terms of phase drift .....	102
5.3) Harmonic Phase Reference (HPR) implementation.....	105
5.3.1 ) Characterization of the Harmonic Phase Reference (HPR).....	107
CHAPTER VI.....	115
6.1) Measurement Results .....	116
CONCLUSIONS .....	129
Appendix A .....	131

MMS-NT screen elements description .....	132
1) Menu Bar .....	132
2) <i>TSet</i> Window.....	135
I)-S-parameter Calibration Procedure .....	138
1) file (.tst) configuration .....	138
1.1) Checking the current calibration standards file (.std) .....	139
1.2) Setting Hardware.....	140
1.3) Setting the frequencies of interest .....	142
1.4) Defining calibration methods .....	143
2) Calibration Standards Measurements .....	145
3) S-parameter Calibration Verification.....	147
II) Power Calibration Procedure.....	149
1) Loading S-parameter Calibration.....	149
2) S-O-L calibration (only if auxiliary port is needed) .....	150
3.1) Power Measurements with auxiliary port .....	153
3.2) Power Measurements without auxiliary port .....	154
4) Power Calibration Verification .....	156
4.1)Load Pull file (.lpx) overview .....	156
4.2)Power calibration verification without/with auxiliary port .....	165
III) Phase Calibration Procedure .....	167
1)Loading S-parameter Calibration.....	167
2)Perform a Power Calibration .....	168
3) Phase Measurements .....	168
4) Phase Calibration Verification.....	171



# **CHAPTER I**

## **INTRODUCTION**

## 1.1) INTRODUCTION

Ruthless competition in the handset market continues to drive manufacturers to search for new opportunities to drive down cost, printed circuit board (PCB) area and power consumption. Simultaneously, the rollout of third-generation (3G) networks has opened the door to a variety of new multimedia and data-based applications, from wireless Internet access and mobile video to text messaging and mobile TV.

As demand for new applications rises and the market becomes more globalized, handset makers face a quandary. How can they support the increasing number of frequency bands to support global platforms and the multiple high-bandwidth technologies needed to deliver these revenue-enhancing services without violating the market's cost, footprint and power constraints? The number of frequencies supported by the latest 3G partnership program (3GPP) standard has increased from three to 10 and will continue to expand. The current frequency bands and their associated bandwidths are shown in Figure 1.1.

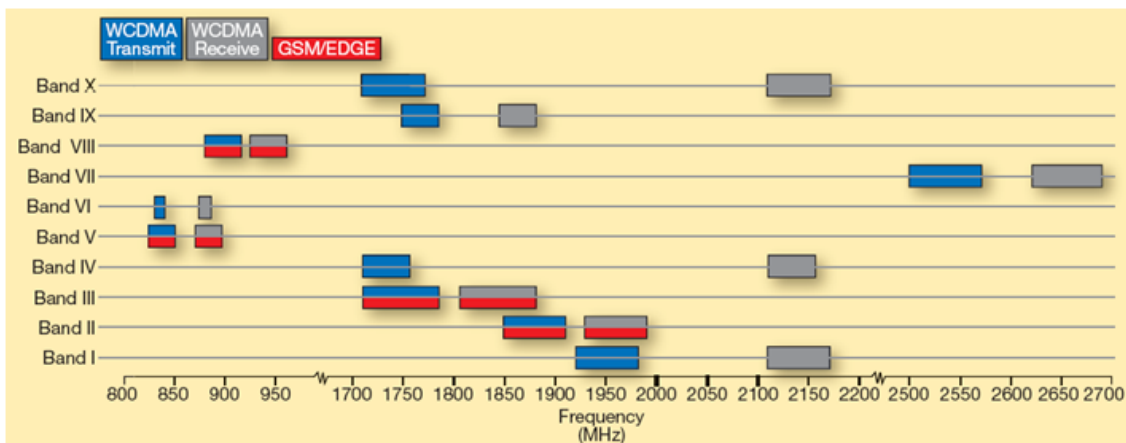


Figure 1.1 3GPP GSM/EDGE and WCDMA frequency bands.

One thing seems clear; to succeed, handset designers need to deliver multiband, multimode capability. At the same time, network operators are continuing to roll out 3G wideband CDMA (WCDMA) networks. Based on the universal mobile telecommunications system (UMTS) network topology, this technology is rapidly becoming the leading global

mobile-broadband solution. Industry analysts predict WCDMA and EDGE will represent the two fastest-growing segments of the handset market over the next few years. To meet demand for IP-based services, a growing number of UMTS operators worldwide are deploying high-speed downlink packet access (HSDPA) capability. High-speed uplink packet access (HSUPA) is ready to follow in the near future. Figure 1.2 offers an overview of each cellular standard and associated up and downlink data rate.

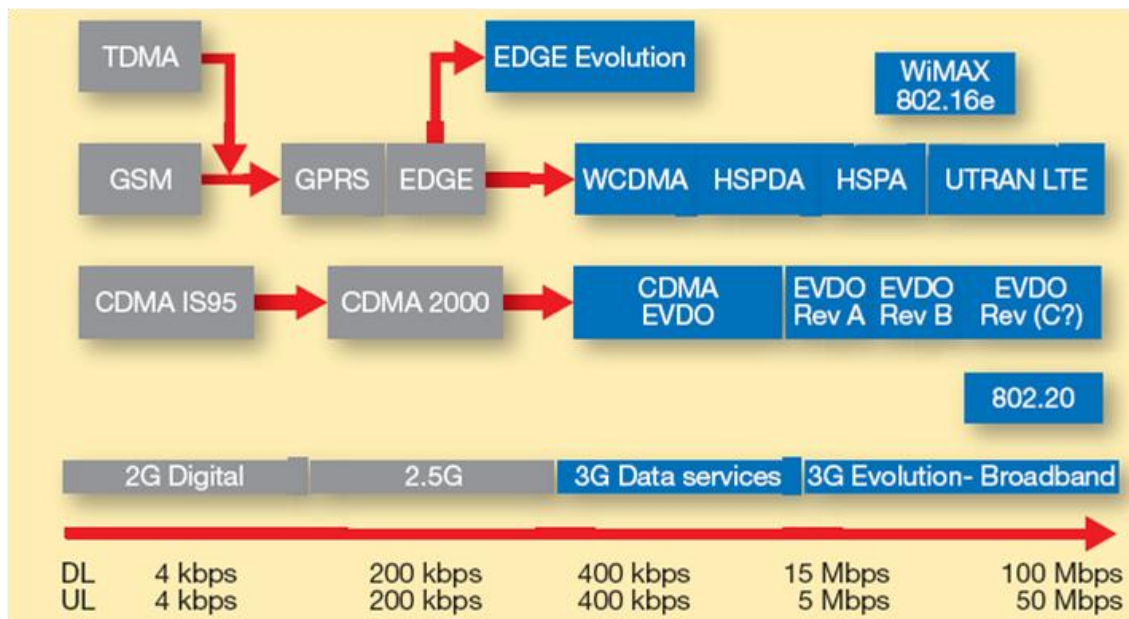


Figure 1.2 Cellular standards evolution.

In other words, the full integration of RF subsystem, demands multiband, multimode and multiple wireless standards such as: Global System Mobil (GSM), General Packet Radio Service (GPRS), Enhanced Data rate for GSM Evolution (EDGE), Wideband Code Division Multiple Access (WCDMA), High-Speed Downlink Packet Access (HSDPA), must be on the same System-on-Chip (SoCs) making an efficient and cost-effective multimode solution essential (see figure 1.3). Solutions that were acceptable for single- or dual-band applications may not be acceptable for triple- and quad-band service where external component cost and size become unacceptable. Transceiver designers must be increasingly forward-looking in anticipation of these factors, while at the same time employ

measured restraint so that present customer demands are well served in the near-term. The RF transceiver is a key ingredient of any multimode solution. Its design presents several challenges that are magnified when distinctly different wireless standards such as GSM and WCDMA must both be hosted.

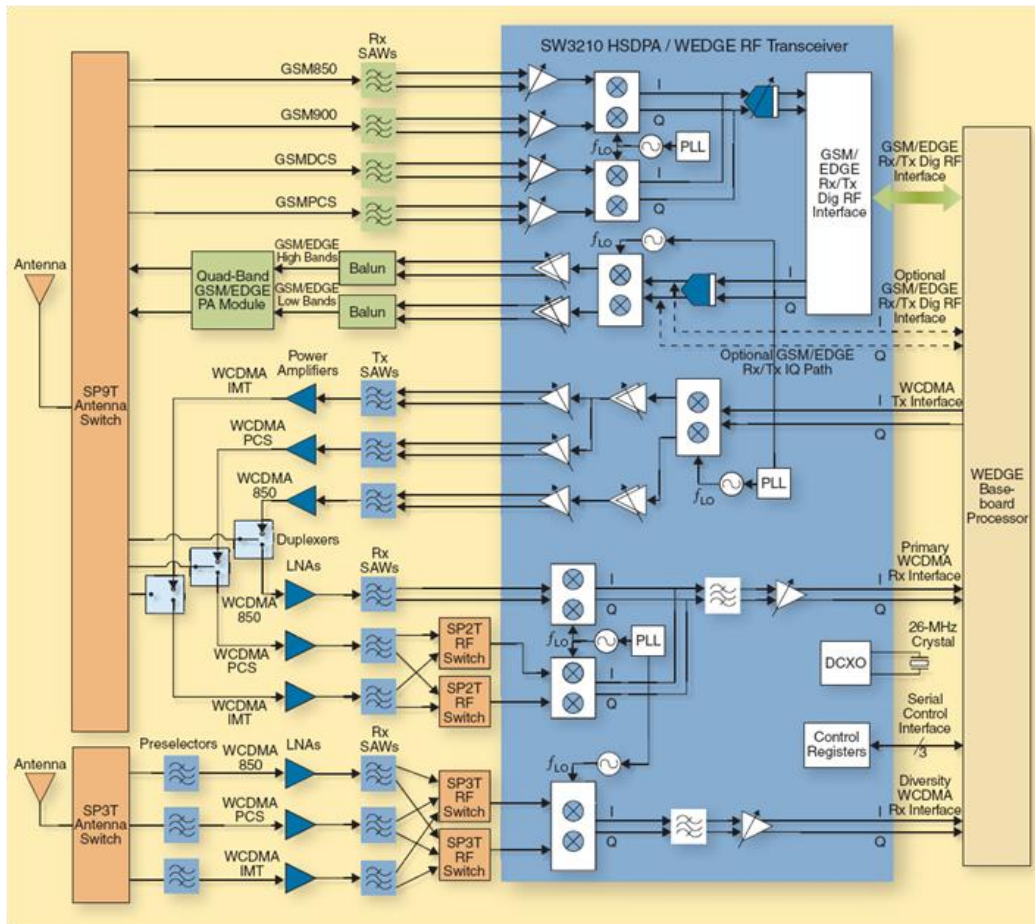


Figure 1.3 Innovative single-chip CMOS RF transceiver that incorporates a complete multiband HSDPA/WCDMA and quad-band GSM/EDGE radio subsystem with receive diversity for multimode wireless applications.

At this high integration level microwave designers struggle with problems such as:

On the receiver side:

-For GSM-EDGE the receiver architecture requires IP2 performance on the order of 50 dBm or more when referred to the antenna input.

-CMOS designs must also contend with fairly severe  $1/f$  noise in the sensitive IQ gain stages that immediately follow the down conversion mixer. Detailed  $1/f$  noise parameters depend significantly on oxide thickness and channel length.

-One of the major problems facing WCDMA receiver design pertains to transmitter leakage that falls through the duplexer filtering into the LNA input. This leakage adversely impacts attaining receiver IP2 and IP3 requirements.

On the transmitter side:

-If the frequency synthesizer will operate on-frequency, relative to the PA output this demands serious attention to oscillator pushing and pulling, and signal dynamic range can also be quite challenging particularly for WCDMA mode.

- If the frequency synthesizer operates on-frequency, relative to the PA output oscillator, re-modulation due to the PA is a particularly serious issue for on-frequency GSM-EDGE designs because a major portion of the modulation spectrum can fall within the frequency synthesizer's closed-loop bandwidth. Since the PA contributions coherently add with the oscillator's own sinusoidal waveform, the net phase error as seen by the phase-locked loop (PLL) cannot be nulled and near-chaotic behavior can result.

- If the frequency synthesizer will not operate on-frequency relative to the PA output, still because of noise considerations, dividers must use a minimum number of active devices in circuit structures.

- Power efficiency is also a challenge. The output power amplification stage consumes a large percentage of the battery capacity in any wireless device. Unlike the power amplifiers (PAs) in GSM-EDGE handsets, which are used in saturated mode, PAs in WCDMA systems operate in linear mode.

-The bandwidth and dynamic range specifications of GSM-EDGE transmitters are less than the demands imposed by WCDMA waveforms.

The latter is a key concept to manage integrated polar modulation based GSM-EDGE-WCDMA solutions in the same signal path as shown in figure 1.4. A single, common transmit path could maximize on-chip circuit re-use, reduce system costs, save PCB area and simplify the design of the handset's front-end. Moreover, since linear PAs consume a large proportion of the battery capacity in handsets, a single transmit path capable of using non-linear power amplifiers (PAs) could dramatically reduce power consumption and extend handset battery life.

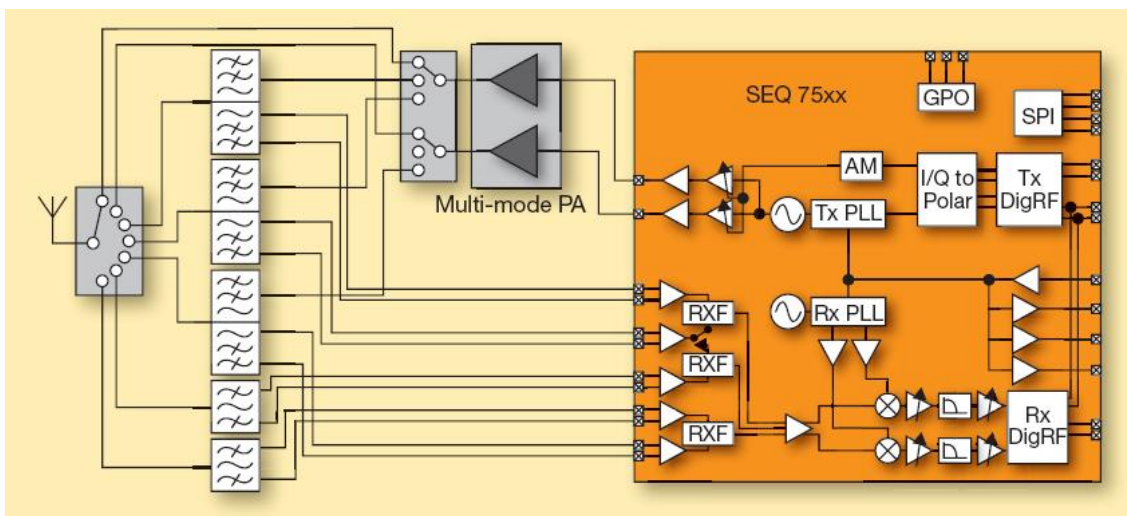
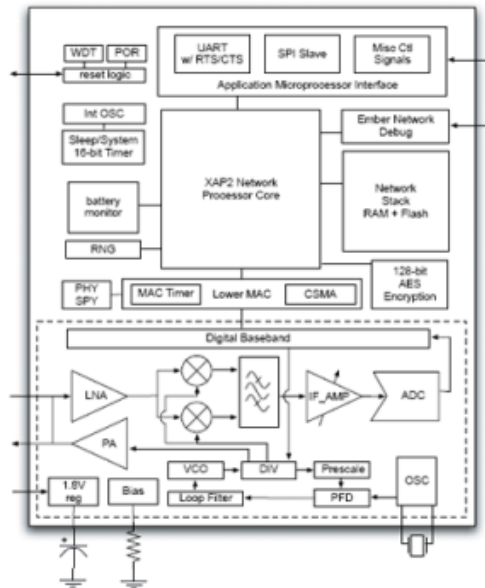


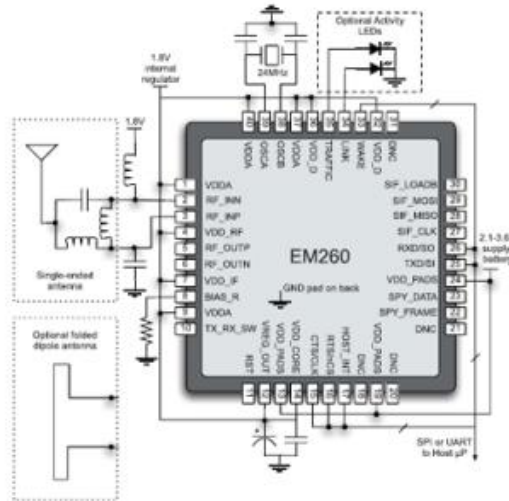
Figure 1.4 Next-generation polar WEDGE solution.

It seems evident that the answer to these constraints is the differential configurations. At present the major building blocks in a highly integrated Tx and Rx paths such as : Power Amplifier (PA), modulator (MOD), power detector (PD), automatic gain control circuit (AGC), voltage-controlled oscillator (VCO), dividers , etc, are built by using differential structures, because their intrinsic nature solves the above constraints automatically. The differential structures also reject the signal coupling due to the highly conductive substrate which allows to integrate high-power blocks with low -power blocks on the same chip as shown in figure 1.5. However, there are strong reasons why the introduction of differential circuits to replace single-ended circuits has been a slow process:

- Double the circuitry versus a single-ended circuit design.
- Twice the current and power consumption.
- Difficult to design and analyze.
- Not easily characterized in both frequency and time domains.



(a)



(b)

Figure 1.5 EM260 from Ember is a ZigBee Network Co-Processor that combines a 2.4GHz IEEE 802.15.4 compliant radio transceiver with a flash-based microprocessor, as example of differential structures benefits.

a) Block diagram b) Circuit Diagram

In this thesis work, will be analyzed time domain techniques in order to measure incident and reflected single-ended power waves (their amplitude  $|.$  and their phases  $\angle$  ) at different harmonics of interest in a multiport DUT, underlining special interest in differential power amplifiers characterization, working in a nonlinear region of operation at microwave frequencies, which requires a special class of test bench setup. The characterization level includes both frequency and time domains and additionally the variation of harmonics mixed mode loads to see how their variations influence the harmonic mixed mode design specifications of differential power amplifiers. Chapter II defines some nonlinear mixed-mode specifications of a differential power amplifier, at the beginning of Chapter III there is an explanation about the error models used at RF frequencies in order to correct measurement data, then the first among the three calibration procedures required is described (S-parameter calibration). Chapter IV continues describing the power and phase calibration procedures. In chapter V the hardware implementation of nonlinear differential power amplifier characterization used in this thesis work is described. Chapter VI shows the RF measurement results obtained by testing two commercially differential power amplifiers. Finally, some conclusions summarizing this thesis work.



# **CHAPTER II**

## **DIFFERENTIAL CIRCUITS**

## 2.1) DIFFERENTIAL CIRCUITS

In microwave frequencies a differential circuit consists of a pair of coupled transmission lines on the input and output which provide physical access points to the differential device under test (DDUT) and allow the propagation of two TEM modes (see figure 2.1).

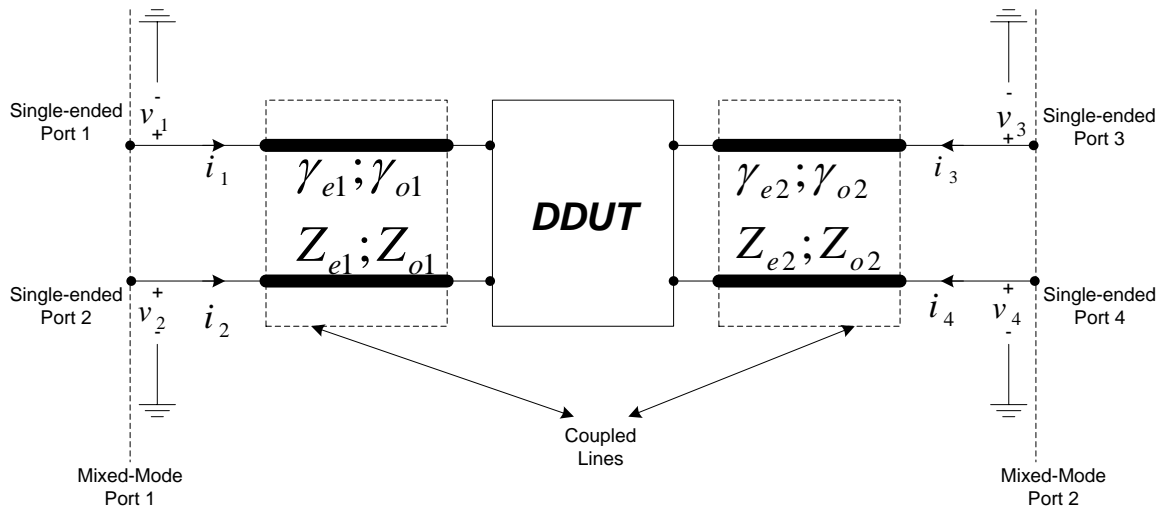


Figure 2.1 Schematic of RF differential two-port network

These two modes are the differential and common mode. The differential mode is defined by means of a signal that propagates between the lines of the access point coupled-pairs at the input and output, these signals are known as differential signals which are described by the difference of voltages and currents at input and output ports as follows:

$$v_{d \frac{i+1}{2}}(x) = v_i - v_{i+1} \quad (2.1)$$

$$i_{d \frac{i+1}{2}}(x) = \frac{i_i - i_{i+1}}{2} \quad (2.2)$$

For  $i=1,3$

On the other hand, the existence of an additional global reference conductor or ground plane allows the common mode propagation, which produces equal signals in respect to ground to each conductor of the access point coupled-pairs at the input and output. This propagation mode is defined by the sum of voltages and currents at input and output as follows:

$$v_{c\frac{i+1}{2}}(x) = \frac{v_i + v_{i+1}}{2} \quad (2.3)$$

$$i_{c\frac{i+1}{2}}(x) = i_i + i_{i+1} \quad (2.4)$$

For  $i=1,3$

This way the definition of differential and common modes springs from the necessity of being consistent with the differential power delivered to a differential load and to define the orthonormal mixed-mode S-parameter basis vectors so that the matrix transformation between standard S-parameters and mixed mode S-parameters is unitary [1]. In others words, in order to obtain:

$$P_{common\ mode\ \frac{i+1}{2}} + P_{differential\ mode\ \frac{i+1}{2}} = P_i + P_{i+1} \quad (2.5)$$

For  $i=1,3$

$$\underline{\underline{S}}^{mm} = \underline{\underline{M}} \underline{\underline{S}}^{std} \underline{\underline{M}}^{-1} \quad (2.6)$$

$$\underline{\underline{M}} \underline{\underline{M}}^{-1} = \underline{\underline{I}}$$

$$\underline{\underline{M}} = \frac{1}{\sqrt{2}} \begin{bmatrix} 1 & -1 & 0 & 0 \\ 0 & 0 & 1 & -1 \\ 1 & 1 & 0 & 0 \\ 0 & 0 & 1 & 1 \end{bmatrix}$$

$P_{common\ mode\ \frac{i+1}{2}}$ : stands for the active power into the common mode at the  $\frac{i+1}{2}$ -th input or output mixed mode port.

$P_{differential\ mode\ \frac{i+1}{2}}$ : stands for the active power into the differential mode at the  $\frac{i+1}{2}$ -th input or output mixed mode port.

$P_x$ : stands for the power at the x-th single-ended access terminal (at the input or at the output) .

The simultaneous propagation of both differential mode and common mode through the access point coupled transmission lines is referred as mixed mode propagation from which mixed mode S-parameters ( $\underline{S}^{mm}$ ) are defined.

When the access points coupled pairs are assumed symmetric, the characteristic impedances of each mode of propagation is defined as the ratio of the voltage to current of the appropriate modes at any point,  $x$ , along the line. These impedances can be expressed in terms of the even- and odd-mode (ground referenced) characteristic impedances ( $Z_{odd-i}$  and  $Z_{even-i}$ ):

$$Z_{di} = 2Z_{odd-i} \quad (2.7)$$

$$Z_{ci} = \frac{Z_{even-i}}{2} \quad (2.8)$$

For  $i=1,2$

This is, because each single-ended voltage and current used into the above differential- and common -mode voltages definitions consists of four propagating modes all referring to ground which are known as odd-mode and even-mode (ground referred).

In this way, both common-mode and differential-mode of propagation are defined by means of voltages  $(v_{d\frac{i+1}{2}}; v_{c\frac{i+1}{2}})$ , currents  $(i_{d\frac{i+1}{2}}; i_{c\frac{i+1}{2}})$  and characteristic impedances  $(Z_{di}, Z_{ci})$ , which also allow to define their normalized power waves at each mixed mode port (1 and 2 in figure 2.1) as follows:

$$a_{mi} = \frac{v_{mi} + i_{mi} Z_m}{2\sqrt{\text{Re}\{Z_m\}}} \quad (2.9)$$

$$b_{mi} = \frac{v_{mi} - i_{mi} Z_m^*}{2\sqrt{\text{Re}\{Z_m\}}} \quad (2.10)$$

For  $m=c,d$  and  $i=1,2$

One has to take into account that the normalized power waves are defined for the coupled pair placed outside of the DDUT at its input and output, in other words, it is a model made for the modeling of coupled transmission lines. In the particular case when the DDUT is a linear time invariant system (LTI), one can relate the DDUT behavior by using the incident and reflected power waves of each propagating mode through the well known mixed mode S-parameter matrix defined as follows (see figure 2.2):

$$\begin{pmatrix} b_{d1} \\ b_{d2} \\ b_{c1} \\ b_{c2} \end{pmatrix} = \begin{bmatrix} \underline{\underline{S}}_{DD} & \underline{\underline{S}}_{DC} \\ \underline{\underline{S}}_{CD} & \underline{\underline{S}}_{CC} \end{bmatrix} \begin{pmatrix} a_{d1} \\ a_{d2} \\ a_{c1} \\ a_{c2} \end{pmatrix} \quad (2.11)$$

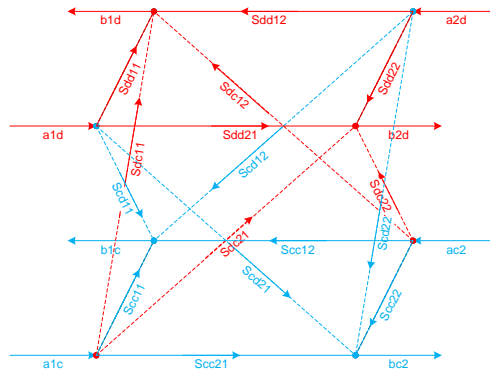


Figure 2.2 Signal flow diagram of mixed-mode two-port linear network.

The mixed mode S-parameters are a powerful design tool even if the DDUT will work in nonlinear mode of operation. This is because differential devices are built to balance as soon as possible. Balanced differential devices by definition have no-mode conversion, it means:

$$\underline{\underline{S}}_{DC} = \underline{\underline{S}}_{CD} = \underline{\underline{0}} \xrightarrow{\text{yields}} \begin{cases} s_{11} = s_{22} \cap s_{33} = s_{44} \text{ (matching condition)} \\ s_{12} = s_{21} \cap s_{34} = s_{43} \text{ (matching isolation condition)} \\ s_{31} = s_{42} \cap s_{13} = s_{24} \text{ (gains condition)} \\ s_{32} = s_{23} \cap s_{41} = s_{14} \text{ (cross terms condition)} \end{cases} \quad (2.12)$$

Particularly balanced differential active devices, offer important benefices such as [2]:

- Improved noise isolation.
- Increased dynamic range for a given supply voltage (3dB).
- Reduced even-order harmonic and intermodulation distortion terms ( $2nf_0$  and  $2f_1+f_2$  or  $2f_2-f_1$ ).
- 3dB odd-order harmonic distortion improvement in respect to single-ended  $((2n+1)f_0)$ .
- Common mode rejection.

On the other hand, when the DDUT is not a linear system the reflected normalized power waves and the incident normalized power waves of each propagating mode can be related by means of a nonlinear vector function defined as (see figure 2.3):

$$\begin{pmatrix} b_{d1} \\ b_{d2} \\ b_{c1} \\ b_{c2} \end{pmatrix} = f_{\text{nonlinear}} \left\{ \begin{pmatrix} a_{d1} \\ a_{d2} \\ a_{c1} \\ a_{c2} \end{pmatrix} \right\} \quad (2.13)$$

This means, in both propagating modes each reflected power wave at a given frequency is a mathematical function of the incident power waves at different frequencies.

In this case, one can look at the DDUT's electrical behavior by measuring directly or indirectly the incident and reflected power waves of each propagating mode at given frequency of interest ( $f_0, 2f_0, \text{etc}$ ), which are related to the single-ended normalized power waves through a linear transformation as:

$$\begin{pmatrix} a_{d1} \\ a_{d2} \\ a_{c1} \\ a_{c2} \end{pmatrix} = \underline{\underline{M}} \begin{pmatrix} a_1 \\ a_2 \\ a_3 \\ a_4 \end{pmatrix} \quad (2.14)$$

$$\begin{pmatrix} b_{d1} \\ b_{d2} \\ b_{c1} \\ b_{c2} \end{pmatrix} = \underline{\underline{M}} \begin{pmatrix} b_1 \\ b_2 \\ b_3 \\ b_4 \end{pmatrix} \quad (2.15)$$

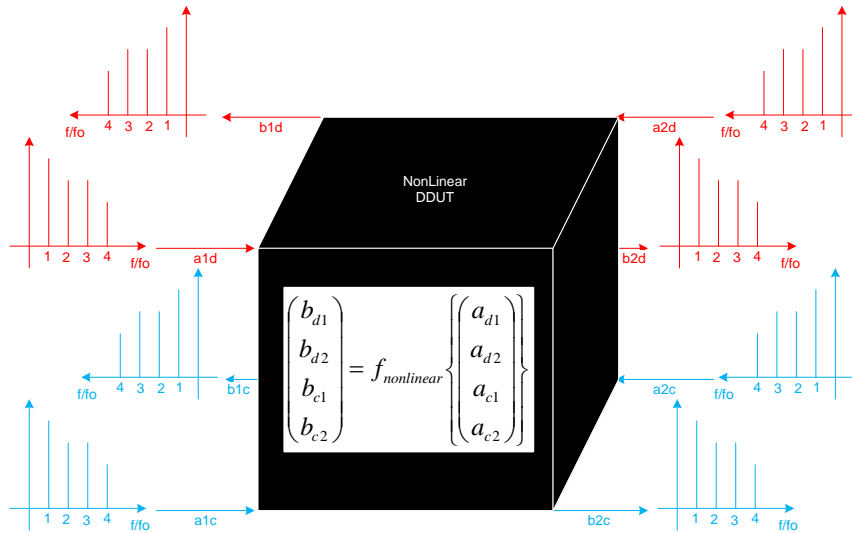


Figure 2.3 Signal flow diagram of mixed-mode two-port nonlinear network.

So, the incident and reflected power waves of each propagating mode give one insight on the nonlinear DDUT electrical behavior at each frequency of interest in both frequency and time domain. Obviously, this power wave measurement based approach is able to be extended to modeling nonlinear DDUTs by using approaches such as Poly-Harmonic Distortion (PHD) applied in separated ways to each propagating mode. Furthermore, tuning the incident and reflected normalized power waves at a given

frequency of interest ( $f_0, 2f_0$ , etc), it's possible to control the harmonic impedances of each propagating mode at the input or output of the DDUT ( $\Gamma_{Smi}$  or  $\Gamma_{Lmi}$ ), which can be useful in microwave DDUT design and optimization. In the particular case of nonlinear differential amplifiers one can get a generic design topology as shown in figure 2.4 [4].

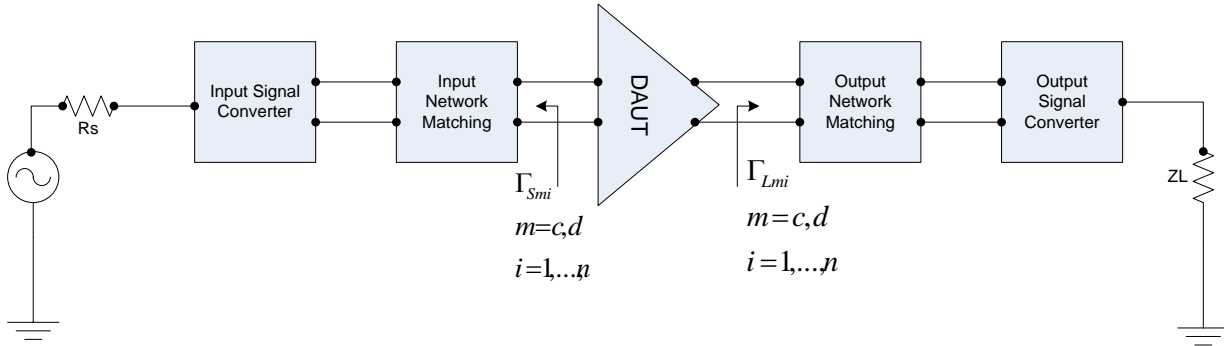


Figure 2.4 Block diagram of differential power amplifier.

The differential Amplifier Under Test (DAUT) can be built by using 1) separate amplifiers that are ideally independent and identical (i.e. push-pull) 2) Two amplifying devices with a common bias current-skin or source (i.e. Cascode differential PA, Cross-Coupled push-pull PA ). The input signal converter is used to interface the single-ended source input with the differential input of the amplifier, similarly the output signal converter is used to interface the differential output of the amplifier with the single-ended load. The input signal converter provides a precisely balanced input signal as possible (to obtain good even-order distortion rejection( $2nf_0$ ) at the output). The output power can be combined at the final stage with a balun (Balanced to Unbalanced ) or left as a differential interface if the post PA SAW filter (Surface Acoustic Wave) is balanced or a dipole type antenna is used. The input and output matching network makes the DAUT “see” proper input and output reflection coefficients at each propagating mode at each frequency of interest ( $f_0, 2f_0, etc$ ).

The microwave test engineer’s task is to find the harmonic loads of each propagating mode in order to optimize a given DAUT performance such as: PAE,  $P_{out-mi}$ ,



$P_{in-mi}$ ,  $G_{P-mi}$ , time domain waveforms shapes ( $V_{1m}(t)$ ,  $V_{2m}(t)$ , etc), common-mode rejection,  $IP(2n+1)$  and  $IP(2n)$ , etc). A PA design's emphasis is on the output power, power gain, linearity and efficiency. The design starts at the output port where the output power contours ( $P_{out-mi}$ ) of the device are characterized. Once the output termination is determined, the matching circuit is designed the same way as the other RF building block's matching circuits.

Characterization of linear and nonlinear differential devices can be done by means of the incident and reflected power waves of each propagating mode at a given frequency of interest, such as when characterizing single-ended non linear devices.

The source ( $\Gamma_{Sm}$ ) and load ( $\Gamma_{Lm}$ ) reflection coefficients of each propagating mode at a given frequency of interest labeled as “ $kf_0$ ” are given by:

$$\Gamma_{Sm} = \frac{Z_{Sm} - Z_{rm}}{Z_{Sm} + Z_{rm}} = \frac{b_{mS}}{a_{mS}} = \frac{a_{m1}}{b_{m1}} = \frac{1}{\Gamma_{INm}} @kf_0 \quad (2.16)$$

$$\Gamma_{Lm} = \frac{Z_{Lm} - Z_{rm}}{Z_{Lm} + Z_{rm}} = \frac{b_{m2}}{a_{m2}} @kf_0 \quad (2.17)$$

For  $m=c,d$

Where:

$Z_{rm}$  : stands for the reference impedance used to map the tuned impedance of the propagating mode. Often  $2Z_{odd}=100\Omega$  for differential-mode and  $\frac{Z_{even}}{2} = 25\Omega$  for common-mode . The latter is because as it's well known, it's difficult to fabricate coupled lines where  $Z_{even}$  does not equal to  $Z_{odd}$ .

The square of the magnitude of the incident and reflected normalized power waves of each propagating mode represents power. Therefore, the power delivered to the m-mode load ( $P_{Lm}$ ) by the m-propagating mode is given by the difference between the incident and reflected power of the m-propagating mode , namely[4]:

$$P_{Lm} = |b_{m2}|^2 - |a_{m2}|^2 = |b_{m2}|^2 (1 - |\Gamma_{Lm}|^2) = P_{OUTm} \quad @kf_0 \quad (2.18)$$

The m-mode input power from a source ( $\mathbf{P}_{INm}$ ) is defined as the m-mode power delivered by the source to an m-mode load, given by:

$$P_{INm} = |a_{m1}|^2 - |b_{m1}|^2 = |a_{m1}|^2 (1 - |\Gamma_{INm}|^2) \quad @kf_0 \quad (2.19)$$

The m-mode power available from a source ( $\mathbf{P}_{AVSm}$ ) is defined as the m-mode power delivered by the source to a conjugate matched m-mode load ( $\Gamma_{Lm} = \Gamma_{Sm}^*$ ) as shown in figure 2.5, given by:

$$P_{AVSm} = |a_{m1}|^2 - |b_{m1}|^2 |_{\Gamma_{INm} = \Gamma_{Sm}^*} = |a_{m1}|^2 (1 - |\Gamma_{Sm}|^2) \quad @kf_0 \quad (2.20)$$

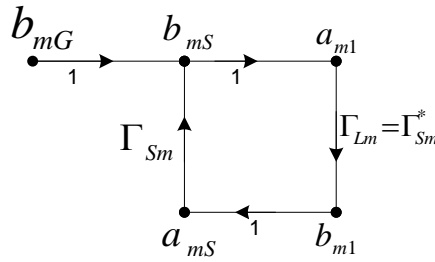


Figure 2.5 Signal flow graph of an m-mode voltage source connected to an m-mode conjugate matched load.

The m-mode transducer power gain, called  $\mathbf{G}_{Tm}$  is defined as the ratio of the m-mode power delivered to an m-mode load to the m-mode power available from the source. From (2.18) and (2.20) one obtains:

$$G_{Tm} = \frac{P_{Lm}}{P_{AVSm}} = \frac{|b_{m2}|^2 - |a_{m2}|^2}{|a_{m1}|^2 - |b_{m1}|^2 |_{\Gamma_{INm} = \Gamma_{Sm}^*}} = \frac{|b_{m2}|^2}{|a_{m1}|^2} \left( \frac{1 - |\Gamma_{Lm}|^2}{1 - |\Gamma_{Sm}|^2} \right) \quad @ f_0 \quad (2.21)$$

Similarly the m-mode operating power gain, called  $\mathbf{G}_{Pm}$  and the m-mode available power gain  $\mathbf{G}_{Am}$  are defined as follows:

$$G_{Pm} = \frac{P_{Lm}}{P_{INm}} = \frac{P_{OUTm}}{P_{INm}} = \frac{|b_{m2}|^2 (1 - |\Gamma_{Lm}|^2)}{|a_{m1}|^2 (1 - |\Gamma_{INm}|^2)} \quad @f_0 \quad (2.22)$$

$$G_{Am} = \frac{P_{AVNm}}{P_{AVSm}} = \frac{P_{OUTm} |_{\Gamma_{Lm} = \Gamma_{OUTm}^*}}{P_{INm} |_{\Gamma_{INm} = \Gamma_{Sm}^*}} \quad @f_0 \quad (2.23)$$

Where :

$$\Gamma_{OUTm} = \left. \frac{b_{m2}}{a_{m2}} \right|_{b_{mG} = 0}$$

On the other hand, the X-dB m-mode gain compression point ( $\mathbf{G_{Pm-XdBm}}$ ) is defined as the m-mode operating power gain ( $\mathbf{G_{Pm}}$ ) where the nonlinearities of the transistor reduces the power gain by X dB over the small-signal linear power gain. That is:

$$G_{Pm-XdB} (dB) = G_{Pm0} (dB) - X (dB) \quad @f_0 \quad (2.24)$$

Where  $\mathbf{G_{Pm0}(dB)}$  is the m-mode small-signal linear power gain in decibels. A typical value of X(dB) is 3dB in differential-mode. Under this condition, ( $\mathbf{G_{Pm-XdBm}}$ ) can be found from (2.18) (2.19) (see figure 2.6) as:

$$P_{OUTm-XdB} = |b_{m2}|^2 - |a_{m2}|^2 = |b_{m2}|^2 (1 - |\Gamma_{Lm}|^2) \quad @f_0 \quad (2.25)$$

$$P_{INm-XdB} = |a_{m1}|^2 - |b_{m1}|^2 = |a_{m1}|^2 (1 - |\Gamma_{INm}|^2) \quad @f_0 \quad (2.26)$$

The output frequency response of a stable nonlinear time-invariant circuit at single dc operating point to a single (or multiple) frequency input can be represented as power series of harmonics. This power series is a mathematical expansion of the nonlinearities that occur at the bias point of the nonlinear circuit. Each harmonic term in the power series expansion of the output signal has a unique coefficient. So, the m-mode large-signal-output response  $v_{Om}$  of a nonlinear differential amplifier can be written as follows:

$$v_{Om} = \sum_{i=0}^{i_{max}} C_{mi} (v_{INm@f_0})^i \tag{2.27}$$

Each i-th harmonic term at a given m-propagating mode has an associated power labeled as  $\mathbf{P}_{mi}$  which can be computed from the measurements readings by using (2.18) and (2.19) at the output and input respectively. The i-th-order harmonic power and the input power at the fundamental ( $P_{INm@f_0}$ ) are related as:

$$P_{mi} = \frac{C_{mi}^2 ((v_{INm@f_0})^2)^i}{Re\{Z_{rm}\}} = k_n P_{INm@f_0}^i \xrightarrow{\text{yields}} P_{mi}(dB) = i P_{INm@f_0}(dB) + k_n(dB) \tag{2.28}$$

The graph shown figure 2.6 shows this relation. This graph allows us to define the i-th-harmonic input-referred intercept point (**IIPi**) and the i-th-harmonic output-referred intercept point (**OIPi**). The i-th-order harmonic intercept point (called **IPI**) is defined as the point where  $P_{OUTm@f_0}$ , and  $P_{OUTm@if_0}$  intercept, when the DDUT is assumed to be linear.

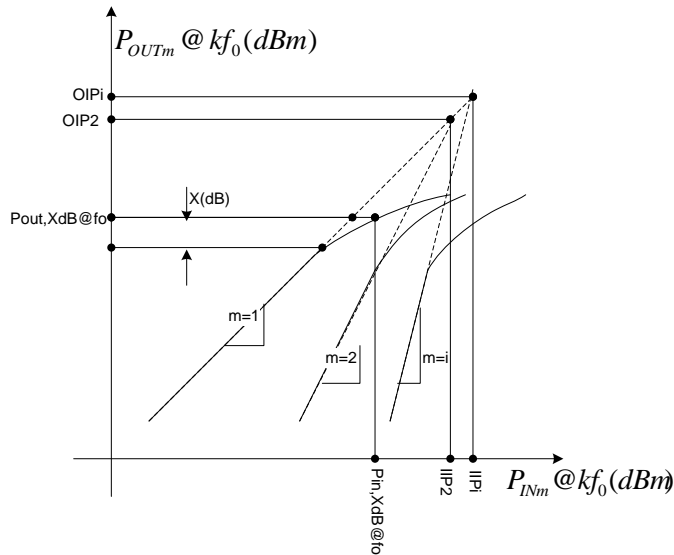


Figure 2.6 Nonlinear Differential Amplifier Pin-Pout curve

A fundamental property of the mixed-mode representation of a differential circuit with no significant mode-conversion is that the differential and common-mode performances ( $P_{OUTm-@kf_0}$ ,  $P_{OUTm-XdB}@f_0$ ,  $G_{Pm}@f_0$ , etc) can be set independently. This

property allows the design of the differential and common mode responses of a circuit to be pursued to independent design goals. So, one could design matching impedances that maximize differential design specifications while simultaneously greatly reducing the common-mode power dependent specifications.

In this sense, one can continue defining all already existent concepts of non-linear two port devices such as: power added efficiency (**PAE**), *i*-th-order Intermodulation Product (**Ii-thP**), Carrier to *i*-th-order intermodulation ratio (**C/Ii-thP**), etc at each propagating mode (*m*, *c*) and at each frequency of interest.

**References**

- [1] D. E. Bockelman, “The theory, measurement, and application of mode specific scattering parameters with multiple modes of propagation,” Ph.D. dissertation, Dept. Elect. Comput. Eng., Univ. Florida, 1997.
- [2] William R. Eisenstadt , Bob Stengel and Bruce M.Thompson “Microwave Differential Circuit Design Using Mixed-Mode S-parameters, Artech House, Boston 2006.
- [3]Jongchan Kang, Jehyung Yoon “A Highly Linear and Efficient Differential CMOS Power Amplifier With Harmonic Control” IEEE Journal of solid-state circuits Vol.41. N° 46 June 2006.
- [4] G. Gonzalez, *Microwave Transistor Amplifiers*, Prentice-Hall, Englewood Cliffs, NJ, 1984.

# **CHAPTER III**

## **ERROR MODELS AND S-PARAMETER CALIBRATION**

### 3.1) INTRODUCTION

Why will we complicate our lives with such complex error models?. The answer to this question is: otherwise we may lose information about what we really want to measure. That is, losses and phase shift in TEM and quasi-TEM transmission mediums increase with the frequency. For instance, in coaxial cables (see figure 2.1) used typically in test benches at microwave frequencies for information transfer, their attenuation is given by [1]:

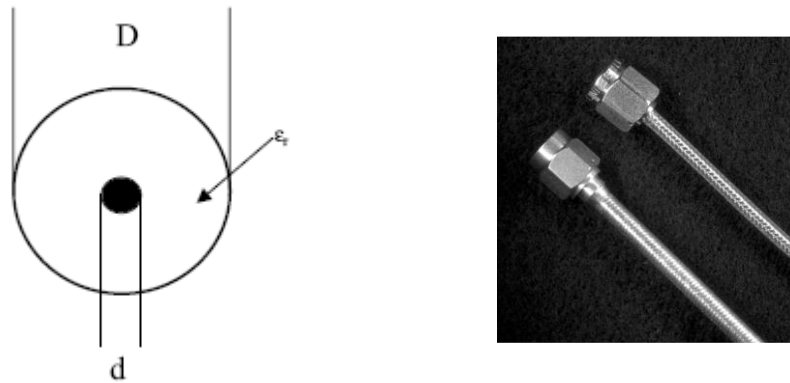


Figure (2.1) Cross-section of a coaxial cable showing outer diameter and inner diameter dimensions (right)/  
Photograph of a solder-coated and braided coaxial cable (left).

$$L_C = \frac{0.435\sqrt{f}}{Z_o.d} \left( \frac{dB}{100ft} \right); \text{ Loss in center conductor} \quad (2.1)$$

$$L_o = \frac{0.435\sqrt{f}}{Z_o.D} \left( \frac{dB}{100ft} \right); \text{ Loss in outer conductor} \quad (2.2)$$

$$L_D = 2.78 \cdot \rho \cdot f \cdot \sqrt{\epsilon_r} \left( \frac{dB}{100ft} \right); \text{ Dielectric loss} \quad (2.3)$$

$$L_{losses\_total} = L_C + L_o + L_D \left( \frac{dB}{100ft} \right); \quad (2.4)$$

Where:

f: frequency in MHz



$\epsilon_r=2.1$  for solid PTFE

1.6 for expanded PTFE

PTFE: (Polytetrafluoroethylene) is the most common dielectric material used to build coaxial cables.

From these expressions it's easy to understand that when working at frequencies above 1GHz, it is only a matter of extract cable's losses from measurements in order to guarantee accurate amplitude measurements.

On the other hand, the phase shift introduced by a piece of coaxial cable with a physical length L over a voltage or current wave traveling across it, at a given frequency f is given by:

$$\theta = \frac{\sqrt{\epsilon_r} \cdot 360 \cdot f \cdot L}{c} \text{ (}^\circ\text{)} \quad (2.5)$$

Once again it's easy to appreciate, how at high frequencies the cables' phase shift is not negligible, and has to be extracted, so as to guarantee accurate phase measurements. One shouldn't to measure a voltage directly by using a sampling oscilloscope at high frequencies without being aware of what one is losing. Besides these two more evident errors present into microwave frequency test benches; one may get a lot of errors which must be extracted from measurements data, in order to guarantee they are correct within a given uncertainty level. Also these magnitude error and phase errors at high frequencies, predict what will be the error correction model found, in order to correct measurement data. The error model will remove magnitude error and/or phase error, in other words, it will consist of complex numbers.

### **3.2) SOURCES AND TYPES OF ERRORS ON VNA MEASUREMENTS SYSTEMS**

Many others types of errors are intrinsic to the test equipments' nature and to the particular nature of the setup used to carry out measurement. For instance, parts of the

measurement setup, such as interconnecting cables and signal-separation devices (as well as the equipments themselves), all introduce variations in magnitude and phase that can mask the actual performance of the test devices. The environment and user may also affect the measurement accuracy. Formally whatever measurement system used, it will include measurement errors that can be separated into two categories depending on whether they might be present or not in the measurement data as follows [2]:

**3.2.1) Raw Errors:** associated with the uncorrected system that are called systematic (repeatable), random (non-repeatable), and drift errors.

**3.2.1.1) Systematic Errors:** are repeatable errors that the system can measure. If they do not vary over time they can be characterized through calibration or error-correction procedure and mathematically removed during the measurements process [3]. In most high frequency measurements the systematic errors are the most significant source of measurement uncertainty. These are errors due to mismatch and leakage in the test setup, isolation between the reference and test signal paths, and system frequency response. These uncertainties are quantified as source-load impedance mismatch, directivity, isolation (crosstalk), and frequency response (tracking) respectively.

**3.2.1.2 ) Random Errors:** are not predictable, they vary randomly as a function of time and cannot be removed through error correction. However, there are things that can be done to minimize their impact on measurement accuracy. The three main sources of random errors are [4].

### **Instrument Noise Errors**

Noise is unwanted electrical disturbances generated in the components of the analyzer (e.g., sampler noise, and IF noise floor) and they affect the measurement equipment's dynamic range [5]. These disturbances include:

**Low level noise (noise floor)** due to the broadband noise floor of the receiver.

**High level noise** or jitter of the trace data due to the noise floor and the phase noise of the LO source inside the test set.

One can reduce both noise errors by doing one or more of the following:

-Increase the source power to the DUT; however this only reduces low-level noise.

-Narrow the IF bandwidth: Reducing the IF receiver bandwidth reduces the effect of random noise on a measurement as shown in figure 2.18 for different RF frequencies and at a given number of measuring points. However, narrower IF bandwidths cause longer sweep times.

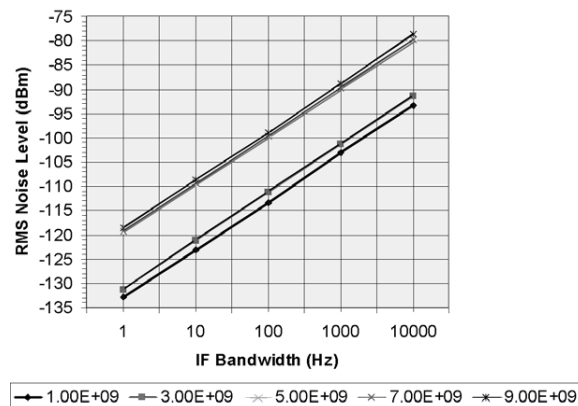


Figure 2.18 RMS noise floor vs. IF BW (n=801 pts) @ 1, 3,5,7,9 GHz

-Apply several measurement sweep averages. Using the averaging function available in most VNA, improve the S/R for every factor increase in averages [5]. It also reduces measurement speed because when two traces must be averaged, measurement time doubles. Table 2.1 compares the two latter techniques so as to reduce the noise floor.

		Noise floor reduction (dB)	Sweep time increase factor
10 KHz	10 averages	10	10
1 KHz	0 averages	10	7.75
10 KHz	100 averages	20	100
100 Hz	0 averages	20	74.8
100 Hz	10 averages	10	10
10 Hz	0 averages	10	9.9
100 Hz	100 averages	20	100
1 Hz	0 averages	20	99.5

Table 2.1 Sweep time impact respect to IF bandwidth and averaging points

In both cases it's important to note that each option to improve the dynamic range and then reduce these type of random errors is often time consuming.

### Switch Repeatability Errors

Mechanical or Solid state RF switches are used in the measurement test equipment to switch the sources, attenuator, loads, etc. (see figure 2.19). When mechanical RF switches are activated, the contacts close differently from when they were previously activated. When this occurs, it can adversely affect the accuracy of a measurement. For solid state RF switches, their port-to-port isolation characteristic is the more important specification.

One can reduce the effects of switch repeatability errors by avoiding switching setups, or account for them by applying the well known switch error correction procedure.

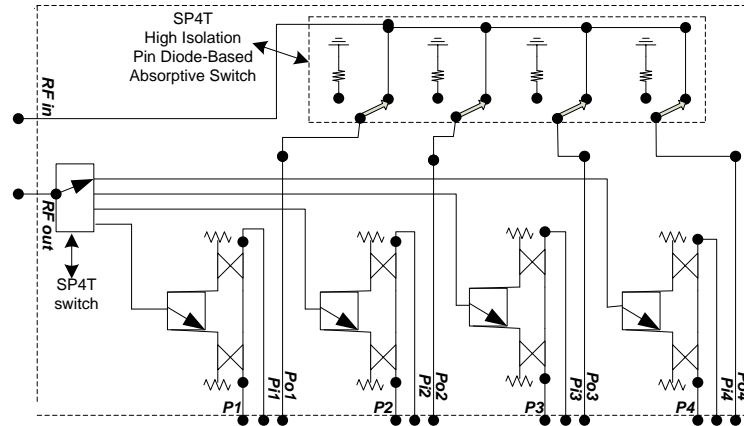


Figure 2.19 Block diagram of basic four port unit.

### Connector Repeatability Errors

Connector repeatability is the random variation encountered when connecting a pair of RF connectors. Variations in both reflection and transmission can be observed. Connector wear causes changes in electrical performance. One can reduce connector repeatability errors by practicing good connector care methods.

**3.2.2) Residual Errors:** are the errors that remain after calibration or error correction procedure. So they may include Raw Errors terms depending on whether they may be removed or not through the error correction procedure, furthermore they include other non-Raw Errors terms such as: the uncertainty measurement specification of the VNA's system which includes the system's dynamic accuracy, the connector type's repeatability, system repeatability, stability, and noise level. They are also determined by the quality of calibration standards and how well "known" they are.

### 3.3) ERROR MODELS

A key concept related with multiport nonlinear active device characterization is that one can characterize linear or non linear systems by using a linear one. The latter is

characterized by means of and during a complete error correction procedure or called calibration. The calibration steps number depends on what DUT's performances one needs to measure and where one needs to do it (on-wafer or coaxial measurement environments). So after a calibration procedure one will be able to remove all desired systematic errors from the measurements data.

When characterizing multiport linear or non linear DUTs, one is required to remove the greatest quantity of systematic errors as possible from the measurement data, so as to guarantee good levels of accuracy. Sometimes, however the amount of systematic errors one can remove from the measurement data and their relationship to the error model's complexity and calibration's steps becomes a compromise; the larger the number of systematic error terms, the more complex the error model and the calibration procedure.

It's important to note that, first one chooses an error model to be used, and then one tries to get the best calibration procedure (algorithm) in order to find the error model's unknowns.

On the other hand, as mentioned in Section 3.1.1.2, one has to account that some systematic errors can be completely removed from the measurement data, however others can be simply reduced, even if they aren't explicit in the error model. The rest of the error terms cannot be removed or reduced and they establish the measurement's uncertainty.

### **3.4) ERROR MODEL'S GENERATION PROCESS**

One is required to characterize the measurement setup in order to extract the systematic error terms from the measurements data. Figure 3.1 shows a generic multiport VNA system (based on a complete reflectometer architecture [6]) when carrying out linear DUT's measurements like S-parameters. This topology will be used to generate the Error Models by using a similar approach to [7]. In figure 3.1: the source section is connected by means of a high isolation absorptive SPnT switch, which is connected at the signal

separation section whose function is taking a part of the incident and reflected waves from the DUT and route them to the mixer/sampler-based receiver, where they will be down converted at a given IF frequency to finally being digitized. It's important to emphasize that often the signal separation section acts like a interface between two different types of measurement environments labeled as “k” and “j” in figure 3.1.

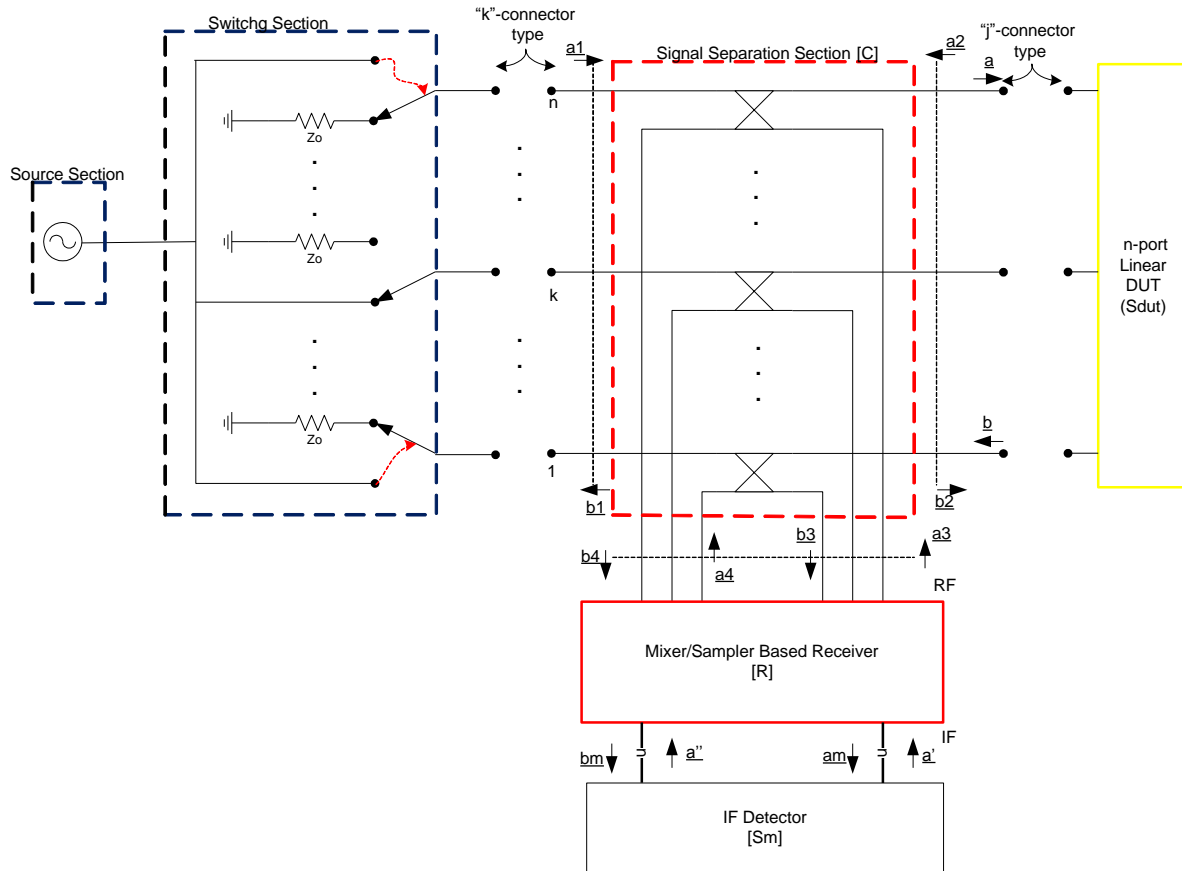


Figure 3.1. Generic multiport VNA setup when carrying out S-parameter measurements.

Where:

$$\underline{a}_i = \begin{pmatrix} a_{1i} \\ a_{2i} \\ \vdots \\ a_{ni} \end{pmatrix}; \quad \underline{b}_i = \begin{pmatrix} b_{1i} \\ b_{2i} \\ \vdots \\ b_{ni} \end{pmatrix} \text{ For } i=1, \dots, 4$$

$$\underline{\mathbf{a}}_m = \begin{pmatrix} a_{m1} \\ a_{m2} \\ \vdots \\ a_{mn} \end{pmatrix}; \underline{\mathbf{b}}_m = \begin{pmatrix} b_{m1} \\ b_{m2} \\ \vdots \\ b_{mn} \end{pmatrix}; \underline{\mathbf{x}} = \begin{pmatrix} x_1 \\ x_2 \\ \vdots \\ x_n \end{pmatrix}; \text{ for } \mathbf{x}=\mathbf{a}', \mathbf{a}'$$

$$\underline{\mathbf{a}} = \begin{pmatrix} a_1 \\ a_2 \\ \vdots \\ a_n \end{pmatrix}; \underline{\mathbf{b}} = \begin{pmatrix} b_1 \\ b_2 \\ \vdots \\ b_n \end{pmatrix}$$

As an initial hypothesis, it will be assumed that the signal separation section, the mixer/sampler-based receiver, and the DUT, are Linear Time-Invariant Systems, in this way, they will be characterized by defining their S-parameter matrixes:  $\underline{\underline{\mathbf{C}}}$ ;  $\underline{\underline{\mathbf{R}}}$ ;  $\underline{\underline{\mathbf{S}}}_{dut}$  respectively.

Figure 3.1 allows us define  $\underline{\underline{\mathbf{C}}}$ ;  $\underline{\underline{\mathbf{R}}}$  as follow:

$$\begin{pmatrix} \underline{a_3} \\ \underline{a_4} \\ \underline{a_m} \\ \underline{b_m} \end{pmatrix} = \underline{\underline{\mathbf{R}}} \begin{pmatrix} \underline{b_3} \\ \underline{b_4} \\ \underline{a'} \\ \underline{a''} \end{pmatrix} \quad (3.1)$$

$$\begin{pmatrix} \underline{b_1} \\ \underline{b_2} \\ \underline{b_3} \\ \underline{b_4} \end{pmatrix} = \underline{\underline{\mathbf{C}}} \begin{pmatrix} \underline{a_1} \\ \underline{a_2} \\ \underline{a_3} \\ \underline{a_4} \end{pmatrix} \quad (3.2)$$

Since, commonly in practical applications one has physical access to “j” and “k” measurement environments ( $\underline{b_1}$ ;  $\underline{b_2}$ ;  $\underline{a_1}$ ;  $\underline{a_2}$ ), and additionally one can obtain  $\underline{b_m}$  and  $\underline{a_m}$  readings from the VNA system, mathematical expressions will be sought in other to relate them to each other, even if they might not have physical meaning.



To find these mathematical expressions one could begin by substituting  $\underline{a}_i = \underline{\Gamma}_i^{-1} \underline{b}_i$  for  $i=3,4$  into expression (3.1) and (3.2), and then fitting them, to obtain  $(\underline{b}_m; \underline{a}_m)$  in (3.1) and  $(\underline{b}_1; \underline{b}_2; \underline{a}_1; \underline{a}_2)$  in (3.2) like independent variables, after that, they can be rewritten as:

$$\begin{pmatrix} \underline{a}_m \\ \underline{b}_m \end{pmatrix} = \underline{R}' \begin{pmatrix} \underline{b}_3 \\ \underline{b}_4 \end{pmatrix} \quad (3.1)'$$

$$\begin{pmatrix} \underline{a}_1 \\ \underline{b}_1 \\ \underline{a}_2 \\ \underline{b}_2 \end{pmatrix} = \underline{C}' \begin{pmatrix} \underline{b}_3 \\ \underline{b}_4 \end{pmatrix} \quad (3.2)'$$

By substituting  $\begin{pmatrix} \underline{b}_3 \\ \underline{b}_4 \end{pmatrix}$  from (3.1)' into (3.2)' one gets:

$$\begin{pmatrix} \underline{a}_1 \\ \underline{b}_1 \\ \underline{a}_2 \\ \underline{b}_2 \end{pmatrix} = \begin{bmatrix} \underline{D}_{11} & \underline{D}_{12} \\ \underline{D}_{21} & \underline{D}_{22} \\ \underline{D}_{31} & \underline{D}_{32} \\ \underline{D}_{41} & \underline{D}_{42} \end{bmatrix} \begin{pmatrix} \underline{a}_m \\ \underline{b}_m \end{pmatrix} = \begin{bmatrix} \underline{D}_{11} & \underline{D}_{12} \\ \underline{D}_{21} & \underline{D}_{22} \\ -\underline{M} & \underline{K} \\ -\underline{H} & \underline{L} \end{bmatrix} \begin{pmatrix} \underline{a}_m \\ \underline{b}_m \end{pmatrix} \quad (3.2)''$$

Expression (3.2)'' establishes that “k” and “j” measurement environments are related to VNA’s system readings by means of an equivalent Linear Time Invariant System defined by a  $4 \times 2 \times 2 \times 2$   $\underline{D}$  matrix, furthermore it establishes that each of these relationships can be treated in a separate fashion, it means, there is a relationship between each measurement environment “j” or “k” and the total VNA’s system readings  $\begin{pmatrix} \underline{a}_m \\ \underline{b}_m \end{pmatrix}$ :

$$\begin{pmatrix} \underline{a}_1 \\ \underline{b}_1 \end{pmatrix} = \begin{bmatrix} \underline{D}_{11} & \underline{D}_{12} \\ \underline{D}_{21} & \underline{D}_{22} \end{bmatrix} \begin{pmatrix} \underline{a}_m \\ \underline{b}_m \end{pmatrix} = \underline{D}_1 \begin{pmatrix} \underline{a}_m \\ \underline{b}_m \end{pmatrix} \quad (3.3)$$

$$\begin{pmatrix} \underline{a_2} \\ \underline{b_2} \end{pmatrix} = \begin{bmatrix} -\underline{M} & \underline{K} \\ -\underline{H} & \underline{L} \end{bmatrix} \begin{pmatrix} \underline{a_m} \\ \underline{b_m} \end{pmatrix} = \underline{D_2} \begin{pmatrix} \underline{a_m} \\ \underline{b_m} \end{pmatrix} \quad (3.4)$$

Expressions (3.3) and (3.4) are the input and output waves de-embedding equations respectively. It's clear that once  $\underline{D_1}$  and  $\underline{D_2}$  are completely known, one can reconstruct that that is happening at the “k” and “j” measurement environments in both frequency or time domains through  $\begin{pmatrix} \underline{a_m} \\ \underline{b_m} \end{pmatrix}$  readings. Because  $\begin{pmatrix} \underline{a_m} \\ \underline{b_m} \end{pmatrix}$  is the result of a superposition of that that happens at both “k” and “j” measurement environments, adding (3.3) and (3.4) result :

$$\begin{pmatrix} \underline{a_m} \\ \underline{b_m} \end{pmatrix} = 2 \left( \underline{D_1}^{-1} \begin{pmatrix} \underline{a_1} \\ \underline{b_1} \end{pmatrix} + \underline{D_2}^{-1} \begin{pmatrix} \underline{a_2} \\ \underline{b_2} \end{pmatrix} \right) = \begin{pmatrix} \underline{a_{m1}} \\ \underline{b_{m1}} \end{pmatrix} + \begin{pmatrix} \underline{a_{m2}} \\ \underline{b_{m2}} \end{pmatrix} \quad (3.5)$$

Expressions (3.i) for i=3,..,5 establish some important facts:

-First, that which one measures with a VNA  $\left( \begin{pmatrix} \underline{a_{m1}} \\ \underline{b_{m1}} \end{pmatrix} + \begin{pmatrix} \underline{a_{m2}} \\ \underline{b_{m2}} \end{pmatrix} \right)$  is a superposition of two different effects: one of them occurs at the “j” measurement environment  $\begin{pmatrix} \underline{a_{m2}} \\ \underline{b_{m2}} \end{pmatrix}$  and the other one occurs at the “k” measurement environment  $\begin{pmatrix} \underline{a_{m1}} \\ \underline{b_{m1}} \end{pmatrix}$ .

-It's possible to know each partial contribution  $\begin{pmatrix} \underline{a_{mi}} \\ \underline{b_{mi}} \end{pmatrix}$  for i=1,2 from the total VNA's readings  $\begin{pmatrix} \underline{a_m} \\ \underline{b_m} \end{pmatrix}$  added by each “j” or “k” measurement environment.

$\underline{D_i}$  For i=1,2 matrixes' shape will be able to describe physical effects between ports of the “j” or “k” measurement environments independently.

One has to account that  $\underline{\underline{D}}_i$  (for  $i=1,2$ ) matrixes spring from the electrical interaction between two LTI systems (receiver and signal separation section) each with incoming and outgoing power waves ( $a_i, b_i$ ) defined at each  $i$ -th transmission media, and this has a physical meaning according to figure 3.1. For instance, in that figure each pair of waves ( $a_i'', b_{mi}$ ) travels through a physical medium ( i.e. a coaxial cable ), in a similar way to which ( $a_i', a_{mi}$ ) travels through another physical medium. However, (3.4) is able to be rewritten as (note that  $\begin{pmatrix} a_2 \\ b_2 \end{pmatrix} = \begin{pmatrix} b_{dut} \\ a_{dut} \end{pmatrix}$ ):

$$\begin{pmatrix} b_m \\ a \end{pmatrix} = \begin{bmatrix} \underline{\underline{\Gamma}}_{00} & \underline{\underline{\Gamma}}_{01} \\ \underline{\underline{\Gamma}}_{10} & \underline{\underline{\Gamma}}_{11} \end{bmatrix} \begin{pmatrix} a_m \\ b \end{pmatrix} = \underline{\underline{S}}_e \begin{pmatrix} a_m \\ b \end{pmatrix} \tag{3.4}'$$

Where:  $\underline{\underline{\Gamma}}_{10} = \underline{\underline{L}} \underline{\underline{K}}^{-1}$  ;  $\underline{\underline{\Gamma}}_{11} = -(\underline{\underline{H}} + \underline{\underline{L}} \underline{\underline{K}}^{-1} \underline{\underline{H}})$ ;  $\underline{\underline{\Gamma}}_{00} = \underline{\underline{K}}^{-1}$  ;  $\underline{\underline{\Gamma}}_{01} = -\underline{\underline{K}}^{-1} \underline{\underline{M}}$

This mathematical expression suggests that it has been modeled by means of a LTI system characterized by a  $\underline{\underline{S}}_e$  matrix as shown in figure (3.2).

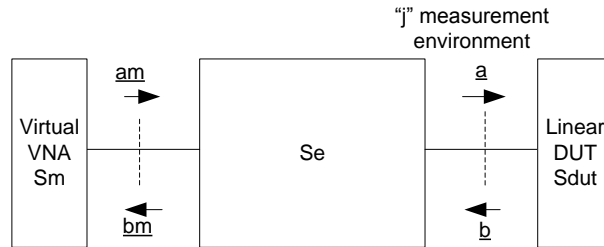


Figure 3.2 physical meaning suggested by (3.4)'

By comparing this figure with that shown in figure 3.1 and according to what has been discussed recently concerning ( $a_i'', b_{mi}$ ) or ( $a_i', a_{mi}$ ) power waves, it doesn't make physical sense. It means, (3.4)' represents a mathematical error model not a physical one. However, physical considerations can be taken into account: for instance, in both figures one can consider that the crosstalk between nearby ports might influences a given ( $b_{mi}, a_{mi}$ )

VNA's reading, and this effect could be accounted by changing  $\underline{\underline{S_e}}$  matrix's shape as it will be described in the next section.

### 3.5) TYPES OF MULTI-PORT VNA SYSTEM ERROR MODELS

As was proven in the previous section, the general connection between a real multiport network analyzer and a given multiport device under test (DUT) , can be considered as a cascade of a virtual free error multiport network analyzer, an error box (which includes all error terms) and the device under test (DUT) (see figure 3.3).

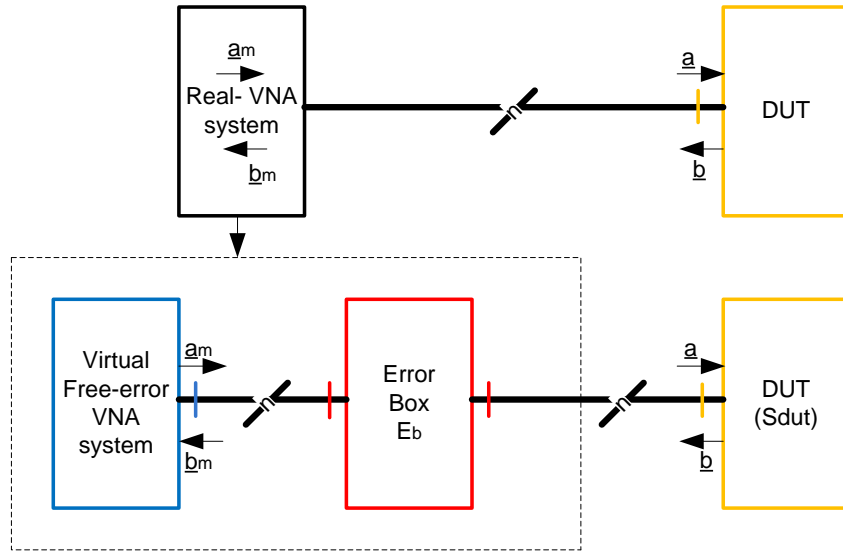


Figure 3.3 Leaky error model

One can define the error box ( $E_b$ ) as follows [8] (see (3.4)):

$$\begin{pmatrix} \underline{a} \\ \underline{b} \end{pmatrix} = \begin{bmatrix} -\underline{\underline{H}} & \underline{\underline{L}} \\ -\underline{\underline{M}} & \underline{\underline{K}} \end{bmatrix} \begin{pmatrix} \underline{a}_m \\ \underline{b}_m \end{pmatrix} \quad (3.11)$$

Where:

$$\underline{a} = \begin{pmatrix} a_1 \\ a_2 \\ \vdots \\ a_n \end{pmatrix}; \quad \underline{a}_m = \begin{pmatrix} a_{m1} \\ a_{m2} \\ \vdots \\ a_{mn} \end{pmatrix}$$

$$\underline{\mathbf{b}} = \begin{pmatrix} b_1 \\ b_2 \\ \vdots \\ b_n \end{pmatrix}; \underline{\mathbf{b}}_m = \begin{pmatrix} b_{m1} \\ b_{m2} \\ \vdots \\ b_{mn} \end{pmatrix}$$

Depending on  $\underline{\underline{H}}, \underline{\underline{K}}, \underline{\underline{L}}, \underline{\underline{M}}$  matrixes' forms, there may exist basically three different types of error models. The first one is the most complete, it accounts for all error terms that can occur between ports. It is represented by means of four full matrixes like in (3.11), it defines the so called **Leaky Error Model** [9] whose block diagram is shown in figure 3.3. As it seems obvious from (3.11) it relies on  $4n^2$  **unknowns**.

The second matrix form is:

$$\begin{bmatrix} -\underline{\underline{H}} & \underline{\underline{L}} \\ -\underline{\underline{M}} & \underline{\underline{K}} \end{bmatrix} = \begin{bmatrix} -\begin{pmatrix} \underline{\underline{H}}_L & \underline{\underline{0}} \\ \underline{\underline{0}} & \underline{\underline{H}}_R \end{pmatrix} & \begin{pmatrix} \underline{\underline{L}}_L & \underline{\underline{0}} \\ \underline{\underline{0}} & \underline{\underline{L}}_R \end{pmatrix} \\ -\begin{pmatrix} \underline{\underline{M}}_L & \underline{\underline{0}} \\ \underline{\underline{0}} & \underline{\underline{M}}_R \end{pmatrix} & \begin{pmatrix} \underline{\underline{K}}_L & \underline{\underline{0}} \\ \underline{\underline{0}} & \underline{\underline{K}}_R \end{pmatrix} \end{bmatrix} \quad (3.12)$$

It defines the well known Partially or **Half Leaky Error Model** [10] [11], whose diagram block is shown in figure 3.4. Owing to in this case one has four matrices, each of them with  $(n^2/2)$  unknowns these add a total of  $2n^2$  **unknowns**. Seeing figure 3.4 it's obvious that this error model assumes that a given port might be only affected by neighbors' leakage. This is useful when working in on-wafer measurement environments where the tips' probe proximity is small, mainly those located in the same tip probe.

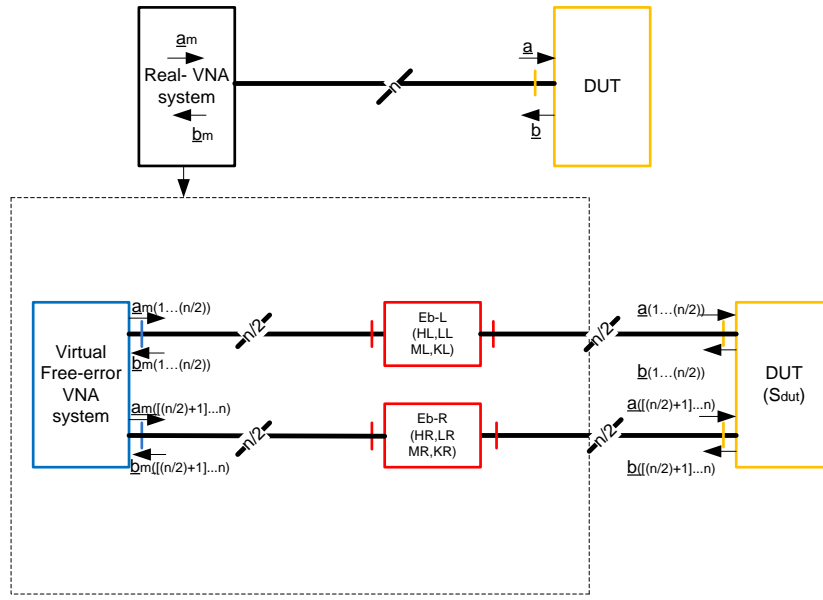


Figure 3.4 Half Leaky Error Model

Finally a third matrix form is:

$$\begin{bmatrix} -\underline{\underline{H}} & \underline{\underline{L}} \\ -\underline{\underline{M}} & \underline{\underline{K}} \end{bmatrix} = \begin{bmatrix} - \begin{pmatrix} h_{11} & 0 & \dots & 0 \\ 0 & h_{22} & 0 & \vdots \\ \vdots & \vdots & \ddots & 0 \\ 0 & 0 & 0 & h_{nn} \end{pmatrix} & \begin{pmatrix} l_{11} & 0 & \dots & 0 \\ 0 & l_{22} & 0 & \vdots \\ \vdots & \vdots & \ddots & 0 \\ 0 & 0 & 0 & l_{nn} \end{pmatrix} \\ - \begin{pmatrix} m_{11} & 0 & \dots & 0 \\ 0 & m_{22} & 0 & \vdots \\ \vdots & \vdots & \ddots & 0 \\ 0 & 0 & 0 & m_{nn} \end{pmatrix} & \begin{pmatrix} k_{11} & 0 & \dots & 0 \\ 0 & k_{22} & 0 & \vdots \\ \vdots & \vdots & \ddots & 0 \\ 0 & 0 & 0 & k_{nn} \end{pmatrix} \end{bmatrix} \quad (3.13)$$

This defines the so called **Non Leaky Error Model**, the most popular one, whose block diagram is shown in figure 3.5. There are 4, nxn-diagonal matrixes defining **4n unknowns**. It doesn't account for crosstalk between ports (considered negligible), which is acceptable when working in measurement coaxial environments. It's also commonly applied in on-wafer measurement environments, although as a compromise between crosstalk levels between nearby ports, error model complexity, and calibration procedure complexity.

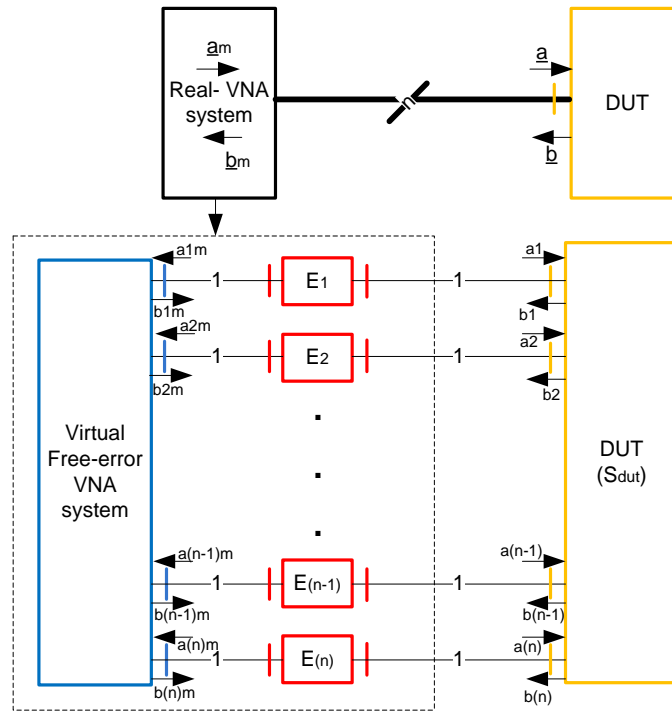


Figure 3.5 Non-Leaky Error Model

### 3.6) S-PARAMETER CALIBRATION

During a S-parameter calibration procedure the task is connecting physical calibration standards where needed (“j” measurement environment ports in figure 3.6) in order to get mathematical conditions that allow us to find  $\underline{H}$ ,  $\underline{K}$ ,  $\underline{L}$ ,  $\underline{M}$  matrixes’ elements over an initially chosen error model. In this way by using physical standards and VNA’s readings  $\begin{pmatrix} a_m \\ b_m \end{pmatrix}$  a total of  $(4n^2-1)$ ,  $(2n^2-1)$  or  $(4n-1)$  error terms are found depending on whether full-leaky, half-leaky or non-leaky error model are chosen respectively. During the S-parameter calibration procedure the setup shown in figure 3.6 will be used. In this figure the assumption is to have only one and two port calibration standards available, this occurs frequently in labs

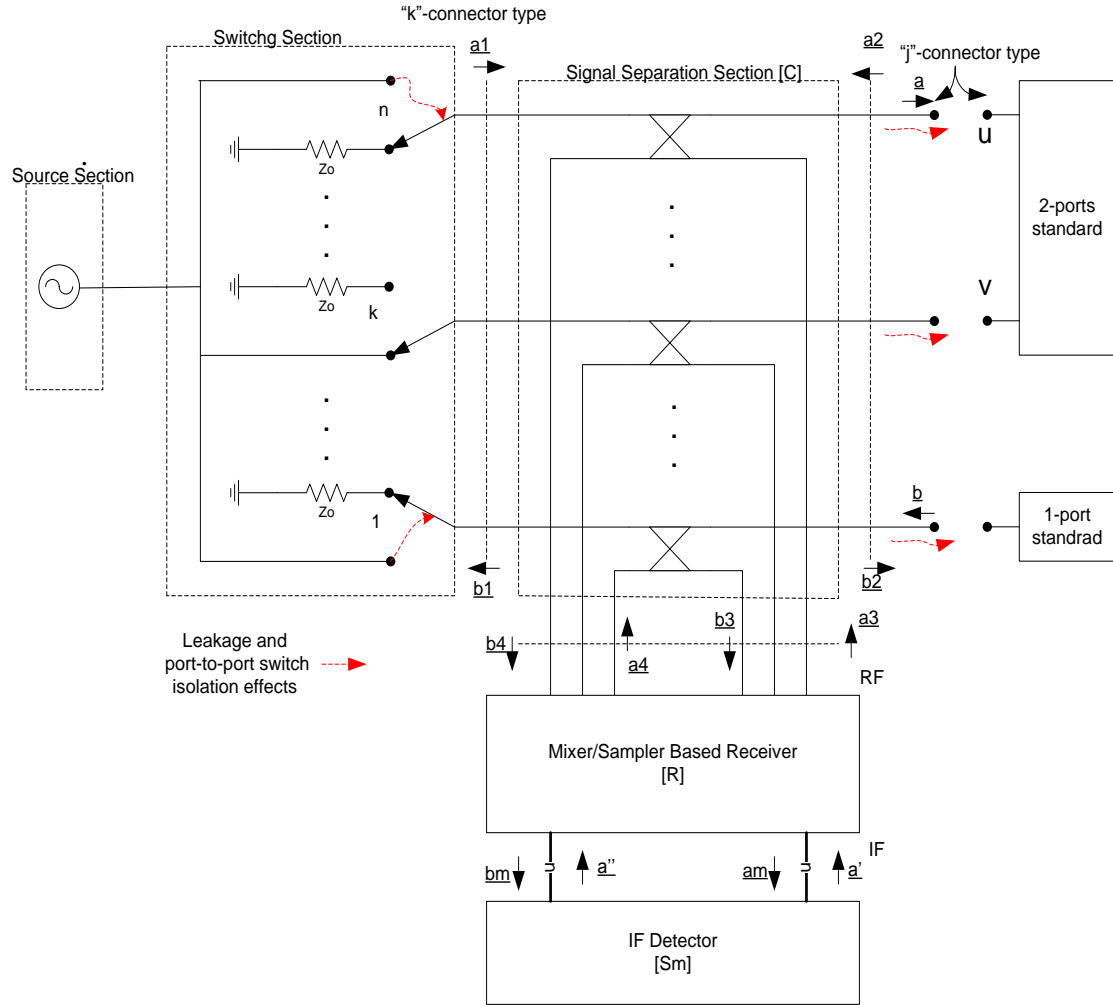


Figure 3.6 s-parameter calibration setup

To find a mathematical expression to relate  $\begin{pmatrix} a_m \\ b_m \end{pmatrix}$  with  $\underline{\underline{H}}, \underline{\underline{K}}, \underline{\underline{L}}, \underline{\underline{M}}$  matrixes' elements equation (3.11) it can be written for each of the n source signal positions, which give n similar equations that can be written in matrix notation as:

$$\begin{bmatrix} \underline{\underline{a}} \\ \underline{\underline{b}} \end{bmatrix}_1 \cdots \begin{bmatrix} \underline{\underline{a}} \\ \underline{\underline{b}} \end{bmatrix}_n = \begin{bmatrix} -\underline{\underline{H}} & \underline{\underline{L}} \\ -\underline{\underline{M}} & \underline{\underline{K}} \end{bmatrix} \begin{bmatrix} \underline{\underline{a}}_m \\ \underline{\underline{b}}_m \end{bmatrix}_1 \cdots \begin{bmatrix} \underline{\underline{a}}_m \\ \underline{\underline{b}}_m \end{bmatrix}_n \quad (3.14)$$



An n-port linear DUT represented by means of its S-parameter matrix  $\underline{\underline{S}}$  establishes:

$$\underline{\underline{b}} = \underline{\underline{S}} \underline{\underline{a}} \quad (3.15)$$

This equation can also be applied for each of the n source position as follow:

$$\left[ (\underline{\underline{b}})_1 \dots (\underline{\underline{b}})_n \right] = \underline{\underline{S}} \left[ (\underline{\underline{a}})_1 \dots (\underline{\underline{a}})_n \right] \quad (3.16)$$

By combining (3.14) with (3.16) one gets [5]:

$$\underline{\underline{S}} \underline{\underline{L}} \underline{\underline{B}}_m - \underline{\underline{S}} \underline{\underline{H}} \underline{\underline{A}}_m - \underline{\underline{K}} \underline{\underline{B}}_m + \underline{\underline{M}} \underline{\underline{A}}_m = \underline{\underline{0}} \quad (3.17)$$

$$\text{Where: } \underline{\underline{A}}_m = \left[ (\underline{\underline{a}}_m)_1 \dots (\underline{\underline{a}}_m)_n \right]; \underline{\underline{B}}_m = \left[ (\underline{\underline{b}}_m)_1 \dots (\underline{\underline{b}}_m)_n \right]$$

This expression allows relating measurement readings with the standards' S-parameter. Each of the  $n^2$  zero elements of the right-hand member in (3.17) can be written similar to (5) in [8] as:

$$\sum_{p=1}^n k_{ip} b_{mpj} + \sum_{p=1}^n s_{ip} \left( \sum_{q=1}^n h_{pq} a_{mpj} \right) - \sum_{p=1}^n s_{ip} \left( \sum_{q=1}^n l_{pq} b_{mpj} \right) - \sum_{p=1}^n m_{ip} a_{mpj} = 0$$

For  $i,=1\dots n \quad j=1\dots n.$  (3.18)

The S-parameter calibration consists of collecting equations similar to (3.18) from an appropriate number of calibration standard measurements. These equations can be stacked together to form an  $4n^2 \times 4n^2$  homogeneous linear system such as:

$$\underline{\underline{C}} \underline{v} = \underline{0} \quad (3.19)$$

Where:

$$\underline{\underline{C}}(a_{mi}, b_{mi}, s_{ij-std})$$

$$\underline{v} = (k_{11} \quad \dots \quad k_{nn} \quad h_{11} \quad \dots \quad h_{nn} \quad l_{11} \quad \dots \quad l_{nn} \quad m_{11} \quad \dots \quad m_{nn})^T$$

As is well known, this homogeneous linear system has got two solutions: the trivial one  $\underline{v} = \underline{0}$  and the nontrivial one  $\underline{v} = \alpha(1 \quad \dots \quad v_{4n^2})^T$ . The latter occurs because one can divide (3.19) among whichever of the  $4n^2$  unknowns, turning it into a non-homogeneous linear system with  $4n^2-1$  unknowns. By selecting arbitrarily  $k_{11}$  as unknown among which dividing (3.19), one gets an equivalent  $(4n^2-1) \times (4n^2-1)$  non-homogeneous linear system as:

$$\underline{\underline{N}} \cdot \underline{u} = \underline{g} \quad (3.20)$$

Where:

$$\underline{\underline{N}}(a_{mi}, b_{mi}, s_{ij-std}) ;$$

$$\underline{u} = (\hat{k}_{12} \quad \dots \quad \hat{k}_{nn} \quad \hat{l}_{11} \quad \dots \quad \hat{l}_{nn} \quad \hat{h}_{11} \quad \dots \quad \hat{h}_{nn} \quad \hat{m}_{11} \quad \dots \quad \hat{m}_{nn})^T$$

$$\underline{g}(b_{mi})$$

$$(\hat{x}_{ij} = \frac{x_{ij}}{k_{11}} \text{ for } x=k,l,m,h \text{ and } i=1..n \text{ } j=1..n)$$

Since, as a mathematical artifice for solving it, one has divided (3.19) among  $k_{11}$ ,  $k_{11}$ 's information has been lost (its modulus and its phase). So, as mentioned earlier, after a S-parameter calibration procedure all the  $(4n^2-1)$ ,  $(2n^2-1)$  or  $(4n-1)$   $\hat{x}_{ij}$ s terms are known depending on whether full-leaky, half-leaky or non-leaky error models are chosen respectively. Introducing them into (3.17) and solving this to find  $\underline{\underline{S}}$  result [6]:

$$\underline{\underline{S}} = (\underline{\underline{K}} \underline{\underline{B}}_m - \underline{\underline{M}} \underline{\underline{A}}_m)(\underline{\underline{L}} \underline{\underline{B}}_m - \underline{\underline{M}} \underline{\underline{A}}_m)^{-1} \quad (3.21)$$

After a S-parameter calibration has been carried out, the fact of not knowing  $k_{11}$  is of no concern to compute the DUT's S-parameter  $s_{ij}$ . Hereby the S-parameter-dependent DUT's performances (like  $G_{op}$ , K-factor,  $G_t$ ,  $G_{tu}$  MSG, MUG, stability circles, etc in linear two-port devices) can be obtained after a complete S-parameter calibration procedure independent of whatever error model was previously chosen .

There are some practical facts related with the passing from (3.17) to (3.20) that are important to point out:

-First, in labs often there is only one unit of the different types of one and two ports calibration standards available (.ie.1-short, 1-load, 1-thru,1-line,etc), this fact constrains things because (3.17) demands knowing all  $s_{ip}$  elements of an hypothetic n-port calibration standard, independently of what error model is chosen.

-For instance, a two port calibration standard (connected between whatever u and v ports among the n available, as shown in figure 3.6) is characterized by a 2x2 S-parameter matrix such as:

$$\underline{\underline{S}} = \begin{bmatrix} S_{uu} & S_{uv} \\ S_{vu} & S_{vv} \end{bmatrix} \quad (3.22)$$

It's evident from (3.17) that when n is greater than 2 one hasn't the others  $s_{ij}$  calibration standard's elements, therefore it doesn't make sense to sweeping the source switch among its n positions. Furthermore, if and only if a non leaky error model is chosen the readings  $a_{mij}$   $b_{mij}$  for all those ports where the two port calibration standard is not connected must be near to zero (red-dotted-arrow in figure 3.6). In this way, by substituting (3.22) in (3.17) will yield four equations similar to (3.18) instead of the 4n-1 required. Each of these equations will have only sixteen addends (or error terms at a time). Something similar occurs with one port standards. For this reason by interchanging the one

and two port calibration standards available in the lab allows the building of a system similar to (3.20).

- On the other hand, when a full or half leaky error model is chosen it's mandatory to rely on  $n$  ports calibration standards (i.e.  $n$ -opens,  $n$ -loads, etc or proper combinations of them) in the lab in order to carry out a complete S-parameter calibration procedure and to sweep the source switch among its  $n$  positions for each  $n$ -port calibration standard connected. This is easily proven because an  $n$ -ports calibration standard measurement gives us just (with  $n^2$  S-parameters)  $n^2$  equations similar to (3.18) which are lesser than the unknowns number of the full-leaky or half-leaky error models, it means,  $n^2 < 4n^2$  or  $n^2 < 2n^2 \quad \forall n$  respectively. Furthermore, since in (3.20) just  $(4n^2-1)$  or  $(2n^2-1)$  linearly independent equations are needed to solve it, the minimum number, say "k", of  $n$ -port calibration standard measurements (or  $n$ -port calibration standards) required in both cases can be found by imposing that:

$$kn^2 \geq 4n^2 - 1 \xrightarrow{\text{yields}} k_{min} = 5 \quad \forall n \quad \text{for full leaky error model.}$$

$$kn^2 \geq 2n^2 - 1 \xrightarrow{\text{yields}} k_{min} = 3 \quad \forall n \quad \text{for half leaky error model.}$$

Unfortunately this  $k_{min}$ 's value transforms (3.20) into a  $(k_{min}n^2 \times 4n^2 - 1)$  or  $(k_{min}n^2 \times 2n^2 - 1)$  over determined system of linear equations respectively, whose solution requires using techniques such as: least square, QR decomposition, etc.

- Depending on the error model chosen one can get in literature the most powerful, efficient, and optimized calibration algorithms in order to solve (3.20). For instance, chosen Leaky Error Model, in [8] a simple calibration algorithm using commercial one and two port calibration standards on multiport systems was proposed and carried out on a 3 port system, in [12] an calibration algorithm was proposed and carried out on 4 port (differential devices) system, by using four-, two- and one -port calibration standards. In

[10] and [11] calibration algorithms were proposed so as to solve (3.20) when applying a Half Leaky Error Model on multiport systems and was carried out on a four-port system, working in coaxial and on-wafer measurement environments respectively. When working with a Non-Leaky Error Model in [13] a powerful and general formulation was proposed, which allows to solve (3.20) in the multiport VNA systems, by using just one- and two-port commercial calibration standards and it was carried out on a 3 port VNA system.

In this thesis work all the experimental results presented in chapter VI required the S-parameter calibrations which were obtained by using Microwave Measurement Software-NT (MMS-NT) [14]: a 32-Bit Visual C++ written windows application. MMS-NT by using (specified by the user): 1)the system port and their connector organization; 2)a proper set of calibration standards (with the electrical model) and their connector type which allows the possibility to plug or to not plug the standard to a specific port 3) calibration algorithm to be used between ports (RSOL,SOL,THRU,Q-SOLT, LRM, TRL, Reciprocal, etc); the MMS-NT : 1) generates the optimum sequence of connections, 2)asks the user to perform and acquire the measurements in correspondence of every standard involved in the calibration, 3)performs vector  $\underline{u}$ 's computation (see equation 3.20) and 4) de-embeds the measurement data through (3.21).(see appendix A). MMS-NT software relies on a set of methods and data structure that are able to compute and manage the error coefficients of multiport measurement systems in dynamic way , it means, there is no fixed standard sequence, owing to the software generates the best one which resolves the connector constrains. Figure 3.7 shows the S-parameter calibration flowchart.

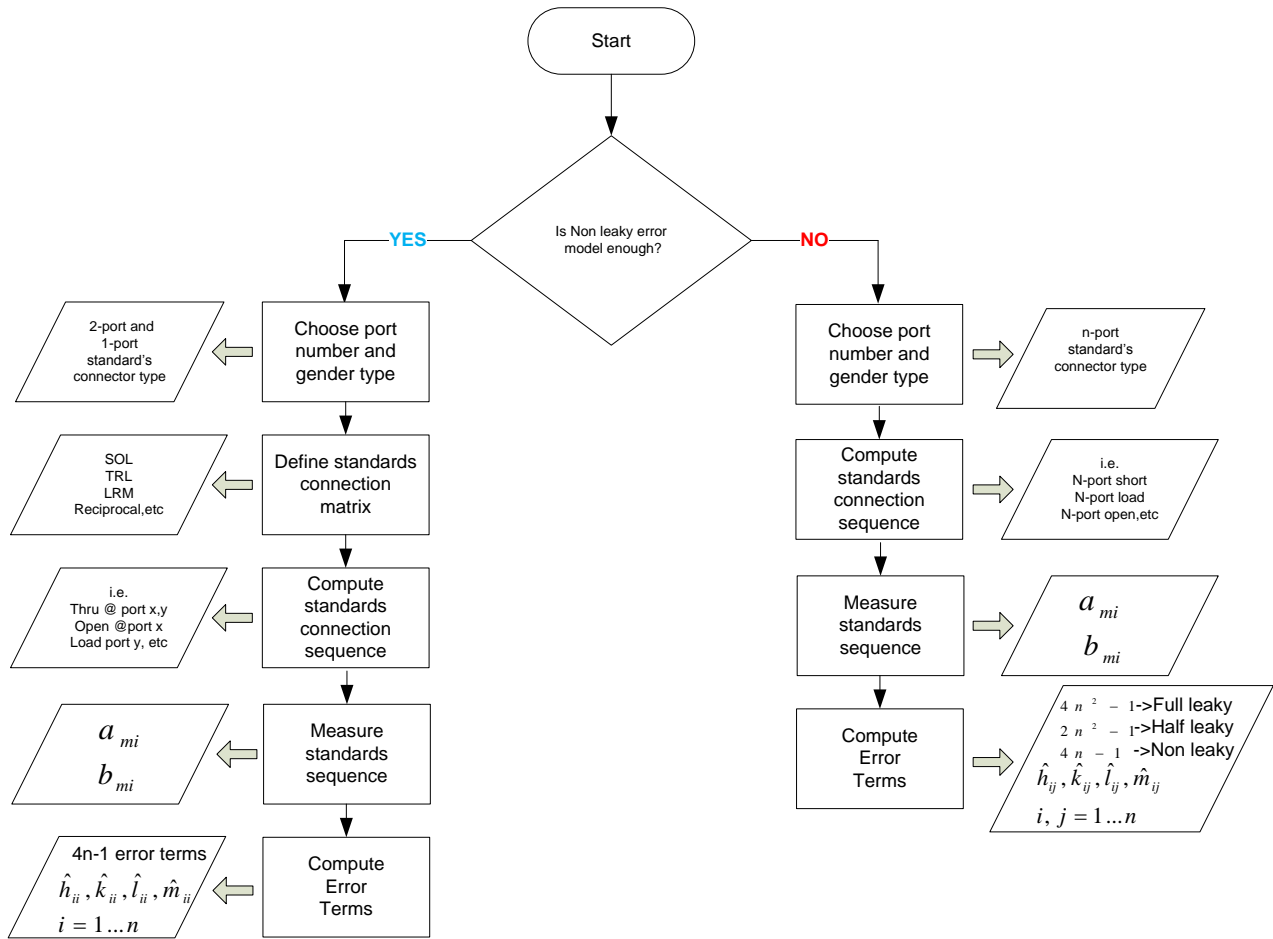


Figure 3.7 S-parameter calibration flowchart

---

**References**

- [1] Golio Mike “ *The RF and Microwave Handbook*” CRC Press LLC US Florida 2001.
- [2] Service Guide Agilent Technologies 8719D/20D/22D Network Analyzers Manufacturing Part Number: 08720-90292 Printed in USA Print Date: February 1999 Supersedes: June 1998.477pages.
- [3]Agilent AN 1287-3 Applying Error Correction to Network Analyzer Measurements
- [4] Agilent PNA Series Network Analyzer Printed Version of PNA Help User’s and Programming Guide Supports Firmware A.08.00 March 12, 2008.
- [5]Agilent Understanding and Improving Network Analyzer Dynamic Range AN-1363-1 09/2000.
- [6] IEEE Transactions on Microwave Theory and Techniques Vol,56,Nº 3 March 2008. “ A Novel Calibration Algorithm for Special Class of Multiport Vector Network Analyzer”. Andrea Ferrero, Senior Member, IEEE, Valeria Teppati Member IEEE, Marco Garelli, Student Member, IEEE and Alessandra Neri.
- [7] A. Ferrero “VNA Measurement and Calibration Intel Class” 17-18 January 2006. Electronic Department, Polytechnic of Turin. Pages 14-16.
- [8] A. Ferrero and F. Sanpietro, “A simplified algorithm for leaky network analyzer calibration,” IEEE Microwave Guided Wave Lett., vol. 5, pp. 119–121, Apr. 1995.
- [9] Speciale, R. A., “Super-TSD. A Generalization of the TSD Network Analyzer Calibration Procedure, Covering n-Port Measurements with Leakage,” 1977 IEEE MTT-S International Microwave Symposium, Digest of Technical Papers, San Diego, California, June 21 23, 1977, IEEE Cat. No. 77CH1219-5 MTT, pp. 114-117.
- [10] V. Teppati, A. Ferrero, D. Parena, and U. Pisani, “A simple calibration algorithm for partially leaky model multiport vector network analyzers,” in 65th ARFTG Dig., Jun. 2005, pp. 1–4.
- [11] Ieee Transactions On Microwave Theory And Techniques, Vol. 53, No. 11, November 2005 3665 On-Wafer Calibration Algorithm for Partially Leaky Multiport Vector Network Analyzers Valeria Teppati, Member, IEEE, and Andrea Ferrero, Member, IEEE.

[12] D. E. Bockelman, “The theory, measurement, and application of mode specific scattering parameters with multiple modes of propagation,” Ph.D. dissertation, Dept. Elect. Comput. Eng., Univ. Florida, 1997.

[13] A. Ferrero, F. Sanpietro, and U. Pisani, “Multiport vector network analyzer calibration: A general formulation,” *IEEE Trans. Microw. Theory Tech.*, vol. 42, no. 12, pp. 2455–2461, Dec. 1994.

[14] Ing. Chiara Soragna-PAF, Prof. Andrea Ferrero-Polytechnic of Torino “MMS LINE Multiport S-parameter System” <http://www.pafmicro.com/products.htm>:



# **CHAPTER IV**

## **POWER AND PHASE CALIBRATION**

## 4.1) POWER CALIBRATION

Power Calibration procedure springs from microwave engineers' necessity to measure power –dependent multiport DUT's performances such as [1-3]:

$P_{in}$ : Input Power towards a given i-th port @ $kf_0 = |a|^2 - |b|^2$

$P_{out}$ : Output Power from a given i-th port @ $kf_0 = |b|^2 - |a|^2$

$P_{Din}$ : Differential-Mode Input Power towards a given i-th differential-mode port @ $kf_0 = |a_D|^2 - |b_D|^2$

$P_{Cin}$ : Common-Mode Input Power towards a given i-th common-mode port @ $kf_0 = |a_C|^2 - |b_C|^2$

$P_{Dout}$ : Differential-Mode Output Power from a given i-th differential-mode port @ $kf_0 = |b_D|^2 - |a_D|^2$

$P_{Cout}$ : Common –Mode Output Power from a given i-th common-mode port @ $kf_0 = |b_C|^2 - |a_C|^2$

Where “@ $kf_0$ ” stands for the respective power ( $P_x$ ) measured only at the k-th harmonic of a fundamental frequency labeled as  $f_0$ .

These quantities define in general a lot of DUT's design specifications, which depend on the DUT's application field, most of them can be computed simply by using s-parameter measurements only if linear DUTs are considered [4], unfortunately, often for microwave design engineers, this is not common, on the other hand, they have to optimize power-dependent design specifications in nonlinear DUTs like power amplifiers, oscillators, frequency doublers, mixer, etc[5]. Some of these specifications are: operative and transducer gains ( $G_{op}$  and  $G_t$ ), Power Added Efficiency (PAE), output power at  $G_t$ 's 3dB compression point ( $P_{out|3dB}$ ), Harmonic Intermodulation Products, Intermodulation

Distortion, Conversion Gain (CG), Spectral Purity (SP), and so on ,depending on the DUT type [6].

The S-parameter calibration's output information: ( $\hat{x}_{ij} = \frac{x_{ij}}{k_{11}}$  for x=k,l,m,h and i=1..n j=1...n) (see 3.20) not being enough to compute the above power-dependent design specifications (when working with non linear DUTs), a power calibration will be performed based on [7-9]. To carry it out, one can begin rewriting (3.11) as:

$$\begin{pmatrix} \underline{a} \\ \underline{b} \end{pmatrix} = k_{11} \begin{bmatrix} -\underline{\hat{H}} & \underline{\hat{L}} \\ -\underline{\hat{M}} & \underline{\hat{K}} \end{bmatrix} \begin{pmatrix} \underline{a}_m \\ \underline{b}_m \end{pmatrix} \quad (4)$$

Where:

$$\underline{a} = \begin{pmatrix} a_1 \\ a_2 \\ \vdots \\ a_n \end{pmatrix}; \underline{a}_m = \begin{pmatrix} a_{m1} \\ a_{m2} \\ \vdots \\ a_{mn} \end{pmatrix}; \underline{b} = \begin{pmatrix} b_1 \\ b_2 \\ \vdots \\ b_n \end{pmatrix}; \underline{b}_m = \begin{pmatrix} b_{m1} \\ b_{m2} \\ \vdots \\ b_{mn} \end{pmatrix}$$

$$(\hat{x}_{ij} = \frac{x_{ij}}{k_{11}} \text{ for } x=k,l,m,h \text{ and } i=1..n \text{ } j=1...n)$$

As is well known, after an s-parameter calibration procedure all the  $(4n^2-1)$ ,  $(2n^2-1)$  or  $(4n-1)$   $\hat{x}_{ij}$  terms are known depending upon if a full-leaky, half-leaky or non-leaky error model is chosen respectively. Each incident ( $a_i$ ) and reflected ( $b_i$ ) wave from (4) at the DUT's ports can be written as:

$$a_i = k_{11} (\sum_{j=1}^n -\hat{h}_{ij} a_{mj} + \sum_{j=1}^n \hat{l}_{ij} b_{mj}) = k_{11} \hat{a}_i \quad (4.1)$$

$$b_i = k_{11} (\sum_{j=1}^n -\hat{m}_{ij} a_{mj} + \sum_{j=1}^n \hat{k}_{ij} b_{mj}) = k_{11} \hat{b}_i \quad (4.2)$$

$\hat{a}_i$  and  $\hat{b}_i$  are computed with the s-parameter calibration's information and the VNA's readings. Obviously these expressions become simpler depending on the error model chosen during the s-parameter calibration.

By using (4.1) and (4.2) one can find easily the input and output power at given DUT's port as:

$$P_{in-i} = |k_{11}|^2 (|\hat{a}_i|^2 - |\hat{b}_i|^2) \quad (4.3)$$

$$P_{out-i} = |k_{11}|^2 (|\hat{b}_i|^2 - |\hat{a}_i|^2) \quad (4.4)$$

The power calibration's task is to find  $|k_{11}|$  which is enough to compute the outgoing and incoming normalized power waves to/from the DUT's ports. The setup required during a power calibration procedure demands that one performs the next steps:

- choose whatever "k" port from the n available to connect the signal separation section with the DUT's port as shown in figure (4.1), in order to be able to connect a power sensor.

- inject a CW power signal (at given frequency of interest) into the other side of the signal separation's coupler.

In this way by using (4.3) since  $P_{in-i}$  can be measured with the power meter,  $|k_{11}|$  can be found as:

$$|k_{11}| = \sqrt{\frac{P_{in-i}}{(|\hat{a}_i|^2 - |\hat{b}_i|^2)}} = \sqrt{\frac{P_{meas}}{(|\hat{a}_i|^2 - |\hat{b}_i|^2)}} \quad (4.5)$$

$|k_{11}|$ 's computation has to be done for all frequencies of interest where one intends measure power-dependent DUT's performances.

Unfortunately sometimes it isn't possible to directly connect the power sensor such as in figure 4.1 to the DUT's measurement environment, for instance, in on-wafer DUT's environments. In this case it is needed the use of that proposed in [10]. It means, using (3.3) from section 3.2 applied to whatever port (from the (n-1) available called auxiliary port) on the other side of the signal separation section's couplers, where surely it's possible to connect a power meter as shown in figure 4.2. This will allow us by applying the reciprocity principle to the signal separation section's coupler (with cables and connectors involved) to compute  $|k_{11}|$ .

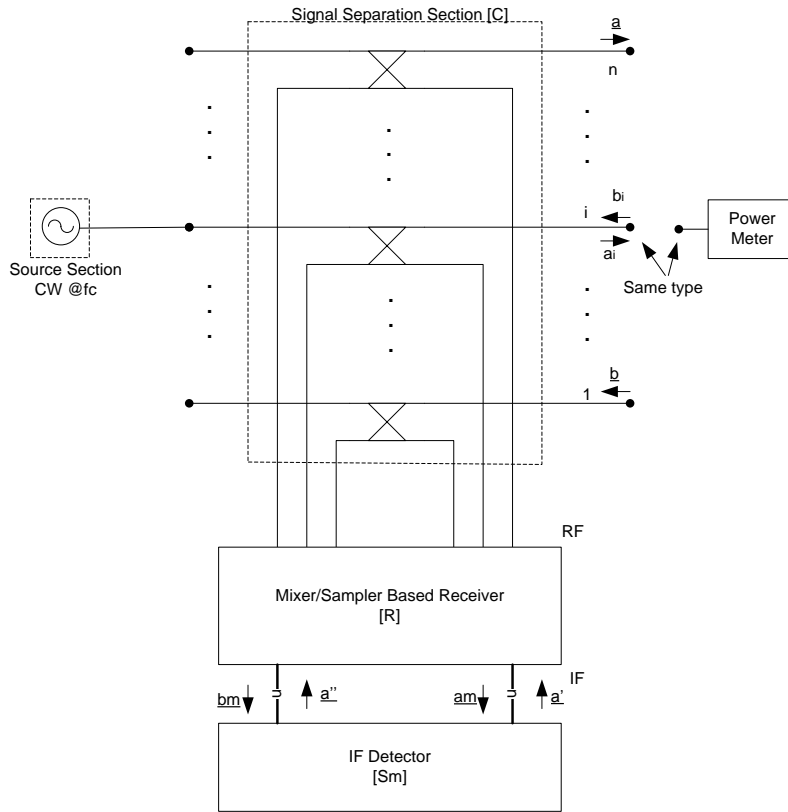


Figure 4.1 Power calibrations setup when measurement's environment problems aren't present.

Furthermore, to simplify things it will be assumed a non leaky error model characterizes  $\underline{\underline{H}}$ ,  $\underline{\underline{K}}$ ,  $\underline{\underline{L}}$ ,  $\underline{\underline{M}}$  (see equation 3.4) and  $\underline{\underline{D}}_1$  (see equation 3.3) matrixes. Obviously

this is a compromise to simplify  $|k_{11}|$ 's computation. So from (3.13) it's evident that (3.3) can be rewritten for whichever initially chosen  $i$ -th auxiliary port, as follows:

$$\begin{pmatrix} a_{i-aux} \\ b_{i-aux} \end{pmatrix} = \begin{bmatrix} -h_{ii-aux} & l_{ii-aux} \\ -m_{ii-aux} & k_{ii-aux} \end{bmatrix} \begin{pmatrix} a_{mi} \\ b_{mi} \end{pmatrix} \quad (4.6)$$

Which after an S-O-L calibration procedure applied to the  $i$ -th auxiliary port chosen it can be written as:

$$\begin{pmatrix} a_{i-aux} \\ b_{i-aux} \end{pmatrix} = k_{ii-aux} \begin{bmatrix} -\hat{h}_{ii-aux} & \hat{l}_{ii-aux} \\ -\hat{m}_{ii-aux} & 1 \end{bmatrix} \begin{pmatrix} a_{mi} \\ b_{mi} \end{pmatrix} \quad (4.7)$$

Where similar to (4), in this case three error terms:  $-\hat{h}_{ii-aux}$ ,  $\hat{l}_{ii-aux}$   $-\hat{m}_{ii-aux}$  are completely known.

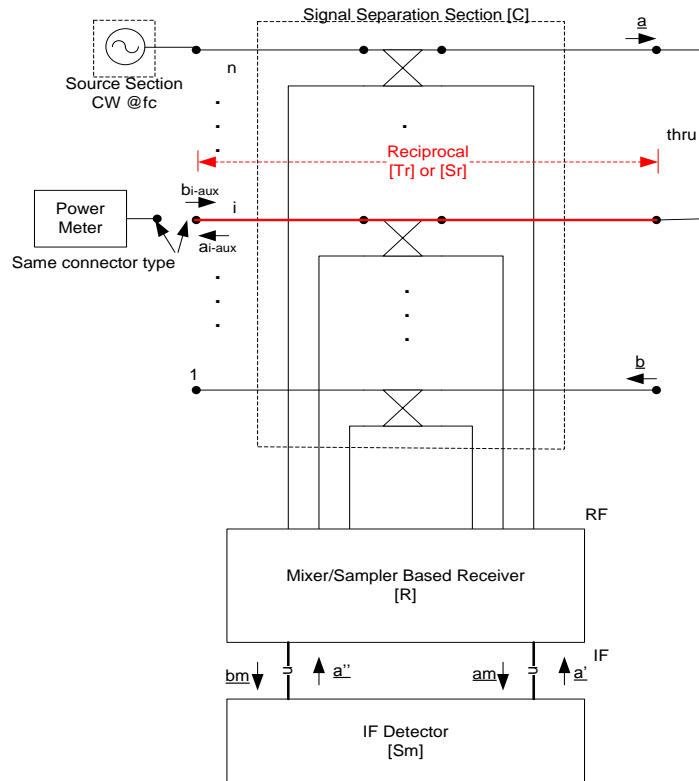


Figure 4.2 Power Calibration when measurement environment problem are present

In similar way as before, the incident ( $b_{i-aux}$ ) and reflected ( $a_{i-aux}$ ) waves at the  $i$ -th auxiliary port's reference plane chosen are:

$$a_{i-aux} = k_{ii-aux} (-\hat{h}_{ii-aux} a_{mi} + \hat{l}_{ii-aux} b_{mi}) = k_{ii-aux} \hat{a}_{i-aux} \quad (4.8)$$

$$b_{i-aux} = k_{ii-aux} (-\hat{m}_{i-aux} a_{mi} + b_{mi}) = k_{ii-aux} \hat{b}_{i-aux} \quad (4.9)$$

Where  $\hat{a}_{i-aux}$  and  $\hat{b}_{i-aux}$  are computed by means of the previous S-O-L calibration applied to the  $i$ -th auxiliary port chosen and the VNA's readings.

By combining (4.8) and (4.9) one can find easily the output power at the  $i$ -th auxiliary port chosen as (see figure 4.2):

$$P_{out-i-aux} = |k_{ii-aux}|^2 (|\hat{a}_{i-aux}|^2 - |\hat{b}_{i-aux}|^2) \quad (4.10)$$

In order to get  $|k_{ii-aux}|$  which will allow us to compute that that is really needed ( $|k_{11}|$ ), the next steps must be carried out in the setup of figure 4.2:

-choose whatever two ports from the  $n$  available to connect the signal separation section with the DUT's port as shown in figure (4.2), and connect them by using a thru or a transmission line.

- Use the two adjacent sides of the signal separation section's couplers : one to inject a CW signal (at a given frequency of interest) and the other one to connect the power sensor (see figure 4.2). This is in order to set a power level that can be measured by the power meter.

In this way by using (4.10) since  $P_{out-i-aux}$  can be measured with the power meter,  $|k_{ii-aux}|$  can be found as:

$$|k_{ii-aux}| = \sqrt{\frac{P_{out-i-aux}}{(|\hat{a}_{i-aux}|^2 - |\hat{b}_{i-aux}|^2)}} = \sqrt{\frac{P_{meas}}{(|\hat{a}_{i-aux}|^2 - |\hat{b}_{i-aux}|^2)}} \quad (4.11)$$

$|k_{ii-aux}|$ 's computation has to be done for all frequencies of interest where one intends to measure power-dependent DUT's performances. Next, in order to compute  $|k_{11}|$  through  $|k_{ii-aux}|$  the reciprocity principle is applied to the cables, through arm's couplers, and connectors (placed between the  $i$ -th auxiliary port chosen to connect the power sensor and the  $i$ -th port used to connect the signal separation section with the  $i$ -th DUT's port), which can be characterized by means of a transmission matrix  $\underline{T}_r$  (see red line in figure 4.2) defined as follow [11]:

$$\begin{pmatrix} b_i \\ a_i \end{pmatrix} = \underline{T}_r \begin{pmatrix} b_{i-aux} \\ a_{i-aux} \end{pmatrix} \quad (4.12)$$

On the other hand, with the assumption of a non leaky error model and after a proper  $s$ -parameter calibration, (4) can be written for whichever  $i$ -th DUT's port as:

$$\begin{pmatrix} a_i \\ b_i \end{pmatrix} = k_{11} \begin{bmatrix} -\hat{h}_{ii} & \hat{l}_{ii} \\ -\hat{m}_{ii} & \hat{k}_{ii} \end{bmatrix} \begin{pmatrix} a_{mi} \\ b_{mi} \end{pmatrix} \quad (4.13)$$

In this way by combining (4.7) with (4.13)  $\underline{T}_r$  can be found as function of  $|k_{11}|$  as:

$$\underline{T}_r = \left( \frac{k_{11}}{k_{ii-aux}} \right) \underline{\hat{T}}_r \quad (4.14)$$

Where:

$$\underline{\hat{T}}_r = \left( \frac{1}{\hat{m}_{ii-aux} \hat{l}_{ii-aux} - \hat{h}_{ii-aux}} \right) \begin{bmatrix} \hat{k}_{ii} \hat{m}_{ii-aux} - \hat{m}_{ii} & \hat{m}_{ii} \hat{l}_{ii-aux} - \hat{k}_{ii} \hat{h}_{ii-aux} \\ \hat{l}_{ii} \hat{m}_{ii-aux} - \hat{h}_{ii} & \hat{h}_{ii} \hat{l}_{ii-aux} - \hat{l}_{ii} \hat{h}_{ii-aux} \end{bmatrix}$$



Since the reciprocal condition establishes  $\text{Det}\{\underline{T}_r\} = 1$ ,  $|k_{11}|$  can be found from (4.14) as:

$$|k_{11}| = \left| \frac{k_{ii-aux}}{\sqrt{\text{Det}\{\underline{T}_r\}}} \right| \quad (4.15)$$

$|k_{11}|$ 's computation has to be done for all frequencies of interest where one intends to measure power-dependent DUT's performances.

This general approach to compute  $|k_{11}|$  can be applied to whatever number of setup's ports (n), whether there is or isn't mechanical constrains to connect the power sensor with the DUT's measurement environment. For instance, when characterizing Differential Devices (4 ports) or single end Devices (2 ports) in on-wafer or mm-coaxial environments. Figure 4.3 shows the power calibration's flowchart.

In this thesis work all the experimental result presented in chapter VI required the power calibration procedure which was performed by using the Microwave Measurement Software (MM-NT) [12]: a powerful 32-Bit Visual C++ written windows application which based on (specified by the user): 1)source's power port's number 2)auxiliary port's number and its connector type (if needed) or simply the port's number where connect the power sensor. The MMS-NT Cal software : 1) establishes the sequence of connections to perform the S-O-L calibration when auxiliary port is required,1.1)asks the user to perform and acquire the measurements in correspondence to every standard involved in the S-O-L calibration,1.2) computes  $-\hat{h}_{ii-aux}$ ,  $\hat{l}_{ii-aux}$   $-\hat{m}_{ii-aux}$  (see equation 4.7) 1.3) and asks the user to perform and acquire the power measurements in correspondence to the power meter's connection to the auxiliary port chosen previously (see figure 4.2).If auxiliary port is not required MMS-NT 2) asks the user to perform and acquire the power's measurements in correspondence to the power meter's connection to whatever port among the n-1s

available as shown in figure 4.1. Obviously to carrying out the power's measurement MMS (via PC) synchronizes itself with the power meter (see appendix A).

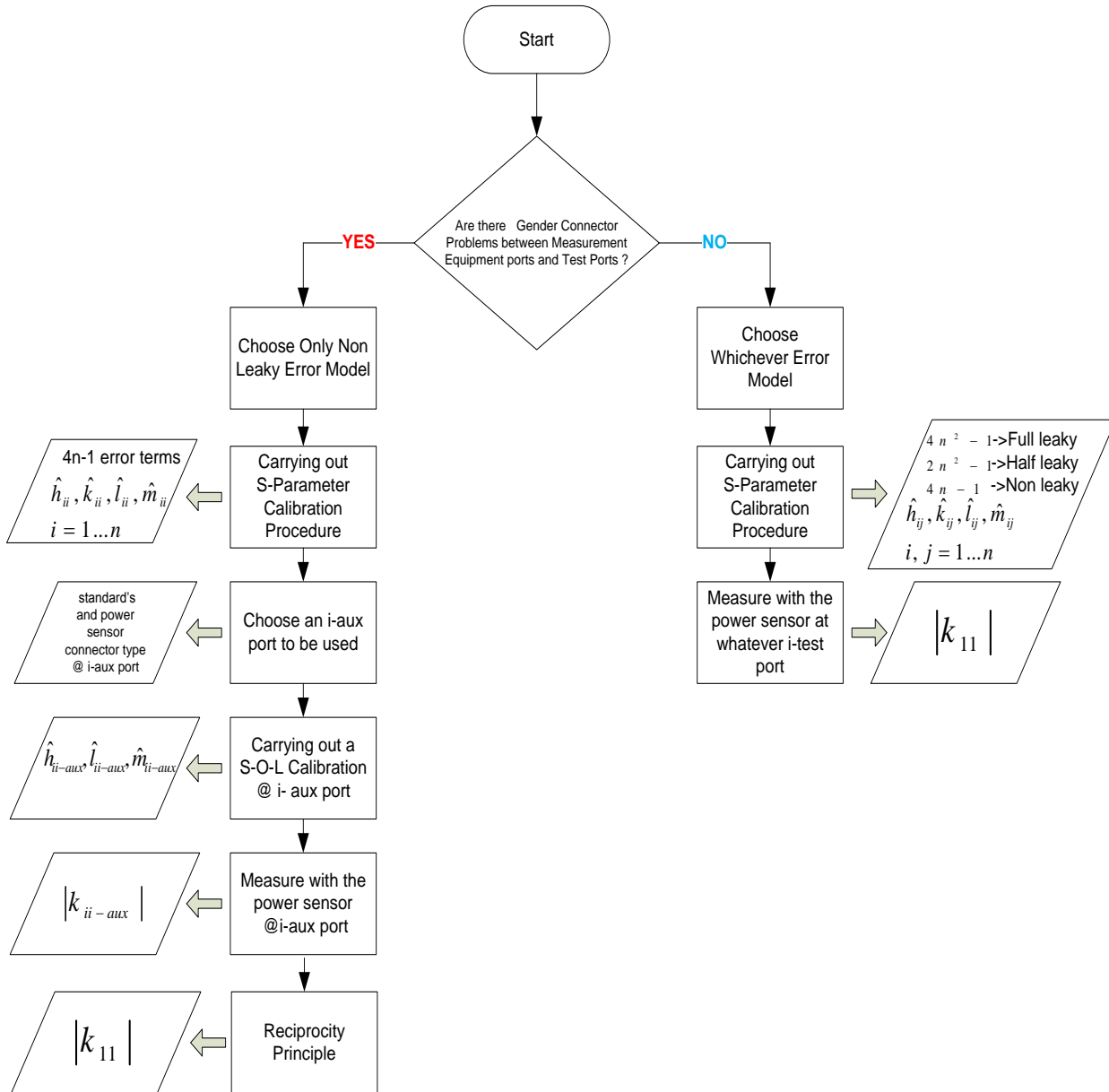


Figure 4.3 Power Calibration flow diagram

## 4.2) PHASE CALIBRATION

As power calibration springs from microwave engineers' necessity to measure power dependent DUT's performances, and as time-domain information is most useful for microwave designers to visualize circuit operation, phase calibration springs to measure time domain waveforms. However, in this case a wider application fields is favored such as:

-Time Domain oscilloscope measurements with vector correction applied, it means, time domain voltages and currents with measurement plane at DUT's terminals.

-Measurement of the absolute amplitude and phase relationship of each frequency components (harmonics) to/from a DUT with vector correction applied with reference plane at DUT's terminals, useful to analyze and design high efficiency power amplifiers such as class E – F, and frequency multipliers.

-Measurement of components intended for tens-Gb/s systems, whose performance specifications typically are made in time-domain terms such as edge rise time, allowable error band ,etc. These time-domain dependent design specifications can be strongly affected at high frequencies. For instance, the eye diagram of a tens-Gb/s signal can be closed significantly by a few inches of cable and a few transitions [13].

-Measurement of multi-tone stimulus/response to/from DUT's measurement planes with vector correction applied and measurement of the amplitude and phase of intermodulation products.

-View and analyze dynamic memory signatures in non linear devices with vector correction applied [14].

-Measure modeling coefficients and others nonlinear device parameters such as: dynamic load line (I(t)-V(t) curves),  $a_i(t)$  and  $b_i(t)$  time domain waveforms, X-parameters[14],etc.

In order to make all these time domain capabilities possible on a multiport VNA system a proper phase calibration must be done. After a S-parameter and power calibrations procedure one has got: ( $\hat{x}_{ij} = \frac{x_{ij}}{k_{11}}$  for  $x=k,l,m,h$  and  $i=1..n$   $j=1..n$ ) (see 3.20) and  $|k_{11}|$  (see 4.5 and 4.15) respectively as output information. This information allows one to rewrite (3.11) as:

$$\begin{pmatrix} \underline{a} \\ \underline{b} \end{pmatrix} = (|k_{11}| \angle k_{11}) \begin{bmatrix} -\underline{\hat{H}} \\ \underline{\hat{L}} \\ -\underline{\hat{M}} \\ \underline{\hat{K}} \end{bmatrix} \begin{pmatrix} \underline{a}_m \\ \underline{b}_m \end{pmatrix} \quad (4.16)$$

Where:

$$\underline{a} = \begin{pmatrix} a_1 \\ a_2 \\ \vdots \\ a_n \end{pmatrix}; \underline{a}_m = \begin{pmatrix} a_{m1} \\ a_{m2} \\ \vdots \\ a_{mn} \end{pmatrix}; \underline{b} = \begin{pmatrix} b_1 \\ b_2 \\ \vdots \\ b_n \end{pmatrix}; \underline{b}_m = \begin{pmatrix} b_{m1} \\ b_{m2} \\ \vdots \\ b_{mn} \end{pmatrix}$$

$$(\hat{x}_{ij} = \frac{x_{ij}}{k_{11}} \text{ for } x=k,l,m,h \text{ and } i=1..n \text{ } j=1..n)$$

$\angle k_{11}$ : stands for the phase of  $k_{11}$

As it is well known, after a S-parameter calibration procedure depending on whether a full-leaky, half-leaky or non-leaky error model is chosen one gets respectively:  $(4n^2-1)$ ,  $(2n^2-1)$  or  $(4n-1)$   $\hat{x}_{ij}$ s error terms. At the DUT's ports each incident ( $a_i$ ) and reflected ( $b_i$ ) power wave can be written in the frequency domain from (4.16) as:

$$a_i = (|k_{11}| \angle k_{11}) (\sum_{j=1}^n -\hat{h}_{ij} a_{mj} + \sum_{j=1}^n \hat{l}_{ij} b_{mj}) = (|k_{11}| \angle k_{11}) \hat{a}_i \quad (4.17)$$

$$b_i = (|k_{11}| \angle k_{11}) (\sum_{j=1}^n -\hat{m}_{ij} a_{mj} + \sum_{j=1}^n \hat{k}_{ij} b_{mj}) = (|k_{11}| \angle k_{11}) \hat{b}_i \quad (4.18)$$

Where:

$a_i = a_i(f)$ : stands for the incident power wave to the  $i$ -th DUT port in the frequency domain labeled as "f".

$b_i = b_i(f)$ : stands for the reflected power wave from the  $i$ -th DUT port in the frequency domain labeled as “F”.

Where  $\hat{a}_i$ ,  $\hat{b}_i$  and  $|k_{11}|$  are computed with S-parameter and power calibration’s information and VNA’s readings. Obviously depending on the error model chosen during the S-parameter calibration (4.17) and (4.18) become simpler.

Looking at (4.17) and (4.18), it’s easy to understand that by now, if one wants to know  $a_i$  and  $b_i$  in the frequency domain one is required to know  $\angle k_{11}$  at each frequency of interest, fortunately the phase calibration has this purpose. In a similar way to power calibration, to carry it out one must consider two conditions: 1) when there are and 2) when there aren’t measurement environment problems. It means, when measurement equipment connectors can’t be physically connected to test ports (i.e. : probe tips in on-wafer environments, special coaxial connector class, etc). This is an important fact, since the approach to be used in order to perform the phase calibration procedure (proposed for the first time in [15][16]) uses sampler-based time domain receiver [17] such as: Microwave Transition Analyzer (MTA) or Sampling Oscilloscope (SO) to carry out phase measurements, whose input port’s coaxial connector demands specific test port’s connector type.

In the first case when mechanical connection problems are not present things are very simple: One can get  $\angle k_{11}$  from time domain receiver readings, however, some considerations must be given to what one measures using a time domain receiver (MTA/SO). A time domain receiver doesn’t separate the incident ( $V_i^+(z, f)$ ) and reflected ( $V_i^-(z, f)$ ) voltage waves at its reference plane ( $z_r$ ) and measure them in separated way such as a VNA; instead of this, it measures the total voltage wave at its reference plane ( $z_r$ ) defined as follow [11]:

$$V_{r-i}(z_r, f) = V_i^+(z_r, f) + V_i^-(z_r, f) = \sqrt{Z_0}(a_r + b_r) \quad (4.19)$$

Where:

$V_{r-i}(z_r, f)$ : stands for the total voltage wave at the time domain receiver's reference plane in the frequency domain labeled as "f".

$z_r$ : stands for the reference plane of the time domain receiver (MTA/SO).

$a_r$ : stands for the incident power wave to the time domain receiver's reference plane in the frequency domain labeled as "f".

$b_r$ : stands for the reflected power wave to the time domain receiver's reference plane in the frequency domain labeled as "f".

$Z_0$ : the complex characteristic impedance of the transmission line at the time domain receiver's reference plane (often  $50\Omega$ ).

On the other hand, it's evident from (4.17-4.19) that  $\angle V_{r-i}(z_r, f)$  must be known at all frequencies of interest where S-parameter calibration was done in order to find  $\angle k_{11}$ . To accomplish it one performs next steps:

- choose whichever "i-th" test port from the n available (used to connect the signal separation section with the DUT's port) to mechanically connect this port to the time domain receiver (MTA/SO) as shown in figure (4.4).

- connect an HPR (as those described in chapter I) which provides a rich in harmonics signal with all harmonics of interest where one intends to characterize the DUT ( $f_0, 2f_0, \text{etc}$ ), into the other side of the signal separation's coupler (chosen previously).

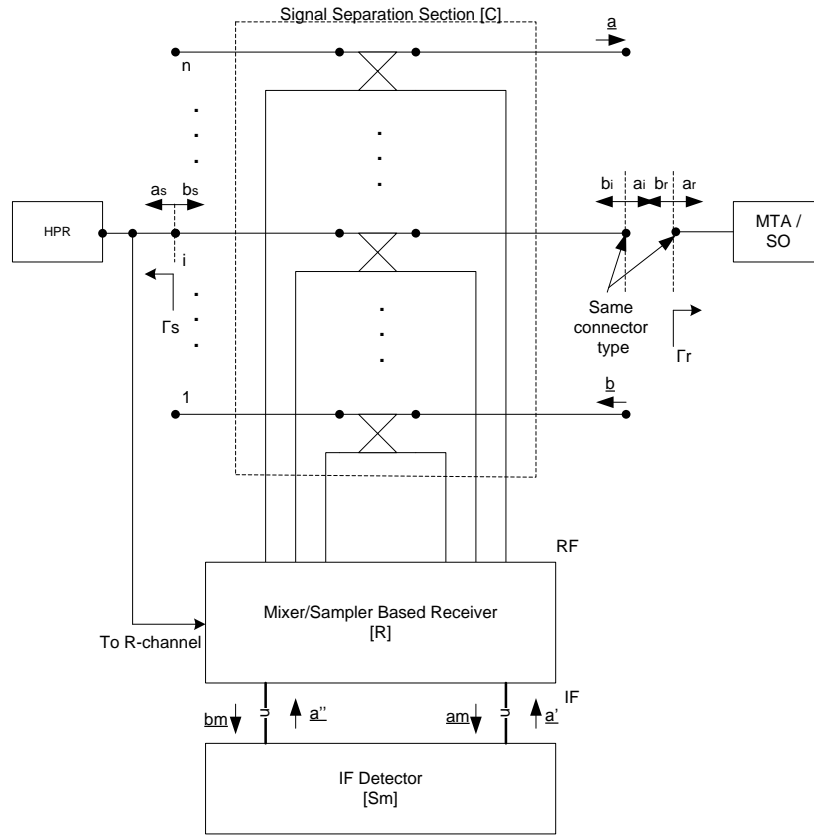


Figure 4.4 Phase calibration setup when gender connector problem aren't present

In this way, because  $\angle V_{r-i}(z_r, f)$  can be obtained from the time domain receiver's (MTA/SO) readings (see (4.19)), and VNA readings allow one to get  $\hat{a}_i, \hat{b}_i$  in the frequency domain (see (4.17) and (4.18)), by combining both readings at the time domain receiver's reference plane ( $z_r$ ), when the time domain receiver is connected to the  $i$ -th test port chosen previously (see figure 4.4) one gets:

$$V_{r-i}(z_r, f) = \sqrt{Z_0}(a_r + b_r) = \sqrt{Z_0}k_{11}(\hat{a}_i + \hat{b}_i) \quad (4.20)$$

From which one finds easily  $\angle k_{11}$  as:

$$\angle k_{11} = \angle V_{r-i}(z_r, f) - \angle(\hat{a}_i + \hat{b}_i) \quad (4.21)$$

From (4.21) it's very important to note that:

- since  $\hat{b}_i$  and  $\hat{a}_i$  depend on both  $a_{mj}$  and  $b_{mj}$  (for  $j=1\dots n$ ) VNA's readings, the latter's phase information must be as accurately known ( $\angle a_{mj}, \angle b_{mj}$ ) as possible. As pointed out in chapter I, this fact demands that the reference channel of the multiport VNA system phase locks with an HPR signal which must be as phase-amplitude stable as possible at each frequency of interest (see figure 4.4).

- $\angle(\hat{a}_i + \hat{b}_i)$  and  $\angle V_{r-i}(z_r, f)$  measurements must be done at each frequency where one intends to characterize the DUT. The former requires more time than the latter, due to the necessity of the VNA to phase lock onto each frequency of interest ( $f_0, 2f_0, \text{etc}$ ) at a time, whereas the time domain receiver (MTA/SO) measures all harmonic components of the HPR signal inside its bandwidth simultaneously.

- the approach used in this thesis work, gets  $\angle k_{11}$  without demanding measurement data of the HPR's long-term characterization such as in LSNA and NVNA technologies [18][19] which use it as a "phase calibration standard". Specifically, these technologies, to compute  $\angle k_{11}$ , demand prior knowledge of the spectral components' phase of the HPR signal ( $\angle a_s$  in figure 4.4) and the input reflection coefficient of the HPR ( $\Gamma_s$  in figure 4.4) at each frequency of interest, unlike, the approach used here which just demands an amplitude – phase stable HPR signal (without pre-characterizing it) which can be obtained easily with "in house made" HPRs built in the lab. In other words,  $\angle k_{11}$ 's accuracy in the approach used here depends on the VNA and time domain receiver's capacity to carry out phase measurements and the HPR's short-term stability, connected to the R-channel and to the i-th test port chosen, during phase calibration procedure (see figure 4.4). In contrast, in LSNA and NVNA technologies  $\angle k_{11}$ 's accuracy depends on the VNA's capacity to measure phase, the long-term stability of the pre-characterized HPR used as "phase calibration standard" connected to the i-th test port chosen and the short-term stability of a second HPR connected to the R-channel during phase calibration procedure.



In the second case when mechanical connection problems are present things are less simple: in this case it isn't possible to directly connect test ports to the time domain receiver (MTA/SO) such as in figure 4.4, for instance, this can occur in on-wafer measurement environments where probe tips can't be connected mechanically with say a 2.4mm coaxial connector from the time domain receiver input port. As in the power calibration procedure it will be required to use the approach proposed in [10]. It means, using (3.3) from section 3.2 applied to whichever port (among the n-1s available, called auxiliary port) on the other side of the signal separation section's couplers, where surely it's possible to connect the time domain receiver (MTA/SO) as shown in figure 4.5.

Furthermore, to simplify things it will be assumed a non leaky error model to characterize  $\underline{\underline{H}}, \underline{\underline{K}}, \underline{\underline{L}}, \underline{\underline{M}}$  (see equation 3.4) and  $\underline{\underline{D}}_1$  (see equation 3.3) matrixes. Obviously, this is a compromise to simplify  $\angle k_{11}$ 's computation. So from (3.13) it's evident that (3.3) can be written for whichever i-th auxiliary port chosen as follow:

$$\begin{pmatrix} a_{i-aux} \\ b_{i-aux} \end{pmatrix} = \begin{bmatrix} -h_{ii-aux} & l_{ii-aux} \\ -m_{ii-aux} & k_{ii-aux} \end{bmatrix} \begin{pmatrix} a_{mi} \\ b_{mi} \end{pmatrix} \quad (4.22)$$

Which after an S-O-L calibration procedure applied to the i-th auxiliary port chosen it can be rewritten as:

$$\begin{pmatrix} a_{i-aux} \\ b_{i-aux} \end{pmatrix} = (|k_{ii-aux}| \angle k_{ii-aux}) \begin{bmatrix} -\hat{h}_{ii-aux} & \hat{l}_{ii-aux} \\ -\hat{m}_{ii-aux} & 1 \end{bmatrix} \begin{pmatrix} a_{mi} \\ b_{mi} \end{pmatrix} \quad (4.23)$$

This allows writing the reflected ( $b_{i-aux}$ ) and incident ( $a_{i-aux}$ ) power waves at the i-th auxiliary port chosen as:

$$a_{i-aux} = k_{ii-aux} (-\hat{h}_{ii-aux} a_{mi} + \hat{l}_{ii-aux} b_{mi}) = (|k_{ii-aux}| \angle k_{ii-aux}) \hat{a}_{i-aux} \quad (4.24)$$

$$b_{i-aux} = k_{ii-aux} (-\hat{m}_{ii-aux} a_{mi} + b_{mi}) = (|k_{ii-aux}| \angle k_{ii-aux}) \hat{b}_{i-aux} \quad (4.25)$$

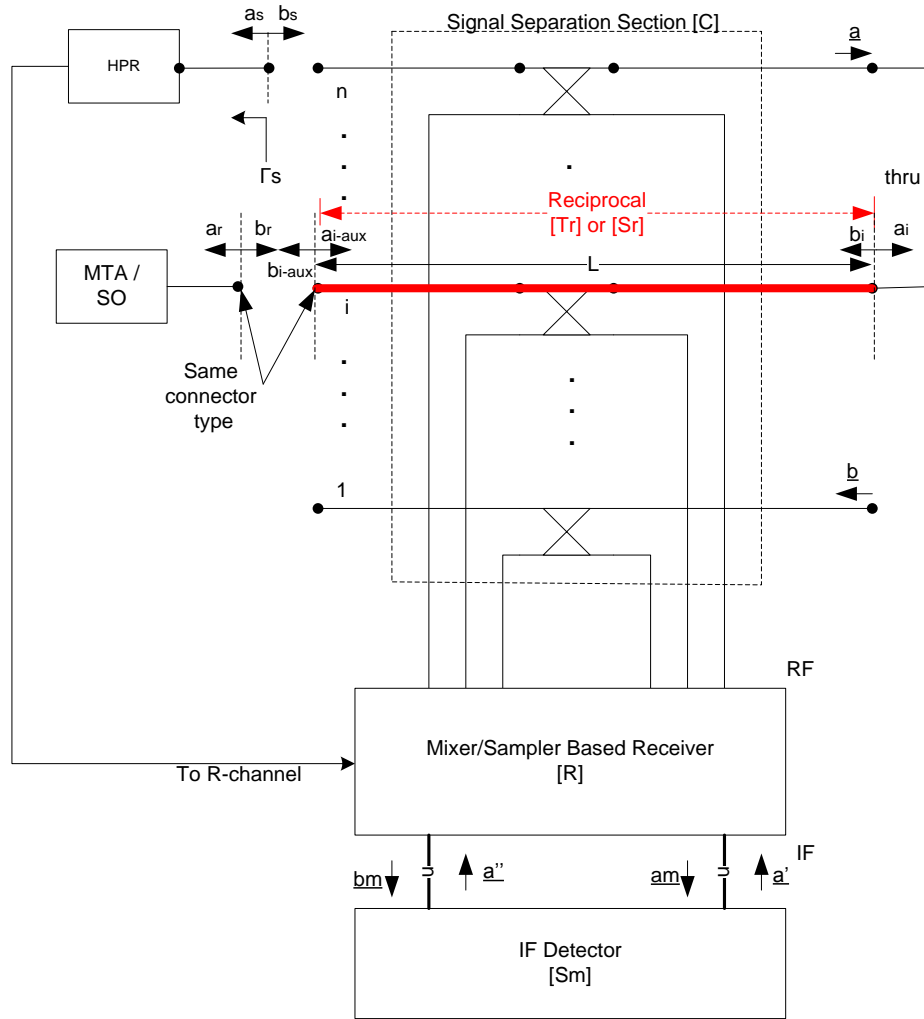


Figure 4.5 phase calibration setup when gender connector problems are present.

Where  $\hat{a}_{i-aux}$  and  $\hat{b}_{i-aux}$  are computed by means of the S-O-L calibration's results applied to the  $i$ -th auxiliary port chosen ( $-\hat{h}_{ii-aux}, \hat{l}_{ii-aux} - \hat{m}_{ii-aux}$ ) and from VNA's readings,  $|k_{ii-aux}|$  is completely known from power calibration procedure.

In order to get  $\angle k_{ii-aux}$  which will allow computing ( $\angle k_{11}$ ) which is really needed, it's required to:

-choose two ports among  $n$  available (used to connect the signal separation section with the DUT's port) and connect them by using a thru or a transmission line as shown in figure 4.5.

- use the two adjacent ports of the signal separation section's couplers : one to inject the HPR signal and the other one to connect the time domain receiver (see figure 4.5). This is done, in order to set a power level at each frequency of interest ( $f_0$ ,  $2f_0$ , etc) that can be measured by the time domain receiver (MTA/SO).

In this way, because  $\angle V_{r-i}(z_r, f)$  can be obtained from the time domain receiver (MTA/SO) readings (see (4.19)), and since VNA readings allow get  $\hat{a}_i$ ,  $\hat{b}_i$  (see (4.17) and (4.18)), by combining both readings at the time domain receiver's reference plane ( $z_r$ ), when the time domain receiver is connected to the  $i$ -th auxiliary port previously chosen (see figure 4.5) one gets:

$$V_{r-i}(z_r, f) = \sqrt{Z_0}(a_r + b_r) = \sqrt{Z_0}k_{ii-aux}(\hat{b}_i + \hat{a}_i) \quad (4.27)$$

From which one finds easily  $\angle k_{ii-aux}$  as:

$$\angle k_{ii-aux} = \angle V_{r-i}(z_r, f) - \angle(\hat{b}_i + \hat{a}_i) \quad (4.28)$$

The same considerations pointed out for  $\angle k_{11}$ 's computation, when gender connector problems are not present given by (4.21), must be done on the  $\angle k_{ii-aux}$ 's computation given by (4.28): ( $\angle a_{mj}$ ,  $\angle b_{mj}$ ) accuracy, the HPR signal must be as phase-amplitude stable as possible at each frequency of interest,  $\angle(\hat{b}_i + \hat{a}_i)$  and  $\angle V_{r-i}(z_r, f)$  measurements must be done at each frequency where one intends to characterize the DUT, etc.

Next, in order to compute  $\angle k_{11}$  through  $\angle k_{ii-aux}$  :one must characterize the cables, through arm's couplers, and connectors placed between the  $i$ -th auxiliary port

chosen (used to connect the time domain receiver (MTA/SO)) and the  $i$ -th test port (used to connect the signal separation section with the  $i$ -th DUT's port), by means of a S-parameter matrix  $\underline{\underline{S}}_r$  (see red line in figure 4.5) defined as follow [11]:

$$\begin{pmatrix} a_i \\ b_{i-aux} \end{pmatrix} = \underline{\underline{S}}_r \begin{pmatrix} b_i \\ a_{i-aux} \end{pmatrix} \quad (4.29)$$

On the other hand, with the assumption of a non leaky error model and after a suitable S-parameter calibration, (4) can be written for whichever  $i$ -th test port as:

$$\begin{pmatrix} a_i \\ b_i \end{pmatrix} = k_{11} \begin{bmatrix} -\hat{h}_{ii} & \hat{l}_{ii} \\ -\hat{m}_{ii} & \hat{k}_{ii} \end{bmatrix} \begin{pmatrix} a_{mi} \\ b_{mi} \end{pmatrix} \quad (4.30)$$

In this way, by combining (4.23) and (4.30)  $\underline{\underline{S}}_r$  can be found as function of  $\angle k_{11}$  as:

$$\underline{\underline{S}}_r = \begin{bmatrix} S_{r-11} & \left(\frac{|k_{11}| \angle k_{11}}{k_{ii-aux}}\right) \hat{s}_{r-12} \\ \left(\frac{k_{ii-aux}}{|k_{11}| \angle k_{11}}\right) \hat{s}_{r-21} & S_{r-22} \end{bmatrix} = \begin{bmatrix} S_{r-11} & S_{r-12} \\ S_{r-21} & S_{r-22} \end{bmatrix} \quad (4.31)$$

Where:

$$S_{r-11} = \frac{\hat{h}_{ii} \hat{l}_{ii-aux} - \hat{l}_{ii} \hat{h}_{ii-aux}}{\hat{m}_{ii} \hat{l}_{ii-aux} - \hat{k}_{ii} \hat{h}_{ii-aux}}$$

$$S_{r-22} = -\frac{\hat{k}_{ii} \hat{m}_{ii-aux} - \hat{m}_{ii}}{\hat{m}_{ii} \hat{l}_{ii-aux} - \hat{k}_{ii} \hat{h}_{ii-aux}}$$

$$\hat{s}_{r-12} = \frac{(\hat{l}_{ii} \hat{m}_{ii-aux} - \hat{h}_{ii} \hat{m}_{ii}) - S_{r-11} (\hat{k}_{ii} \hat{m}_{ii-aux} - \hat{m}_{ii})}{(\hat{m}_{ii-aux} \hat{l}_{ii-aux} - \hat{h}_{ii-aux})}$$

$$\hat{s}_{r-21} = \frac{(\hat{m}_{ii-aux} \hat{l}_{ii-aux} - \hat{h}_{ii-aux})}{(\hat{m}_{ii} \hat{l}_{ii-aux} - \hat{k}_{ii} \hat{h}_{ii-aux})}$$

The reciprocity condition applied to (4.31) establishes  $s_{r-21} = s_{r-12}$ , which yields  $\angle k_{11}$ 's ambiguity sign given by:

$$\angle k_{11} = \begin{cases} \frac{\angle\left\{\left(\frac{\hat{s}_{r-21}}{\hat{s}_{r-12}}\right)(k_{ii-aux})^2\right\}}{2} \\ \pi + \frac{\angle\left\{\left(\frac{\hat{s}_{r-21}}{\hat{s}_{r-12}}\right)(k_{ii-aux})^2\right\}}{2} \end{cases} \quad (4.32)$$

Because this ambiguity sign occurs at each frequency of interest ( $f_0$ ,  $2f_0$ , etc) it can be handled by an approach software-hardware such as in [20], however this could be a time consuming task. The strategy used in this thesis work (performed by “in house made” software) in order to solve  $\angle k_{11}$ 's ambiguity sign is quite different: it's based on getting  $\angle s_{r-21} = \angle s_{r-12}$  from calibration's measurements at each frequency of interest ( $f_0$ ,  $2f_0$ , etc). A reason to carry it out is that by combining  $T_{r-11}$  from (4.14) and  $S_{r-21}=S_{r-12}$  from (4.29) one can get  $\angle k_{11}$  uniquely defined as follow:

$$T_{r-11} = \frac{1}{S_{r-12}} = \left(\frac{k_{11}}{k_{ii-aux}}\right) \hat{T}_{r-11} \quad (4.33)$$

$$\angle k_{11} = \angle k_{ii-aux} - \angle S_{r-12} - \angle \hat{T}_{r-11} \quad (4.34)$$

Where:

$$\hat{T}_{r-11} = \left(\frac{\hat{k}_{ii} \hat{m}_{ii-aux} - \hat{m}_{ii}}{\hat{m}_{ii-aux} \hat{l}_{ii-aux} - \hat{h}_{ii-aux}}\right)$$

It's evident from (4.34) that owing to  $k_{ii-aux}$  and  $\hat{T}_{r-11}$  are completely known after proper power and S-parameter calibration procedures to get  $\angle k_{11}$  only  $\angle S_{r-12} = \angle S_{r-21}$  is required at each frequency of interest ( $f_0, 2f_0$ , etc) which can be found through  $\angle\{s_{r-21}s_{r-12}\} = \angle\{\hat{s}_{r-21}\hat{s}_{r-12}\}$  (which is completely known from (4.31)) as shown in figure 4.6.

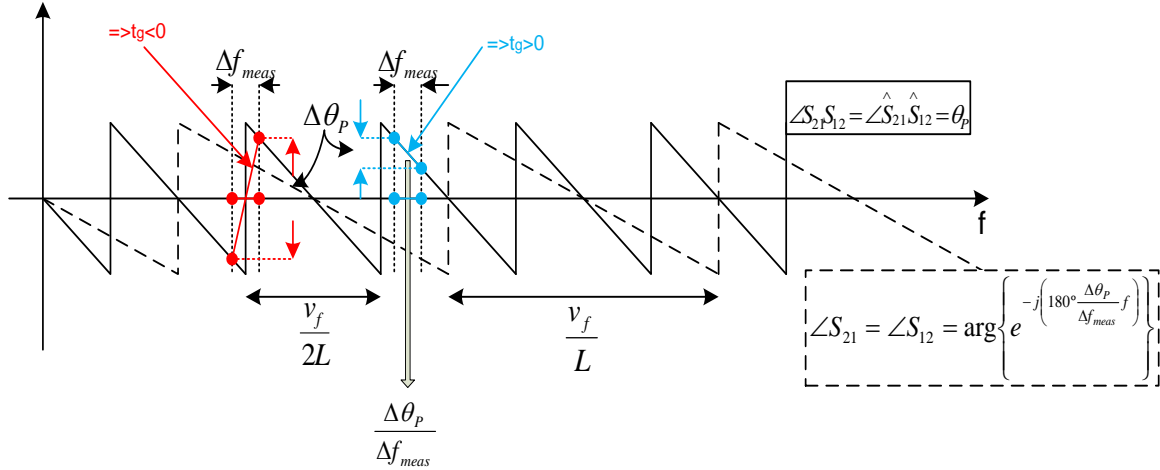


Figure 4.6.  $\angle S_{r-12} = \angle S_{r-21}$ 's computation through  $\angle\{s_{r-21}s_{r-12}\} = \angle\{\hat{s}_{r-21}\hat{s}_{r-12}\}$

Where:

$v_f$  (m/s): stands for the velocity of propagation of the RF signal traveling through cables, through arm's couplers, and connectors placed between the  $i$ -th auxiliary port chosen (used to connect the time domain receiver (MTA/SO)) and the  $i$ -th test port (used to connect the signal separation section with the  $i$ -th DUT's port). It depends on the relative dielectric constant ( $\epsilon_r$ ) of the dielectric material used in cables, through arm's couplers, and connectors. Since coaxial cables have the longest length in the path, (see figure 4.5) one can approximate the overall  $v_f$  as that of a coaxial cable given by [21]:

$$v_f = \frac{1}{\sqrt{\epsilon_r}} c \approx 0.69c \quad (4.35)$$

Where it was accounted that the most common dielectric used to build coaxial cables is the Polytetrafluoroethylene (PTFE) with a  $\epsilon_r=2.1$ .

$L$  (m): is the mechanical length of cables, through arm's couplers, and connectors placed between the  $i$ -th auxiliary port chosen (used to connect the time domain receiver (MTA/SO)) and the  $i$ -th test port (used to connect the signal separation section with the  $i$ -th DUT's port) (see figure 4.5).

The steps to get  $\angle S_{r-12} = \angle S_{r-21}$  through  $\angle \{s_{r-21}s_{r-12}\} = \angle \{\hat{s}_{r-21}\hat{s}_{r-12}\}$  are the following:

1-Given a frequency list which includes all frequencies of interest where one intends to characterize the DUT ( $f_0$ ,  $2f_0$ , etc), due to the  $\angle \{s_{r-21}s_{r-12}\} = \angle \{\hat{s}_{r-21}\hat{s}_{r-12}\}$ 's frequency periodicity  $\left(\frac{v_f}{2L}\right)$  is often lesser than  $f_0$ , then two consecutive points in the frequency list ( $kf_0$ ,  $(k+1)f_0$ ) won't be enough to compute  $\angle S_{r-12} = \angle S_{r-21}$ . Therefore, an additional frequency point ( $f_x$  and/or  $f_y$ ) depending on a differential of frequency labeled as " $\Delta f_{meas}$ " in figure 4.6 must be included in the frequency list.

2- Because  $\Delta f_{meas}$  will be used to compute the group delay ( $t_g$ ) introduced by cables, through arm's couplers, and connectors placed between the  $i$ -th auxiliary port chosen and the  $i$ -th test port (see figure 4.5), it must be chosen lesser than  $\angle \{s_{r-21}s_{r-12}\} = \angle \{\hat{s}_{r-21}\hat{s}_{r-12}\}$ 's frequency periodicity  $\left(\frac{v_f}{2L}\right)$  which by using (4.35) can be estimated as:

$$\Delta f_{meas} \ll \frac{v_f}{2L} \approx \frac{103}{L} \text{ (MHz)} \quad (4.36)$$

3-Once  $\angle \{s_{r-21}s_{r-12}\} = \angle \{\hat{s}_{r-21}\hat{s}_{r-12}\}$  is known at all frequency points in all frequencies of interest ( $f_0$ ,  $2f_0$ , etc), there will be exist two points in the frequency list labeled as  $f_{\theta pmax}$  and  $f_{\theta pmin}$  where  $\angle \{s_{r-21}s_{r-12}\} = \angle \{\hat{s}_{r-21}\hat{s}_{r-12}\}$  has got a maximum and a minimum value respectively, then one can compute the group delay ( $t_g$ ) introduced by cables, through arm's couplers, and connectors by introducing an additional frequency point ( $f_x$  and/or  $f_y$ ) into the frequency list so that:

$$t_g = -\frac{1}{2} \frac{1}{360^\circ} \frac{\Delta\theta_{p1}}{\Delta f_{meas}} = -\frac{1}{2} \frac{1}{360^\circ} \frac{\Delta\theta_{p2}}{\Delta f_{meas}} \quad (4.37)$$

Where:

$$\theta_p = \angle\{s_{r-21}s_{r-12}\} = \angle\{\hat{s}_{r-21}\hat{s}_{r-12}\}$$

$$\Delta\theta_{p1} = \theta_p|_{f=f_{\theta pmax}} - \theta_p|_{f=f_x=f_{\theta pmax} + \Delta f_{meas}}$$

$$\Delta\theta_{p2} = \theta_p|_{f=f_y=f_{\theta pmin} - \Delta f_{meas}} - \theta_p|_{f=f_{\theta pmin}}$$

$$t_g > 0$$

4-Once  $t_g$  is computed from (4.37), one gets easily  $\angle\mathcal{S}_{r-12} = \angle\mathcal{S}_{r-21}$  at all frequencies of interest (required by (3.34) to compute  $\angle k_{11}$ ) as :

$$\angle\mathcal{S}_{r-12} = \angle\mathcal{S}_{r-21} = -360^\circ t_g f \quad (4.38)$$

Obviously (4.37) avoids a situation similar to that shown in figure 4.6 in red color, where even if  $\Delta f_{meas} \ll \frac{v_f}{2L}$ , it may occur that  $t_g < 0$  and it ensures a situation similar to that shown in blue color in the same figure where  $t_g > 0$ . On the other hand, one has to account that since  $\angle\{s_{r-21}s_{r-12}\} = \angle\{\hat{s}_{r-21}\hat{s}_{r-12}\}$  springs from (4.31) the power and S-parameter calibrations procedures must be performed also at  $f_x = (f_{\theta pmax} + \Delta f_{meas})$  and/or  $f_y = (f_{\theta pmin} - \Delta f_{meas})$  new additional frequencies in order to compute  $t_g$  properly.

It's important to note that, independent of whatever mechanism is used in order to solve the  $\angle k_{11}$ 's ambiguity sign, it's clear from (4.34) that  $\angle k_{11}$ 's uncertainty when gender connector problems are present depends on the  $\angle k_{11}$ 's uncertainty when there aren't gender connector problems (included in  $\angle k_{ii-aux}$  term) and in addition on the uncertainty of the S-parameter calibration and SOL calibration performed at the i-th test



port and at the  $i$ -th auxiliary port chosen, respectively. This occurs in a similar way in LSNA and NVNA technologies when gender connector problems are present [20][22]:  $\angle k_{11}$ 's uncertainty depends on all those factor included when there aren't gender connector problems (included in  $\angle k_{ii-aux} = \angle T$  term) and in addition on the uncertainty of the S-parameter calibration, and SOL calibration performed at the test ports and at RF input port 1, respectively. Then differences between the approach used here to perform the phase calibration procedure and that used in LSNA and NVNA technologies are basically: the uncertainty terms that might affect respectively  $\angle k_{ii-aux}$  and  $\angle T$  phases, which can be significantly different.

On the other hand, note that (4.20) and (4.27) can in principle also be used to find the amplitudes of  $k_{11}$  and  $k_{ii-aux}$  respectively. Although this practice can be considered in the future, this is at present not done for the following reasons [21]. It is not easy to accurately determine the voltage of each spectral component of a reference generator ( $V_{r-i}(z_r, f)$ ). Two methods can be considered: measurement with a spectrum analyzer and measurement with a time domain receiver (MTA/SO). Concerning spectrum analyzers, there is a problem of accuracy. A typical specification for state-of-the-art RF spectrum analyzers is an error of about 0.5dB, which is considered to be too high for our application. Concerning time domain receiver (MTA/SO) measurements, one would have to take care of jitter effects, especially considering that the gain of the time domain receiver's samplers is slightly sensitive to temperature variations (this is due to the fact that a diode characteristic is dependent of temperature). This sensitivity is much less for the phase distortion of the time domain receiver which is primarily determined by the transmission path from the input connector to the sampling diodes. Therefore, only  $\angle V_{r-i}(z_r, f)$  term was considered known in (4.20) and (4.27).

In this way, after rights S-parameter, power and phase calibration procedures the total voltages and current waves traveling to/from each  $i$ -th DUT's port can be determined in both frequency and time domains as follow [11]:

$$a_i(t) = \mathfrak{F}^{-1}\{|k_{11}| \angle k_{11}\} \hat{a}_i \quad (4.39)$$

$$b_i(t) = \mathfrak{F}^{-1}\{|k_{11}| \angle k_{11}\} \hat{b}_i \quad (4.40)$$

$$V_i(z_i, f) = \sqrt{Z_0}(a_i + b_i) = \sqrt{Z_0}(|k_{11}| \angle k_{11})(\hat{a}_i + \hat{b}_i) \quad (4.41)$$

$$I_i(z_i, f) = \frac{(a_i - b_i)}{\sqrt{Z_0}} = (|k_{11}| \angle k_{11}) \frac{(\hat{a}_i - \hat{b}_i)}{\sqrt{Z_0}} \quad (4.42)$$

$$V_i(z_i, t) = \mathfrak{F}^{-1}\{\sqrt{Z_0}(|k_{11}| \angle k_{11})(\hat{a}_i + \hat{b}_i)\} \quad (4.43)$$

$$I_i(z_i, t) = \mathfrak{F}^{-1}\left\{\frac{(|k_{11}| \angle k_{11})(\hat{a}_i - \hat{b}_i)}{\sqrt{Z_0}}\right\} \quad (4.44)$$

Where:

$a_i = a_i(f)$ : stands for the incident power wave to the i-th DUT port in the frequency domain labeled as “f”.

$b_i = b_i(f)$ : stands for the reflected power wave from the i-th DUT port in the frequency domain labeled as “f”.

$a_i(t)$ : stands for the incident power wave to the i-th DUT port in the time domain labeled as “t”.

$b_i(t)$ : stands for the reflected power wave from the i-th DUT port in the time domain labeled as “t”.

$V_i(z_i, f)$ : stands for the total voltages wave to the i-th DUT port reference plane ( $z_i$ ) in the frequency domain labeled as “f”.

$I_i(z_i, f)$ : stands for the total current wave to the i-th DUT port reference plane ( $z_i$ ) in the frequency domain labeled as “f”.

$V_i(z_i, t)$ : stands for the total voltages wave to the i-th DUT port reference plane ( $z_i$ ) in the time domain labeled as “t”.

$I_i(z_i, t)$  : stands for the total current wave to the i-th DUT port reference plane ( $z_i$ ) in the time domain labeled as “t”.

$\mathfrak{F}^{-1}$ : stands for the inverse discrete Fourier transform (IDFT).

$$\mathfrak{F}^{-1}\{X(f)\} = x(t) = \text{Re}\{\sum_{h=0}^{h_{max}} X(hf_0)e^{j2\pi hf_0 t}\} \quad (4.45)$$

Where  $f_0$  =fundamental frequency

This general approach to compute  $\angle k_{11}$  can be applied to whatever number of setup’s ports (n), either having or not having mechanical constrains, to connect the time domain receiver (MTA/SO) to the test ports. For instance, when characterizing Differential Devices (4 ports) or single end Devices (2 ports) in on-wafer or mm-coaxial environments. Figure 4.7 shows the phase calibration’s flowchart.

In this thesis work all experimental result presented in chapter VI required the phase calibration procedure which was performed by using Microwave Measurement Software MMS-NT[12]: a powerful 32-Bit Visual C++ written windows application which based on (specified by the user): 1) port number where the HPR signal is connected 2)auxiliary port number and its connector type (if needed) or simply the test port number where connect the time domain receiver (MTA/SO). The MMS-NT cal software : 1) if auxiliary port is required it asks the user to perform and acquire phase measurements in correspondence to the time domain receiver’s connection to the auxiliary port chosen previously (see figure 4.5). Otherwise if auxiliary port is not required 2) it asks the user to perform and acquire phase measurements in correspondence of the time domain receiver’s connection to whichever test port among to the n-1s available as shown in figure 4.4. Obviously to carrying out phase measurements MMS (via PC) synchronizes itself with the time domain receiver (MTA/SO).(see appendix A)

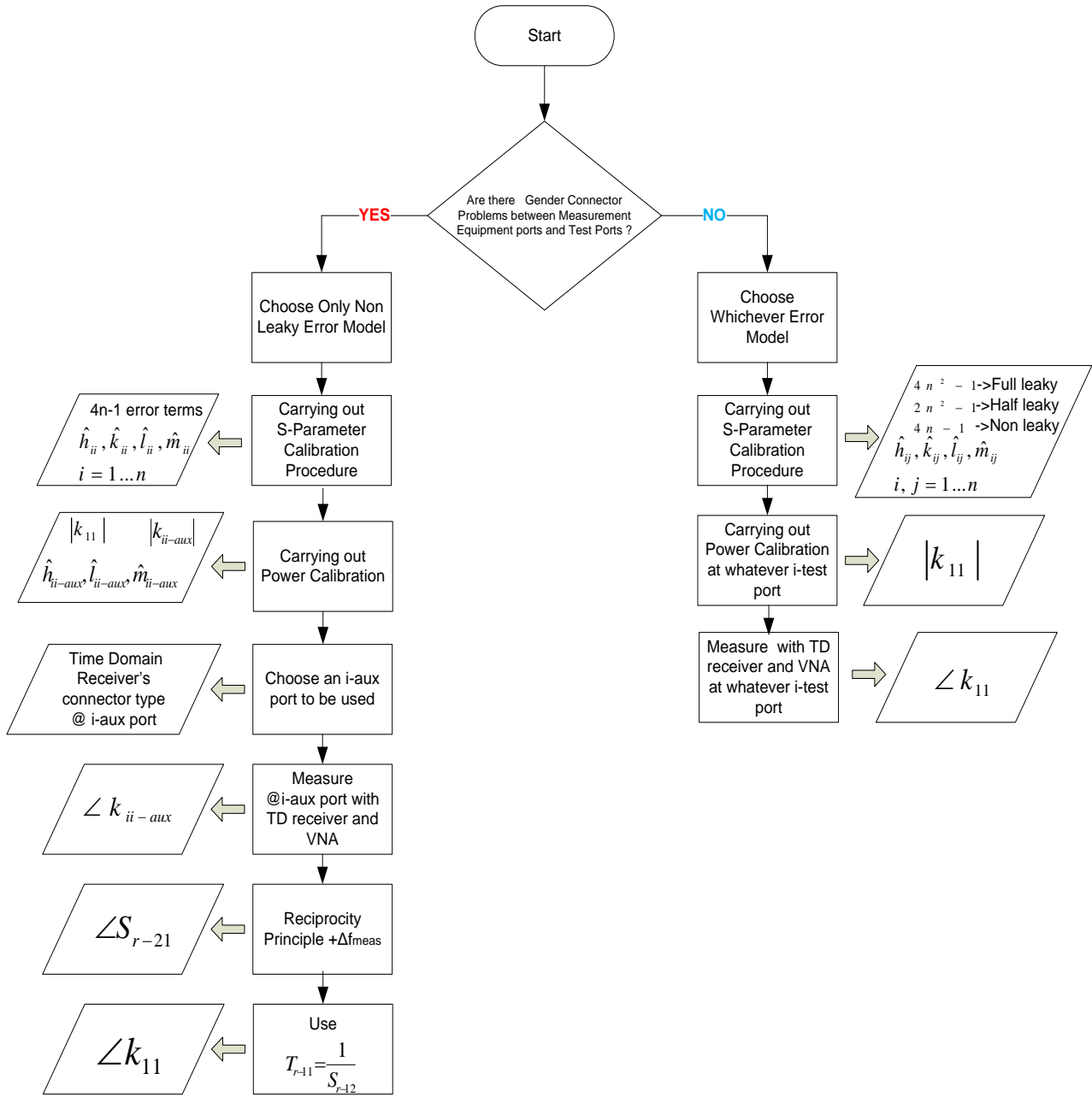


Figure 4.7 Phase Calibration flow diagram

---

**References**

- [1] Kurokawa, K. Power Waves and the Scattering Matrix .Microwave Theory and Techniques, IEEE Transactions on Volume 13, Issue 2, Mar 1965 Page(s): 194 – 202.
- [2] Bockelman, D.E.; Eisenstadt, W.R. Combined differential and common-mode scattering parameters: theory and simulation Microwave Theory and Techniques, IEEE Transactions on Volume 43, Issue 7, Jul 1995 Page(s):1530 - 1539
- [3] D. E. Bockelman, “The theory, measurement, and application of mode specific scattering parameters with multiple modes of propagation,” Ph.D. dissertation, Dept. Elect. Comput. Eng., Univ. Florida, 1997.
- [4] Agilent AN 154 S-Parameter Design. Application Note. Agilent Technologies, Inc. Printed in USA, June 20, 2006.
- [5] Qian Cai, Jason Gerber, Chao-Ren Chang, and Ulrich L. Rhode, “Nonlinear Microwave Circuit Design Using Multi-harmonic Load-Pull Simulation Technique,” Int. J. Microwave Millimeter-Wave Computer-Aided Eng., 1999.
- [6] Ulrich L. Rohde, David P. Newkirk Rf/Microwave Circuit Design For Wireless Applications.2000
- [7] R. Tucker and P.Bradley. “Computer-aided error correction of large-signal load pull measurements”, IEEE Trans, Microwave Theory Tech., vol. MTT-32.pp.296-300.Mar.1984.
- [8] I.Hechet, “Improved error-correction technique for large signal load pull measurements”, IEEE Trans, Microwave Theory Tech., vol. MTT-35,pp.1060-1062,Nov.1987.
- [9] V.Teppati and A.Ferrero, “New perspective in non linear device and amplifier characterization” in GAAS02 Conf.Proc.,Milan.Sept.2002.
- [10] A. Ferrero and U. Pisani,” An Improved calibration Technique for On-Wafer Large-Signal Transistor Characterization,” IEEE Transactions on Instrumentation and Measurement, Vol. 42, No. 2, April 1993.
- [11] G. Gonzalez, *Microwave Transistor Amplifiers*, Prentice-Hall, Englewood Cliffs, NJ, 1984.

- 
- [12] Ing. Chiara Soragna-PAF, Prof. Andrea Ferrero-Polytechnic of Torino “MMS LINE Multiport S-parameter System” <http://www.pafmicro.com/products.htm>
- [13] Ieee Transactions On Microwave Theory And Techniques, Vol. 50, No. 12, December 2002 Enhanced On-Wafer Time-Domain Waveform Measurement Through Removal of Interconnect Dispersion and Measurement Instrument Jitter Jonathan Brereton Scott, Senior Member, IEEE, Jan Verspecht, Babak Behnia, Member, IEEE, Marc Vanden Bossche, Member, IEEE, Alex Cognata, Frans Verbeyst, Mark L. Thorn, Member, IEEE, and Daniel R. Scherrer
- [14] Ieee Transactions On Microwave Theory And Techniques, Vol. 53, No. 11, November 2005 Broad-Band Poly-Harmonic Distortion (PHD) Behavioral Models From Fast Automated Simulations and Large-Signal Vectorial Network Measurements David E. Root, Fellow, IEEE, Jan Verspecht, Senior Member, IEEE, David Sharrit, JohnWood, Senior Member, IEEE, and Alex Cognat.
- [15] A.Ferrero and V.Teppati. “A complete measurement test-set for non linear device characterization” in 58<sup>th</sup> ARFTG Conference Digest. San Diego. USA.Nov.2001.
- [16] V. Teppati, “Microwave device characterization techniques oriented to increase the measurement accuracy” Ph.D. dissertation, Department of Electronics., Polytechnic of Turin . Italy, Dec.2002.
- [17] Sampling Oscilloscope Models and Calibrations Kate A. Remley and Dylan F. Williams National Institute of Standards and Technology, 325 Broadway, Boulder, CO 80305 2003 IEEE MTT-S Int. Microwave Symp. Dig., Philadelphia, PA, June 8-13, 2003, pp. 1507-1510. Presented by Kate Remley.
- [18]Tom Van den Broeck and Jan Verspecht,” Calibrated Vectorial Nonlinear-Network Analyzers,” 1994 IEEE MTT-S International Microwave Symposium Digest, Vol. 2, pp. 1069-1072, May 1994.
- [19] Agilent Technologies “Breakthrough Nonlinear Vector Network Analyzer Applications” **2008-07-17** .
- [20] J.Verspecht, “Calibration of a Measurement System for High Frequency Nonlinear Devices” Ph.D. dissertation, VRIJE Universiteit Brussel Faculteit Toegepaste

Wetenschappen Department ELEC Pleinlaan 2, B-1050 Brussels, Belgium. September 1995.

[21]Golio, Mike "Frontmatter" *The RF and Microwave Handbook* Editor in Chief Mike Golio 2001

[22]Accurate On Wafer Measurement Of Phase And Amplitude Of The Spectral Components Of Incident And Scattered Voltage Waves At the Signal Ports Of A Nonlinear Microwave Device Jan Verspecht, Peter Debie, Alain Barel, Luc Martens Copyright IEEE, 1995 IEEE MTT-S International Microwave Symposium Conference Record, Vol.3, pp.1029-1032.

# ***CHAPTER V***

## **HARDWARE IMPLEMENTATION**

*“Another important area of future research is the non-linear performance of a differential circuit....Measurement methods and systems for non-linear behavior in differential circuits are also needed.”* David E. Bockelman May 1997.



## 5.1) ACTIVE DIFFERENTIAL LOAD AND SOURCE PULL SYSTEM

The Differential Load and Source Pull system used in this thesis work was that proposed for the first time in [1] and subsequently used in [2] to characterize and optimize two power-dependent DUT's performances such as: Power Added Efficiency (PAE) and the differential power gain ( $G_{pD}$ ) of an inverse class F power amplifier. In contrast with some passive systems proposed in [3-5] this active system allows real harmonic mixed-mode reflection coefficient's control, specifically: it allows pulling  $\Gamma_{SD}$ ,  $\Gamma_{SC}$ ,  $\Gamma_{IC}$ ,  $\Gamma_{ID}$  independently at a given  $i$ -th harmonic of interest and keeping them constants under CW input power sweeps at fundamental ( $f_0$ ). Furthermore, this hardware coupled with an "in home made" software allows, true differential and/or common modes characterization in both frequency and time domains, being able to obtain power and time domain waveform dependent DUT's performances. The high speed of the VNA joined with the in-line measurements of all DUT's performances, gave to this system the name "real-time". Before carrying out any measurement one is required to perform a proper S-parameter, power and phase calibration procedures, in order to obtain full vector corrected measurement data in both time and frequency domains. In this sense the calibration procedure involves just the hardware in red color in figure 5.1, which shows the block diagram of the overall system. The former is in contrast with [3-5] where tuner pre-calibration is mandatory.

In this section each section of the overall system will be described briefly, these are basically:

- Stimulus Section
- Adder Single-ended Section
- Single-ended coupler Section
- $\Gamma$ 's Measurement Section
- Single-ended to Mixed-Mode De-coupler Section
- Harmonic Mixed-Mode Path Section
- Mixed-Mode to Single-ended Coupler Section
- 4-port vector network analyzer system

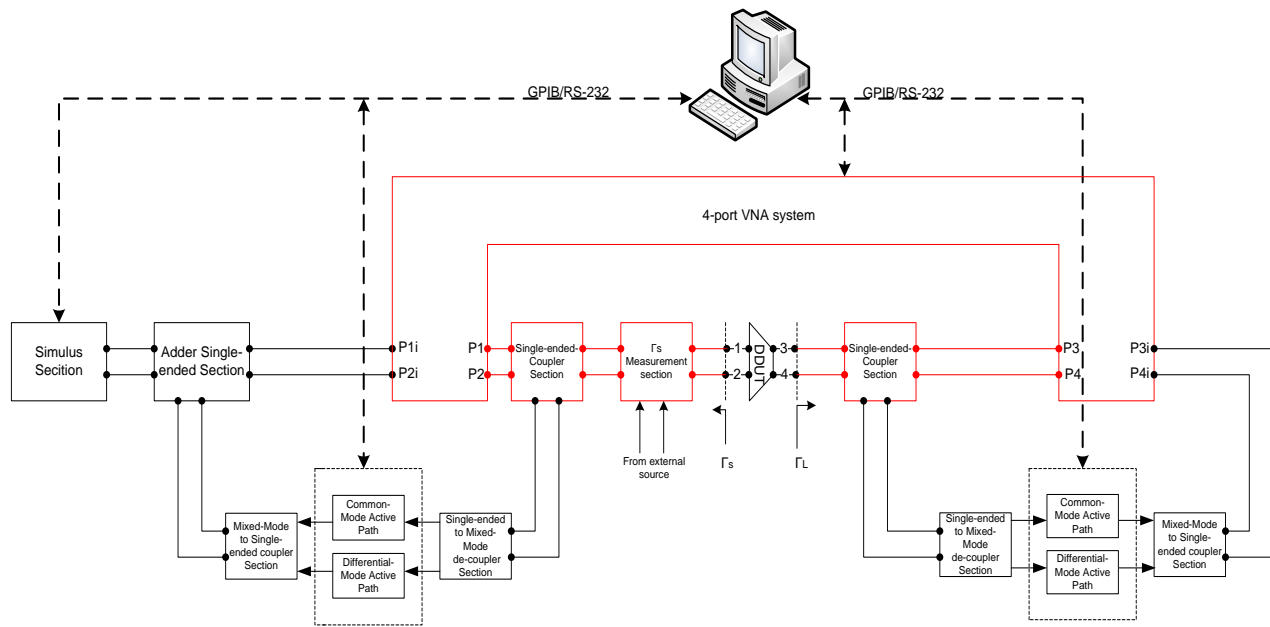


Figure 5.1 Differential Load and Source pull system used in this thesis work.

At the end of this section some practical aspects will be pointed out related to the VNA's reference channel phase locking and its relationship with the drift errors, which are crucial in order to perform reliable measurements when using the four-port vector network analyzer system shown in figure 5.1

### 5.1.1) Stimulus Section

This section is used to drive a true-balanced differential stimulus to the differential device under test (DDUT) at the fundamental frequency of interest @ CW. It's built by using a CW microwave generator whose output power is tuned via PC. This tuned power is split and routed into two different physical paths in order to introduce different electrical delays producing two single-ended signals with  $180^\circ$  of phase difference and with the same amplitude. These tasks are performed by using a  $180^\circ$  3dB hybrid power splitter, which splits the RF signal into two signals with nominally equal amplitudes and  $180^\circ$  phase difference, thus generating the differential-mode RF stimulus signal. Note that the 3dB hybrid has its unused port terminated in 50W load (see figure 5.2). Furthermore, by

interchanging the RF signal and termination, the 3dB hybrid again splits the RF signal into two signals, in this case with nominally equal amplitudes and  $0^\circ$  phase difference, thus generating the common-mode RF stimulus signal.

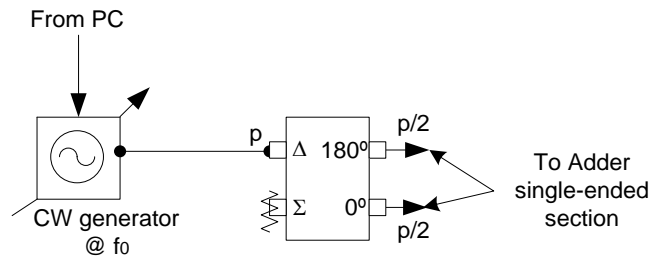


Figure 5.2 Stimulus Section

The most important specification of the  $180^\circ$  3dB hybrid power splitter's are: its magnitude and phase balance, as was proven in [6] these specifications influence its Common Mode Rejection Ratio (CMRR), in other words, its capacity to also produce common-mode excitation (under a given single-ended signal applied to the input) to the DDUT input. In this sense, one has to take care to maintain a balance (in amplitude and phase) from the hybrid ports to the DDUT's input ports. However, depending on the DDUT's nature (its mode conversion behavior) one might stimulate it with a simple single-ended excitation [7]. This will be useful to characterize the power or time domain dependent differential performance, in other cases, one can implement more sophisticated true differential or common mode stimulus such as that proposed in [8] to characterize more specific DDUT.

### 5.1.2) Adder-Single-ended section

It's the most simple one and its function is to add the voltages outgoing from both the Mixed-Mode to Single-ended de-coupler section and from the Stimulus section in order to produce a signal whose harmonic content is the sum of the fundamental ( $f_0$ ) and that produced by the Harmonic Mixed-Mode Path Section ( $k.f_0$ ). It's made up of two 3dB power

splitters whose more important specifications are their magnitude and phase balance. (See figure 5.3).

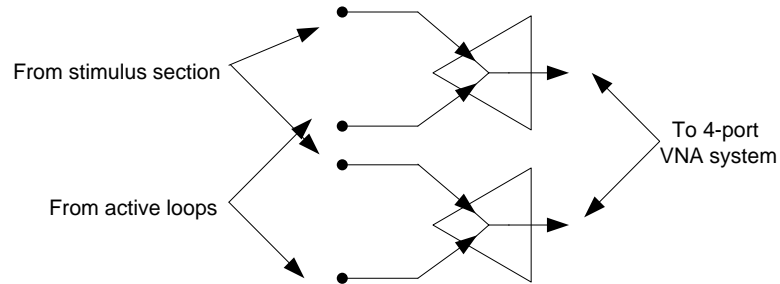


Figure 5.3 Adder single-ended section

### 5.1.3) Single-ended-Coupler Section

Its function is to separate all reverse (at the DDUT's output and at the DDUT's input) signals at each single-ended port (i.e. nodal waves) [6] and route them to the Single-ended to Mixed-Mode De-coupler Section. (See figure 5.4). It consists of a directional coupler at each single-ended port of the DDUT.

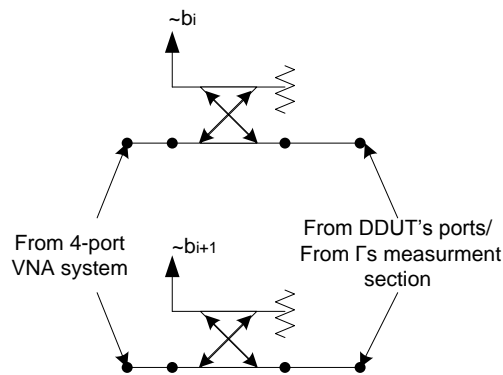


Figure 5.4 Coupler-single-ended section

#### 5.1.4) $\Gamma$ 's Measurement Section

It's made up of a pair of directional couplers at each single-ended input port of the DDUT. In this way, by injecting signal from an external source as shown in figure 5.5 one can compute  $\Gamma_{sC} = \frac{a_{C1}}{b_{C1}}$  or  $\Gamma_{sD} = \frac{a_{D1}}{b_{D1}}$  @  $kf_0$ . Obviously the latter assumes a low reflection at each single-ended input port of the DDUT which otherwise can be used to compute the differential and common mode source reflection coefficient directly by using  $a_i$  and  $b_i$  from the DDUT. However, there is another approach to measure the source reflection coefficient based on measuring  $a_i$  and  $b_i$  under two different DDUT's bias conditions [9] but this is a time consuming task.

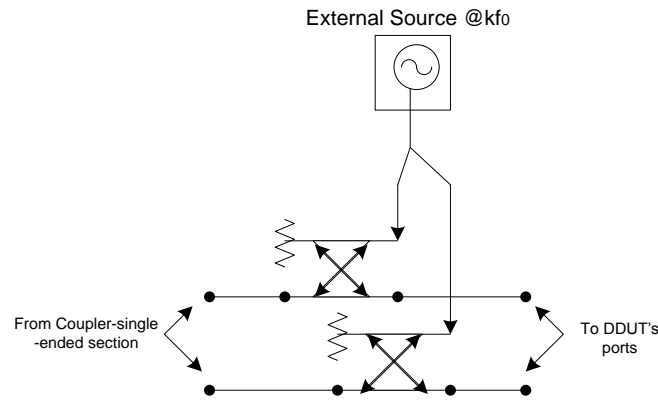


Figure 5.5  $\Gamma$ 's Measurement section

#### 5.1.5) Single-ended to Mixed-Mode De-coupler Section

In this section the nodal waves are combined, in accordance with (5.1) and (5.2), in  $180^\circ$ -3dB hybrid couplers, each providing a (nominal) sum and difference between the corresponding nodal waves. The outputs of these couplers are proportional to the differential and common-mode normalized power waves ( $b_{D1}$ ,  $b_{C1}$ ,  $b_{D2}$ ,  $b_{C2}$ ) [6] to subsequently route them to the Harmonic Mixed-Mode Path Section (see figure 5.6).

$$b_{D1} = \frac{1}{\sqrt{2}}(b_1 - b_2) \quad b_{C1} = \frac{1}{\sqrt{2}}(b_1 + b_2) \quad (5.1)$$

$$b_{D2} = \frac{1}{\sqrt{2}}(b_3 - b_4) \quad b_{C2} = \frac{1}{\sqrt{2}}(b_3 + b_4) \quad (5.2)$$

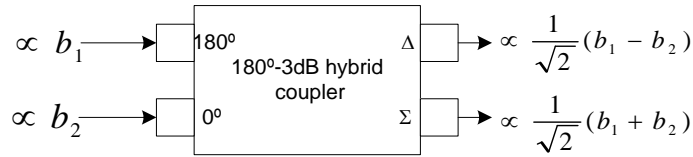


Figure 5.6 Single-ended to Mixed-Mode De-coupler Section

The hybrid coupler’s specifications are crucial in order to guarantee a good isolation between differential and common modes, on other words, it must be as an ideal balanced 4-port device as possible (no mode conversion  $\underline{\underline{S_{DC}}} = \underline{\underline{S_{CD}}} = \underline{\underline{0}}$ ) [6].

### 5.1.6) Harmonic Mixed-Mode Path Section

Its function is to modify modulus ( $|\cdot|$ ) and phase ( $\angle$ ) of the differential and common-mode normalized power waves ( $b_{D1}, b_{C1}, b_{D2}, b_{C2}$ ) outgoing from the Single-ended to Mixed-Mode De-coupler Section, but only at given harmonic frequency of interest ( $kf_0$ ). In this way new modified differential and common-mode normalized power waves ( $b_{D1}', b_{C1}', b_{D2}', b_{C2}'$ ) are obtained. It is basically an improved version of that proposed in [10]. It consists of a chain of circuits establishing a signal path. Its first three circuits are controlled via PC (see figure 5.7):

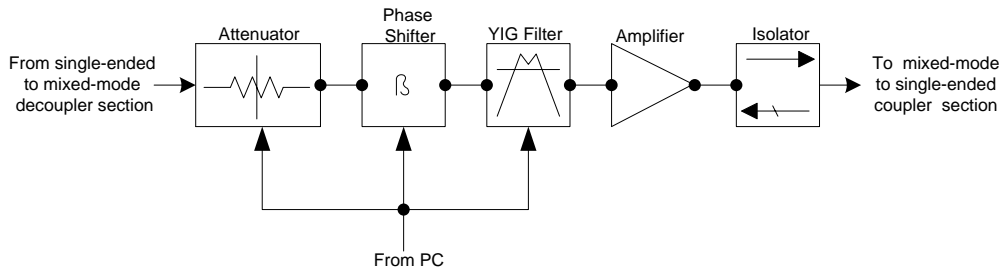


Figure 5.7 Harmonic Mixed-Mode Path Section

### 5.1.6.1) Variable Attenuator

Reduces the power level of the broadband signals ( $b_{D1}$ ,  $b_{C1}$ ,  $b_{D2}$ ,  $b_{C2}$ ). The selection of attenuators for use in this case is generally the easiest of the specification tasks. Because bench testing requirements may vary considerably from project to project, the objective in specifying attenuators for these applications will normally be to provide the broadest possible range of project requirements. Characteristics involved in this concept of versatility will be [11]: broad bandwidth, large attenuation range, high accuracy, longevity of connectors.

### 5.1.6.2) Phase Shifter

Are used to change the transmission phase angle of the broadband signals ( $b_{D1}$ ,  $b_{C1}$ ,  $b_{D2}$ ,  $b_{C2}$ ). Ideal phase shifters provide low insertion loss, and equal amplitude (or loss) in all phase states. Although the loss of a phase shifter is often overcome using an amplifier stage. The phase shifter in the chain is controlled digitally. Digital phase shifters provide a discrete set of phase states that are controlled by using a digital word, however, their mechanism to change the phase may be mechanical or electronic.

### 5.1.6.3) YIG-tuned filter

Is a band pass tuned filter which allows to pass the differential and common-mode normalized power waves ( $b_{D1}$ ,  $b_{C1}$ ,  $b_{D2}$ ,  $b_{C2}$ ) at a given  $k$ -th harmonic of the fundamental ( $kf_0$ ) to the amplifier. It's based on Yttrium Iron Garnet (YIG) technology: a crystal that has very high  $Q$  characteristics. This high  $Q$  provides multi-octave frequency tuning for filters. YIG is a ferrite material that resonates at microwave frequencies when immersed in a DC magnetic field. This resonance is directly proportional to the strength of the applied magnetic field and has very linear "tuning" over multi-octave microwave frequencies. The DC magnetic field is generated using an electromagnet, a permanent magnet or a combination of both. The magnetic field of an electromagnet can be "tuned" using a variable current. Figure 5.8 illustrates a typical YIG filter magnet. In general they are

controlled by a digital command to tuning current or voltages by using a digital driver which is basically an analog driver with a D/A converter at the input.

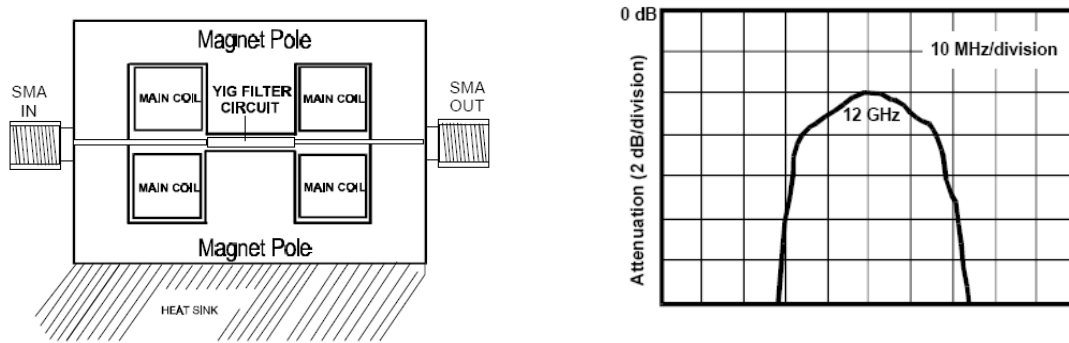


Figure 5.8 Typical open-loop YIG-tuned filter cross section (right) and its typical 3dB bandwidth and insertion loss @12GHz(left).

They can be implemented in open loop (as in figure 5.8) and in closed-loop (see figure 5.9). The former requires manual or computer controlled recalibration during test or after changes in the test parameter, its 3dB bandwidths are up to 15-25 MHz and provides a not predictable center-frequency tuning repeatability [12-13] ; the latter by using frequency discriminator technology, doesn't require recalibration, guarantees 3dB bandwidths lesser than 20 MHz, and provides a center-frequency tuning repeatability within  $\pm 0.5$  MHz (equivalent to less than 0.1dB variation). However, the application field will decide finally what type of technology is the minimum needed to guarantee a good accuracy.

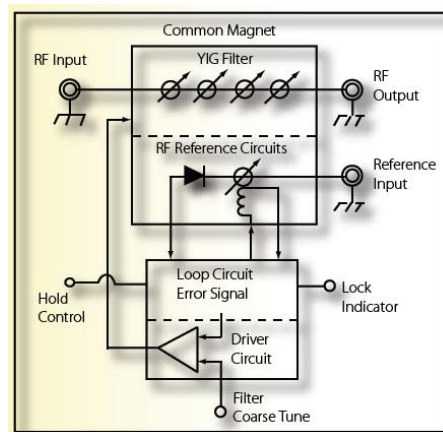


Figure 5.9 Block diagram of a closed-loop YIG-tuned filter.



Taking advantage of its abrupt phase response between its 3dB band pass these kind of filters can be used to electronically fit the phase in the signal path.

#### 5.1.6.4) Amplifier

Its function is to amplify the tones of the differential and common-mode normalized power waves ( $b_{D1}$ ,  $b_{C1}$ ,  $b_{D2}$ ,  $b_{C2}$ ) at a given  $k$ -th harmonic of the fundamental ( $kf_0$ ) outgoing from the YIG-tuned filter in order to increase their amplitude. The most important specifications are high linearity in order to not introduce spurious responses into the signal path and a flat AM-PM response in order to not introduce undesired phase shifts into the signal path. In practice, an amplifier can be used to amplify more than one tone at a time as long as these are from the same mode (i.e.  $b_{D1} @ 2f_0$ ,  $b_{D1} @ f_0$ ).

#### 5.1.6.5) Isolator

Reduces the multiple reflections between the amplifier's output and the Mixed-Mode to Single-ended Coupler Section that might affect the amplitude and phase responses of the signal path [14], and also in order to protect the amplifier from the incident power toward its input.

In this sense it's important to emphasize the fact that, since all the networks in the signal path's chain are linear (cables, amplifier, filter, etc) one must as much as possible guarantee impedance matching between each pair, and to reduce the physical lengths of the chain to improve the flatness in the whole amplitude and phase responses of the signal path[14][10], which influences the magnitude and phase of the DDUT's reflection coefficient when multicarrier signals are used to stimulate the DDUT.

### 5.1.7 Mixed-Mode to Single-ended Coupler Section

In this section the modified differential and common-mode normalized power waves ( $b_{D1}'$ ,  $b_{C1}'$ ,  $b_{D2}'$ ,  $b_{C2}'$ ) @  $k$ -th harmonic of the fundamental ( $f_0$ ) are combined, in

accordance to (5.3) and (5.4), in 180°-3dB hybrid couplers, each providing a (nominal) sum and difference between the corresponding modified differential and common-mode normalized power waves (see figure 5.10). The outputs of these couplers are proportional to the modified nodal power waves ( $b_1', b_2', b_3', b_4'$ ) [6] to subsequently route them to the DDUT's ports to make it “see” a differential and/or common mode reflection coefficient which can be equal or even larger than one.

$$b_1' = \frac{1}{2\sqrt{2}}(b_{D1}' + b_{C1}') \quad b_2' = \frac{1}{2\sqrt{2}}(b_{C1}' - b_{D1}') \quad (5.3)$$

$$b_3' = \frac{1}{2\sqrt{2}}(b_{D2}' + b_{C2}') \quad b_4' = \frac{1}{2\sqrt{2}}(b_{C2}' - b_{D2}') \quad (5.4)$$

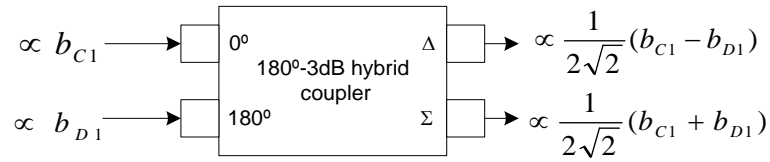


Figure 5.10 Mixed-Mode to Single-ended Coupler Section

Once again the hybrid coupler must be as balanced a 4-port device as possible to ensure isolation between modes which is crucial in order to guarantee true differential and common mode control in the DDUT.

To summarize, in this way each signal path acts independently on the differential and common modes at the DDUT's inputs and/or at outputs. Furthermore, this new active load architecture is inserted in a particular manner inside the overall measurement system: note the position of the loop couplers (Single-ended-coupler Section), as close as possible to the DDUT, and the measurement coupler (inside the 4-port VNA system) inside the loop. This technique is crucial to avoid loop oscillation and it has been patented for single-ended active loop [15].

### 5.1.8) Four-port vector network analyzer system

Its function is basically to sample the incident ( $a_i$ ) and reflected ( $b_i$ ) nodal waves from each DDUT's single-ended port and route them to the receiver channel and finally send the measuring waves' information ( $a_{mi}$ ,  $b_{mi}$ ) to the PC through the GPIB bus. It's made up of three part as shown in figure 5.11:

#### 5.1.8.1) Switch Unit

Used to expand the commercial two-port 8510C VNA [16] up to 4-port [17]. In this unit also each single-ended reflected and incident wave is routed at a time to the 8511A frequency converter module by using SPnT high isolation switches (see figure 5.12).

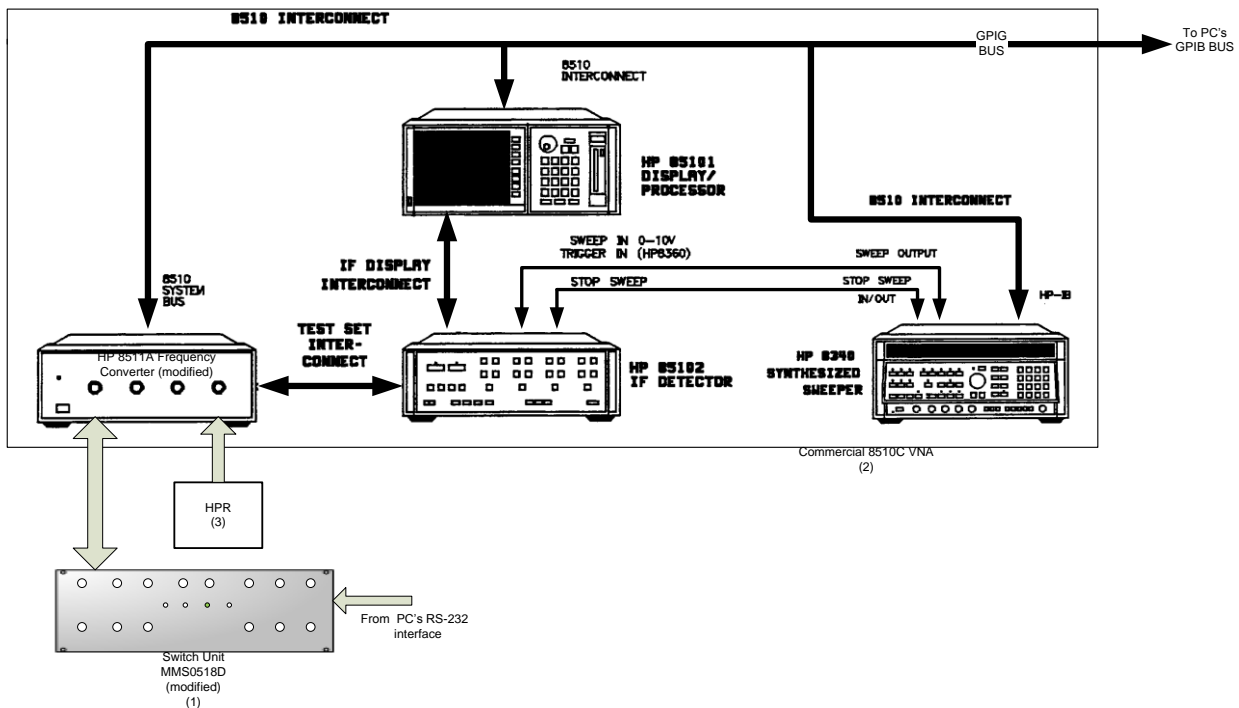


Figure 5.11 Four-port VNA system

---

### 5.1.8.) 8510C Network Analyzer System

Is the heart of the measurement system providing “real time” capability to the overall system. It includes: 1) a sweeper synthesizer generator with frequency range from 0.01 up to 40GHz used during S-parameter calibration, power calibration and S-parameter measurements; 2) A very fast Frequency Converter with frequency range from .045 up to 26.5GHz, used every time. However, during S-parameter, measurement it phase locks itself to the sweeper synthesizer generator (see blue-dotted-line in figure 5.12), otherwise it phase locks itself using external triggering from the harmonic phase reference by choosing a proper HPR’s harmonic near to the frequency where one intends to perform a measurement (see red-dotted-line in figure 5.12).

#### 5.1.8.3) Harmonic Phase Reference (HPR)

Generates a stable-phase frequencies “comb” to be used for 8510C VNA’s phase locking. It’s used during phase calibration, and when characterizing active components in nonlinear mode of operation, allowing one to measure impedances, power and time-domain-dependent DDUT’s performances at fundamental and harmonics , its phase behavior is crucial to the success of this kind of measurements to have good levels of accuracy.

#### 5.1.8.4) R-Channel Phase-Locking considerations

In the 4-port VNA system shown in figure 5.12 when single or two tone tests are performed, the VNA system is used as a very fast receiver, using the frequency list routine to measure the DDUT’s incident and reflected waves according to (4.1) and (4.2) using external triggering (HPR) after a proper s-parameter, power and phase calibration. This requires in general: 1) to introduce an external signal into the frequency converter’s reference channel of the VNA system ( $a_1$  or  $a_2$  in figure 5.12) 2) to introduce the DUT’s incident and reflected waves into the frequency converter module ( $b_1$  in figure 5.12) by

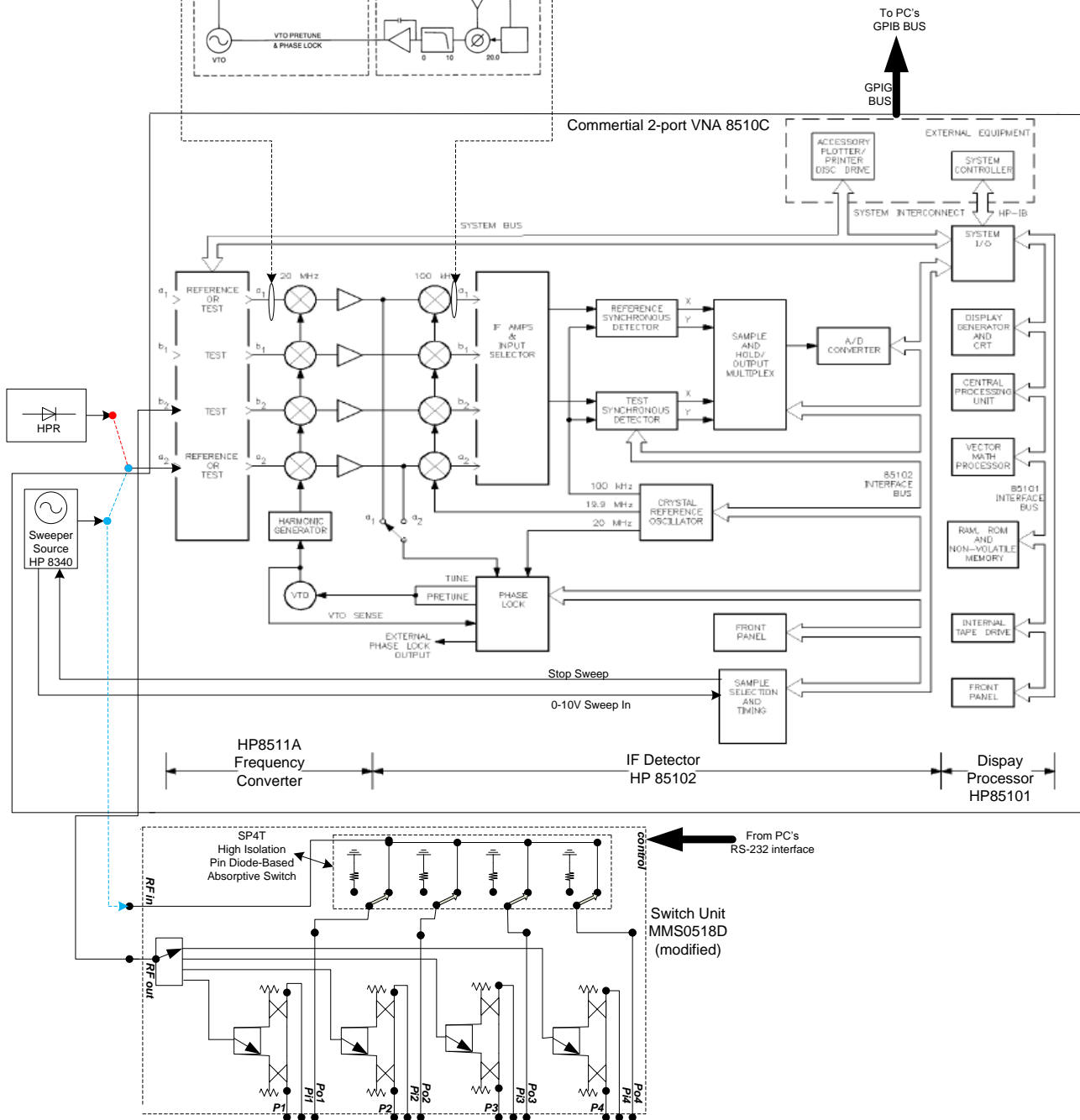


Figure 5.12 Four-port VNA system in detail.

using a proper signal separation section (switch unit). Both HPR and DUT signals must fulfill the next requirements so as to guarantee reliable measurements:

#### 5.1.8.4.1) Power Levels

Often the frequency converter receiver demands a maximum and minimum power level in order to guarantee its mixer/sampler's linearity and phase lock. For the HPR signal, certain requirements must be met so as that the R channel phase locks properly. First, the signal into the R channel must be within a specified power level throughout the entire HPR signal's bandwidth range otherwise proper phase lock will not occur. Obviously since, the HPR signal is a broadband one, proper filtering and/or attenuation at the R-channel port is essential [18], in order to guarantee R-channel phase lock (see table 5.1) throughout the entire frequency range of interest, while ensuring HPR's minimum input power specification (see figure 5.13).

Input Ports			
Connector type:	female 3.5 mm		
Impedance:	50 ohms nominal		
Damage level:	+13 dBm (20 mW) CW RF input <sup>2</sup>		
Port input power for phase lock:	Frequency:	Minimum:	Maximum:
	0.045 to 8 GHz	-40 dBm	-5 dBm
	8 to 20 GHz	-38 dBm	-5 dBm
	20 to 26.5 GHz	-35 dBm	-5 dBm

1. The performance parameters listed are characteristic of the HP 8511A/HP 8510. They are typical or nominal figures and are not field verifiable.

2. Do not exceed -5 dBm input to sampler for proper phase lock operation.

Table 5.1 HP 8510/HP 8511A Frequency converter Characteristics

For the DUT's signal (because phase lock is no matter) this can mean simply adding attenuation between signal separation section's output and the input of frequency converter port to protect the receiver. However, when characterizing hardly nonlinear DDUTs also proper filtering might be required in order to reduce the power in the frequency band of interest. It can also mean adding amplification to the stimulus signal if more power is required.

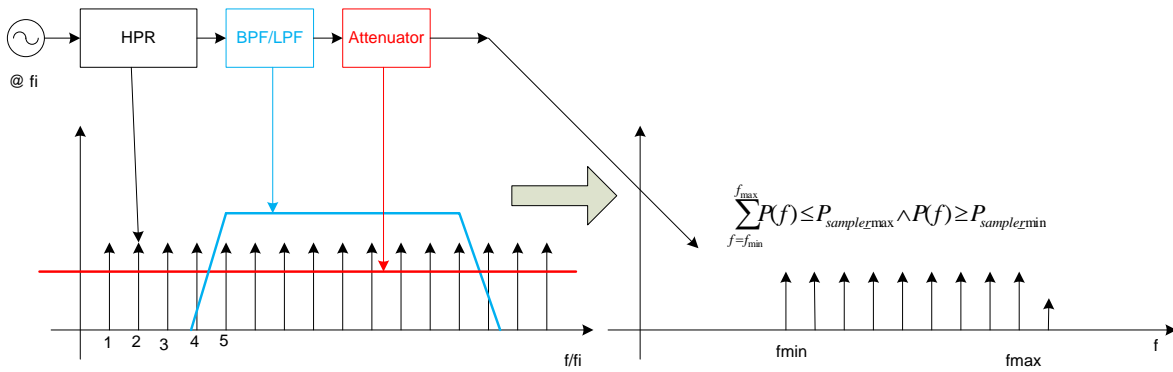


Figure 5.13 Power level on R-channel to guarantee phase lock.

### 5.1.8.4.2) HPR stability

For the 4 port VNA system in figure 5.12, the use of an accurate, stable HPR signal is required for accurate magnitude and relative phase measurements (power and time domain dependent DDUT’s performances). During a measurement the VNA will seek phase-locks automatically at a time onto each frequency of interest stored in its internal frequency list (which includes all frequencies of interest  $f_0, 2f_0, 3f_0, 4f_0$ , etc). Therefore, if the HPR signal is not accurate, the VNA will not receive the anticipated frequency of its internal frequency list due to (see figure 5.14): 1)The HPR might change its power level at a given harmonic of interest ; 2) it might change its phase relationship respect to the input frequency ( $f_i$ ) abruptly 3) or worse it might provide a frequency too far from that desired by the VNA frequency list. In the first and third cases, phase lock can possibly not even occur. In the second case, that inaccuracy is transferred to the measurement results.

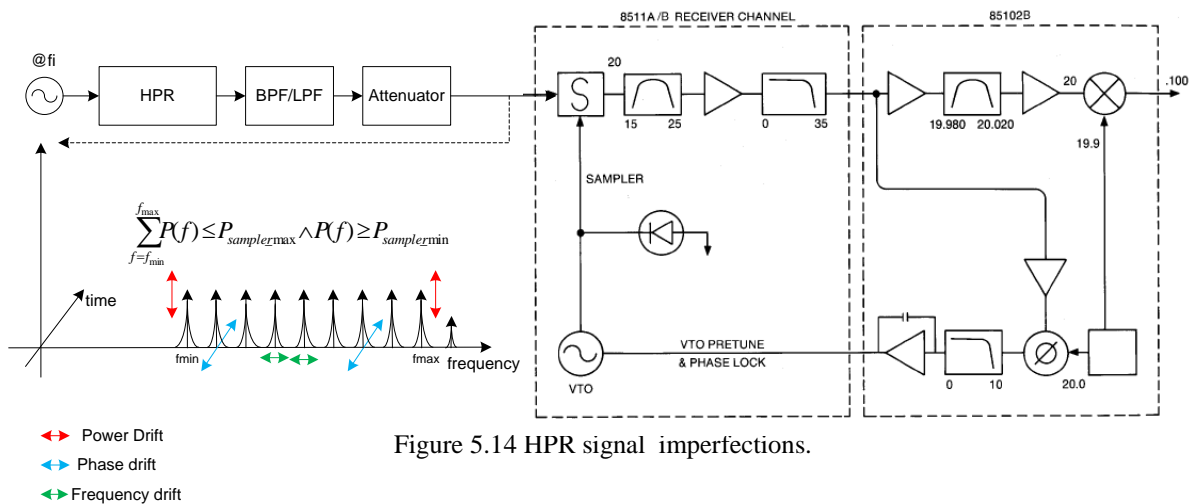


Figure 5.14 HPR signal imperfections.

This HPR signal accuracy and stability requirement can be explained with the help of the figure 5.14. As the HPR signal is present at the R-channel, the 8511A frequency converter is stepped through its internal frequency list range (i.e.  $f_0$ ,  $2f_0$ ,  $3f_0$ ,  $4f_0$ , etc). The 8511A frequency converter phase-locks onto the nearest incoming  $k$ -th harmonic of the input signal ( $kf_i$ ) and down converts it to 20 MHz. This 20 MHz signal continues on, inside the 8510C, and is further down converted to 100 kHz. The 100 kHz signal is then processed by the 8510C internal computer to extract information about the original  $k$ -th harmonic signal ( $kf_i$ ). This information is sent to the PC.

Therefore, the HPR signal must be as stable and accurate as possible in order to provide the  $k$ -th harmonic of the input signal ( $kf_i$ ) signal so that, this will be properly near to the frequency in the internal frequency list. If the  $k$ -th harmonic of the input signal ( $kf_i$ ) is too far from the expected receiver's frequency (i.e.  $f_0$ ,  $2f_0$ ,  $3f_0$ ,  $4f_0$ , etc), then it might lie outside the acquisition range of the PLL. The phase-lock algorithm will not work and a phase-lock error is displayed. However, the latter can be avoided by using the frequency to drive the HPR ( $f_i$ ) as an integer multiple of the fundamental ( $f_0$ ) which one intends to characterize the DDUT. However, since the 8511A is a sampler-based receiver, care must be taken to know how small  $f_i$  could be. In this sense, one has to account for the method that is used to down convert the original HPR signal to 20 MHz in figure 5.14, it is the sampling method which presents all the frequency harmonics of the test set voltage tuned oscillator (VTO) to the incoming HPR signal (see figure 5.14). The VTO is pre-tuned and phase-locked so that one of its harmonics is mixed with the incoming HPR signal to give exactly 20 MHz. An internal 20 MHz band pass filter (BPF) stops all other  $f_i$ 's harmonics and VTO's harmonics, which are not at 20 MHz. However, since the incoming HPR signal is actually composed of many different frequency components, it is possible that: 1) the BPF allows to more than one  $f_i$ 's harmonic to pass through it, this can be avoided, if  $f_i$  is greater than the BPF's pass band (10MHz in figure 5.14). 2) Other components of the HPR signal will combine with a different harmonic of the VTO and also produce a signal at 20 MHz. This spurious response will then proceed through the internal 20 MHz BPF, along with the desired signal, and cause a spurious measurement result that subsequently might



affect the relative phase measurement's accuracy (time domain based DDUT's performances). This spur problem can be handled in software [19]. The other remaining problems related with the HPR signal stability will be treated in the next section.

## 5.2) DRIFT ERRORS

They are errors due to the instruments or test-equipment changes before, during or after error correction procedure, so they cannot be removed from the measurements or measurements carried out during calibration procedure. They are primarily caused by temperature variation and some of them can be removed by additional calibration. The rate of drift determines how frequently additional calibrations are needed. However, by constructing a test environment with a stable ambient temperature, drift errors can usually be minimized. Drift error has two categories: frequency and phase drift of the signal source and instrumentation drift. In this section the former will be described. In figure 5.12 there are basically three types of signal source used by the four-port VNA system [20]:

- **CW Generators (to provide power to both the DDUT and the HPR)**
  - to generate a single frequency, fixed sine wave.
- **Synthesized Sweeper Generators (inside the 8510C VNA system)**
  - to sweep over a range of frequencies
  - may be phase continuous
- **“Comb” Spectrum Generator (HPR)[21]**
  - Frequency, amplitude and phase calibration of broadband receivers.
  - Generation of local oscillator in a totally coherent system.
  - Frequency marking.
  - Generation of reference frequencies for phase locking systems.
  - Sampling phase-lock systems as a gating pulse or as the local oscillator.

It produces simultaneously a line at each multiple of a given input frequency  $f_i$  (from a CW or Swept generator) [22]. They are built by using active devices which can change the reactance between two terminal among two different states abruptly (see figure

5.15). Some technology that is used for this purpose are: Step Recovery Diodes, Non Linear Transmission Line, Indium phosphide monolithic microwave integrated circuit [23], etc.

### 5.2.1) Frequency Drift

As CW and Sweeper Generators depend of the internal or external stable reference oscillator’s precision used in the test bench (each instrument has one) which depends on the temperature and its long-term stability [24]. References, usually at a frequency of 10 MHz, are implemented as temperature-compensated crystal oscillators (TCXO) or oven-controlled crystal oscillators (OCXO) as shown in figure 5.16. The long-term stability is only effective, however, if the instrument remains permanently switched on [25]. If the instrument (or the OCXO) is switched off and on again, measurements take place whereby the oscillator frequency assumes another value. So, it is good practice to select among all the test bench’s measurement equipment that is available, which will be the best used as a frequency reference. If the measurement application requires better frequency accuracy and stability, one can override the internal frequency standard and provide other own high-stability external frequency.

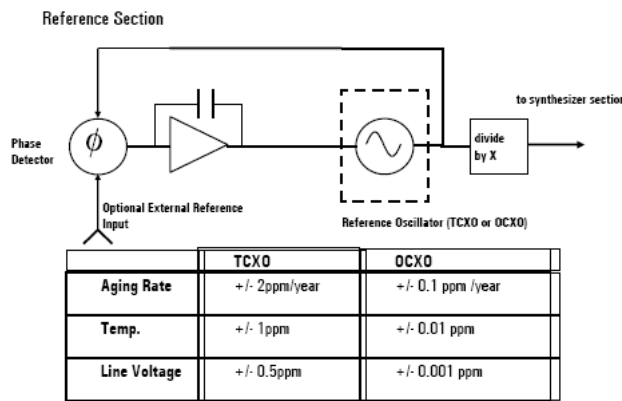


Figure 5.14. Block diagram of a Generator Reference Section

---

On the other hand, for “comb” spectrum generator, because it is driving using a CW or Sweeper generator, the former’s frequency drift specification depends upon the latter’s frequency drift specification, assuming no-frequency modulation effects on the non-linear device used to build the “comb” spectrum generator.

### **5.2.2) Phase Drift**

Includes: -phase noise (specified at a given frequency and at a given frequency offset in respect to the carrier) as shown in figures 5.17,5.18;- phase stability (by keeping temperature controlled); -phase temperature sensitivity; -phase input power sensitivity; -phase harmonic input and output impedance sensitivity [26], and -output phase noise due to changes into the input phase noise [27].

For Synthesized Sweeper Generators or CW generators often it’s only specified by the phase noise, because they don’t generate a broadband signal at their output, in other words, they generate a narrowed frequency signal one at a time (see figure 5.17), unlike “comb” spectrum generators, which generate a broadband signal simultaneously, it means, it generates simultaneously a lot of narrowed frequency signals at each line multiple of the input frequency, so that in this type of generator it’s crucial knowing its behavior when different conditions change (see figure 5.18).

#### **5.2.2.1) Phase noise**

Is spread power over a small range of frequencies around the carrier due to random noise, and is mathematically modeled as random phase modulation. Its units are [dBc/Hz]: dB down from the carrier in a 1 Hz bandwidth. Phase noise is specified at a frequency offset from carrier output. Phase noise may be directly measured from the spectrum of a source. This method requires that the phase noise of the analyzer be much better (~10dB) than the phase noise of the source being tested. Often, the phase noise of a source is measured using test equipment that has been optimized for this purpose.

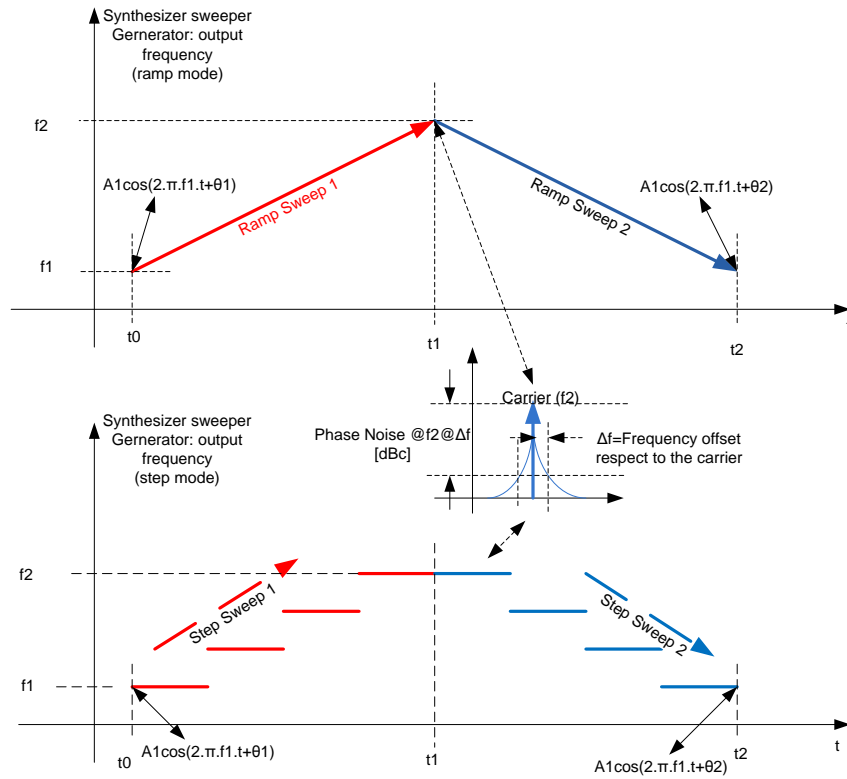


Figure 5.17 Synthesized Sweeper Generator's line spectrum under two mode of operation, and phase noise specification.

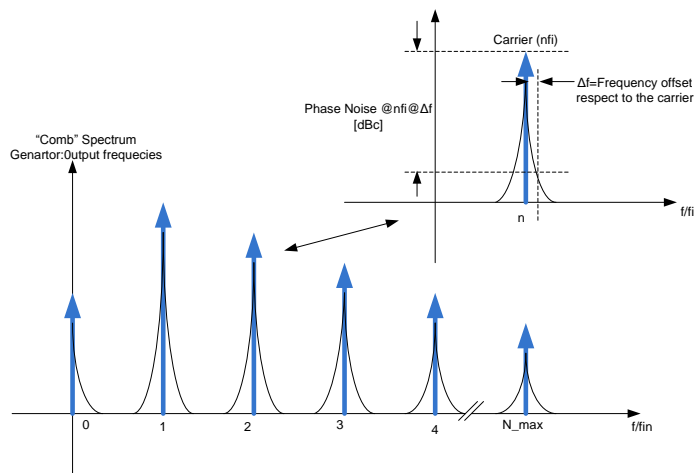


Figure 5.18 "comb" spectrum generator's output line spectrum, and phase noise.

One has to account that as shown in figure 5.15, the “comb” generator’s phase noise specification depends on the input source phase noise [27], so it’s good practice drive them by using low phase noise sources, so that, it may operate at a lower  $f_i$  frequencies. Figure 5.19 shows the phase noise that a comb generator would add to a typical source by plotting the added dB of phase noise for different sources with various amounts of phase noise. This plot assumes that the actual phase noise of the comb generator is fixed to 148dBc/Hz, the number may in fact be lower or higher depending on the comb generator. The plot shows that for a 180dBc/Hz 100MHz source, the added phase noise would be less than 1dB. This data demonstrates that the added phase noise is basically negligible for most practical sources.

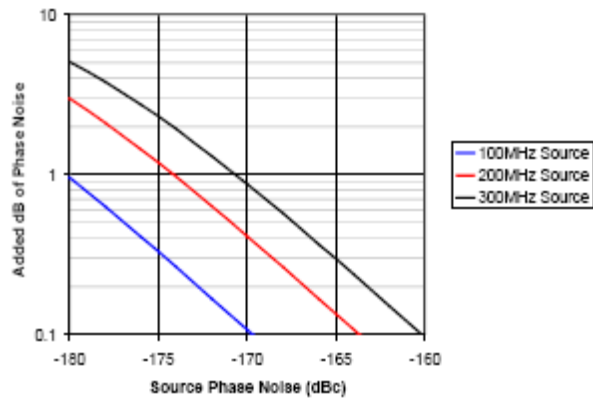


Figure 5.19) Comb Generator output phase noise due to changes on phase noise at the input

Figure 5.20 shows the phase noise specification of a commercial Non Linear Transmission Line (NLTL)-based “comb” generator (blue line), driven with a CW generator at a given input power (not shown in figure). Red line is the comparable phase noise that a crystal oscillator (165dBc/Hz phase noise at 10 kHz) would have if multiplied up to the same harmonic with  $20\log(n)$  rule. This shows that the measured residual phase noise is well below the phase noise due to such a source at the same harmonic.

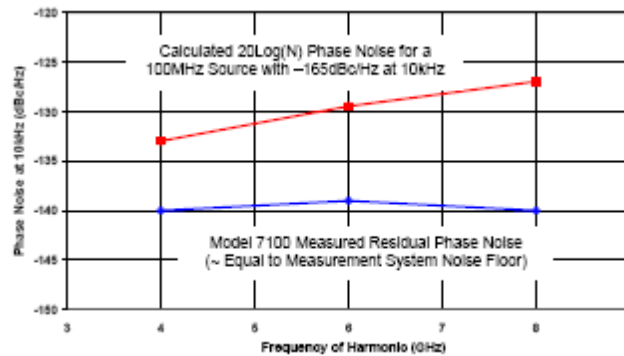
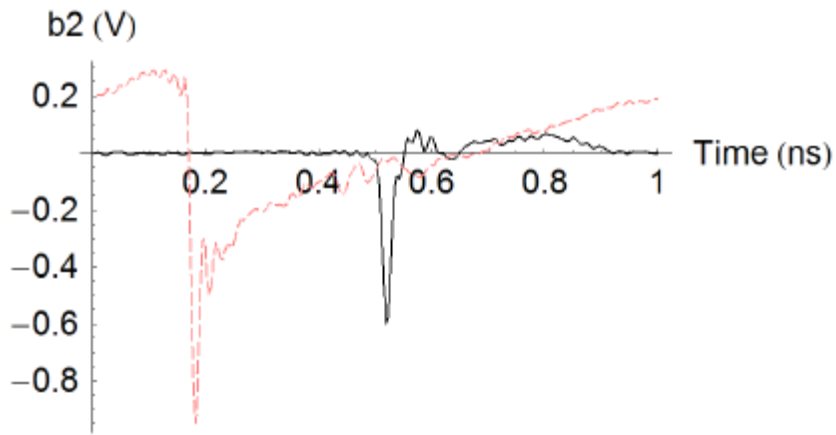


Figure 5.20. Measured Residual Phase Noise of a commercial comb generator (blue line).

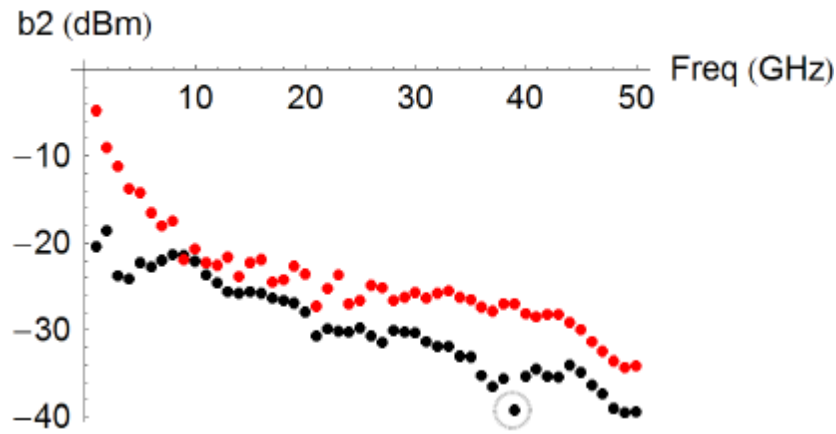
### 5.2.2.2) Others terms of phase drift

As discussed earlier for comb generators, it's crucial to know the parameters such as: phase stability (by keeping temperature controlled), phase temperature sensitivity, phase input power sensitivity, phase harmonic input and output impedance sensitivity. This guarantees that during error correction procedure and measurements, the phase of the reference signal used by the VNA system doesn't change or if it changes, its changes are negligible .

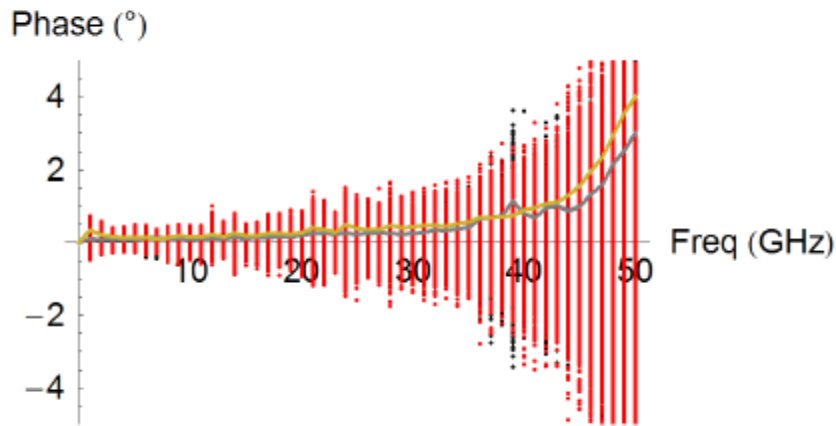
The synthesizer sweeper generator loses the synthesized frequency's phase, sweep to sweep and it cannot be used as a generator which keeps its phase constant in respect to the time. Hereby one must generate simultaneously all the measurement frequencies of interest by using a "comb" spectrum generator and be sure that this way of frequency generation guarantees a well known phase stability under the above conditions. Figure 5.21 shows a comparison between two different commercial "comb" generators (black and red line) under different conditions of operation that one can perform easily in a lab in order to characterize a HPR. This analysis includes time and frequency domain measurements and the measurement's statistical analysis (for each experiment their 1- $\sigma$  standard deviation (straight line) are shown as a function of time only for phase versus frequency graphs).



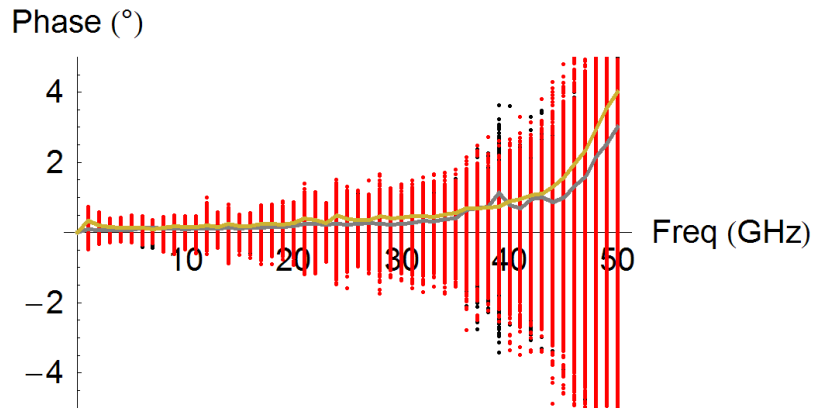
a) Comb generators' Output Pulse Shape



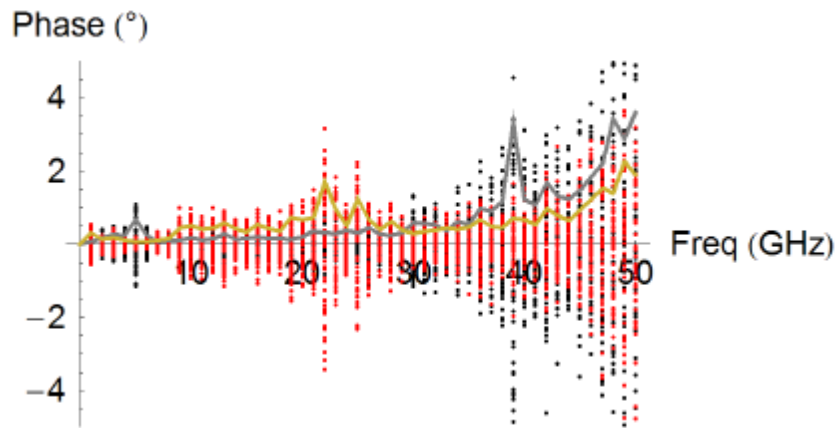
b) Comb generators' output line spectrum



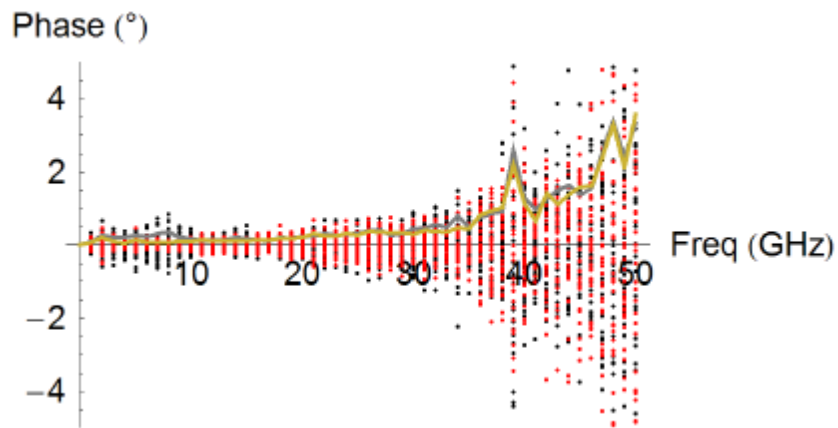
c) Comb generators' phase stability (temperature controlled) (dotted line)



d) Comb Generators' temperature sensitivity (dotted line)

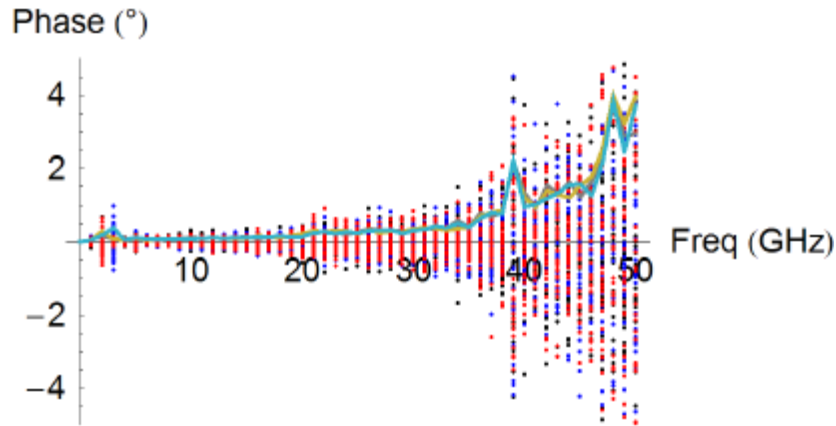


e) Comgenerators' Input power sensitivity(dotted line)



f) Comb generators' harmonic input impedance sensitivity (up to 3fi) (dotted line)





g) Comb generators' Harmonic output impedance sensitivity (up to 3fi) (dotted line)

Figure 5.21 Comb generator's tests

However it's important to point out that depending on the calibration strategies used in order to perform the phase calibration ( $\angle k_{11}$ 's or  $\angle k_{ii-aux}$ 's computation) they will determine what kind of HPR's pre-characterization will be needed and the minimum needed to guarantee good levels of accuracy. For instance, technologies such as LSNA and NVNA [28][29] used to characterize RF devices in non linear region of operation demand a deep knowledge of the HPR.

### 5.3) HARMONIC PHASE REFERENCE (HPR) IMPLEMENTATION

The Harmonic Phase Reference used in this thesis work was constructed as depicted in figure 5.22. The key component is a commercial diode based-detector used as a nonlinear device in order to generate a stable phase-amplitude frequencies' "comb" up to the fifth harmonic of the fundamental ( $5f_0$ ) which will be used for the VNA's R-channel phase locking during the phase calibration procedure and the DDUT's nonlinear behavior measurements. When fed at the input with 0dBm @2GHz ( $f_0$ ) sinusoidal signal, a hardly distorted sinusoidal signal will appear at the output. In the frequency domain this signal represents a multi-harmonic signal existing out of the superposition of a fundamental frequency component of 2GHz and significant harmonics up to about 10GHz. A CW or

sweeper generator can be used to generate the 2GHz ( $f_0$ ) signal, which goes into a power splitter, one part provides the trigger signal that will feed the time domain receiver (MTA/SO) trigger input during phase calibration procedure and also can be used to feed the stimulus section (varying the DDUT's input power level by means of a digital attenuator via PC in figure 5.2), the other part goes into a power amplifier ( $A_1$ ) which boosts the signal power to hit the diode-based detector, whose reflected power wave is coupled by means of a 3dB coupler. The coupled-reflected power wave outgoing from the coupler goes into another power amplifier ( $A_2$ ) which boosts it.

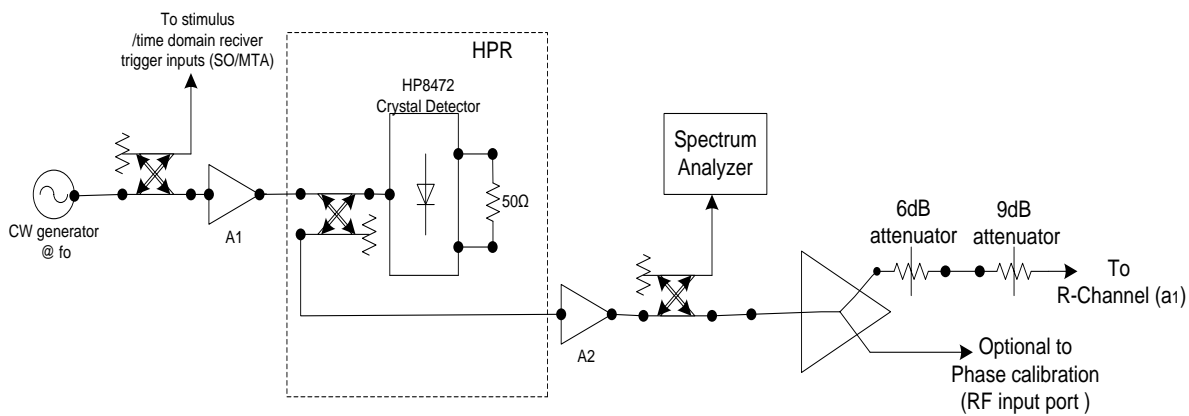


Figure 5.22 Construction of the HPR

A part of the power amplifier's output power ( $A_2$ ) is coupled to the spectrum analyzer (S.A) in order to look at the HPR's line spectrum and fit it (its power level and harmonic number) The other part goes into a power splitter: one part provides the HPR signal required at the RF input port chosen to inject it during phase calibration procedure, the other part goes into a pair of attenuators which will reduce the signal to an acceptable level, such that the HPR signal will not cause nonlinear effects to the VNA's R-channel. Note that, to guarantee conditions depicted in figure 5.13. filtering isn't required because in this case, just a few harmonics are present in the HPR output .

### 5.3.1 ) Characterization of the Harmonic Phase Reference (HPR)

As discussed in chapter IV an appropriate phase calibration and DDUT's nonlinear behavior measurements require an amplitude-phase stable HPR signal in order to guarantee VNA's R-channel phase locking. Furthermore, since to perform the phase calibration procedure the approach used in this thesis work doesn't require an accurate characterization of the HPR such as LSNA/NVNA technologies, just controlled temperature ( $\approx 25$  °C) and without temperature control (environment) measurement conditions have been considered as a perturbation of the "in house made" HPR shown in figure 5.22. On other words, only short-term temperature stability/sensitivity have been examined. The HPR's characterization lasted three days and included the following:

-Day 1: switch on the HPR under temperature controlled conditions, wait until the HPR reaches its steady state, then by using an MTA running 500 magnitude and phase measurements up to the fifth harmonic of interest ( $5f_0$ ).

-Day 2: switch on the HPR without temperature controlled conditions, immediately after by using an MTA running 500 magnitude and phase measurements up to the fifth harmonic ( $5f_0$ ). Then without switching off the HPR, activate the temperature control, wait until the HPR reaches its steady state, an once again launch 500 magnitude and phase measurements up to the fifth harmonic ( $5f_0$ ).

-Day 3: same as Day 1. Measurements results are shown in figures 5.23-26.

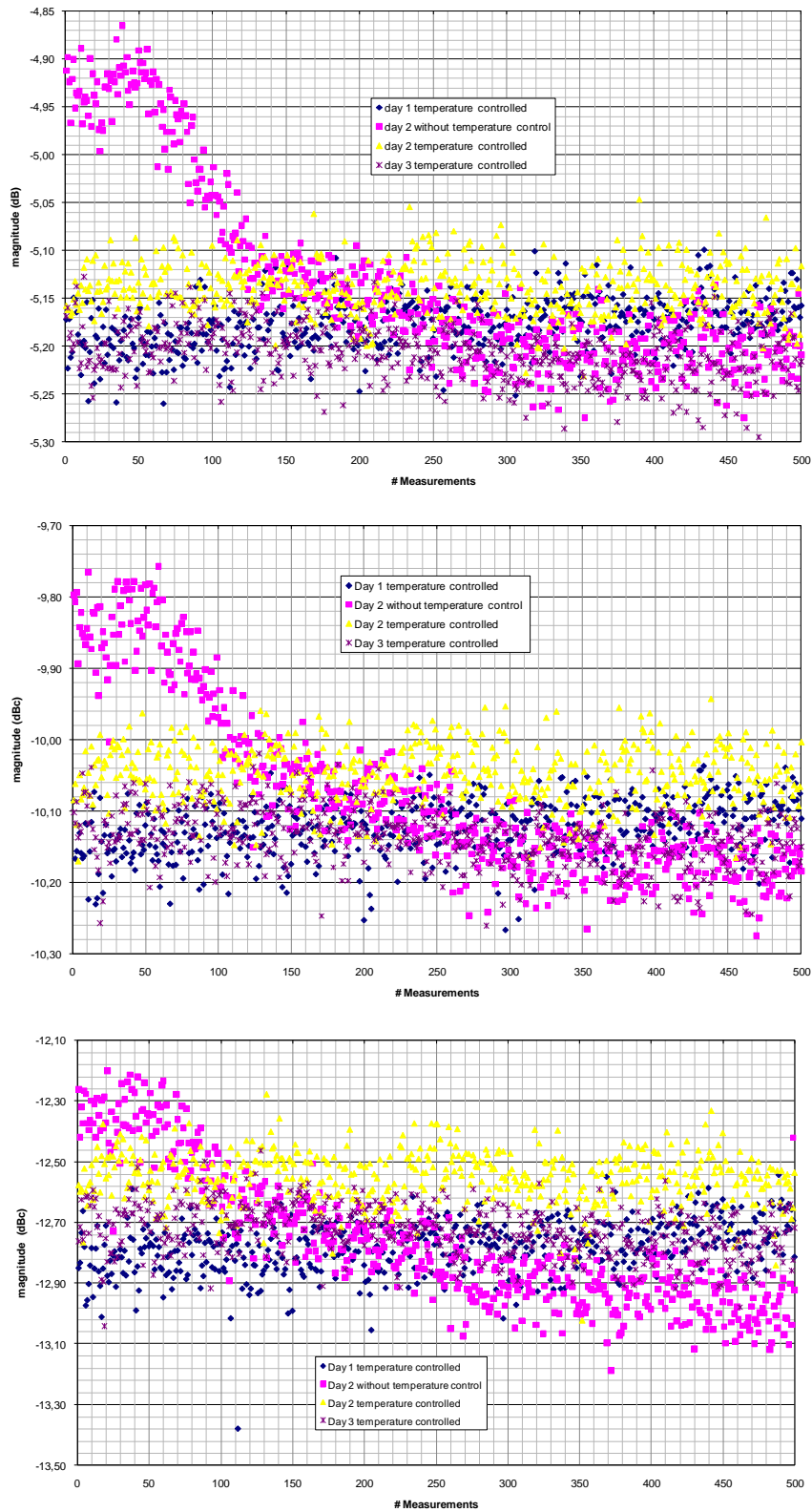


Figure 5.23 Magnitude measurements: upper( $f_0$ ) middle ( $2f_0$ ) lower( $3f_0$ )

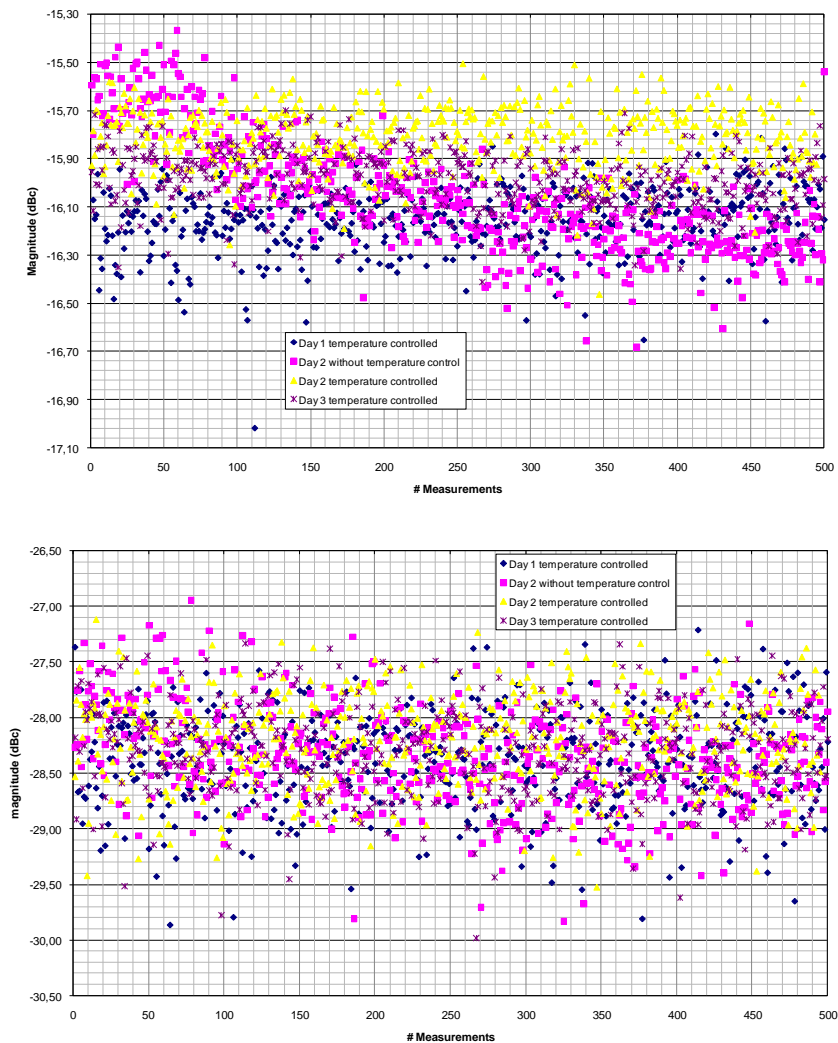


Figure 5.24 Magnitude measurements: upper( $4f_0$ ) lower( $5f_0$ )

Magnitude measurements reveals some important facts:

- the worst case of magnitude deviation occurs while the HPR is reaching its steady state independently of the harmonics considered.

- nearly  $\pm 0.5\text{dBm}$  of the magnitude deviation one can guarantee up to the fourth harmonic ( $4f_0$ ) with or without temperature control.

- the fifth harmonic magnitude variation is nearly  $\pm 3\text{dBm}$  which could be considered unreliable looking at the VNA's R-channel power level specification in table 5.1.

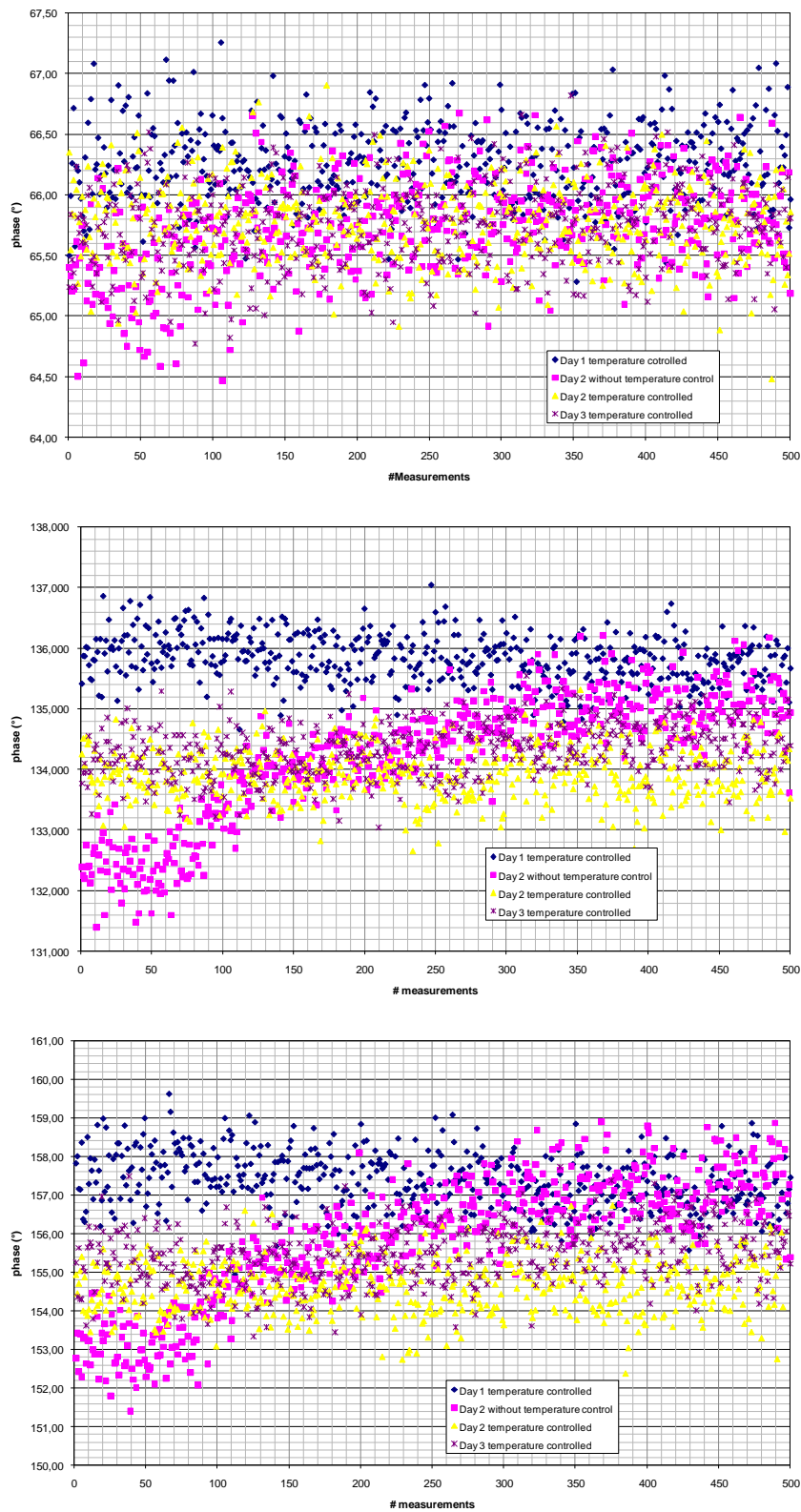
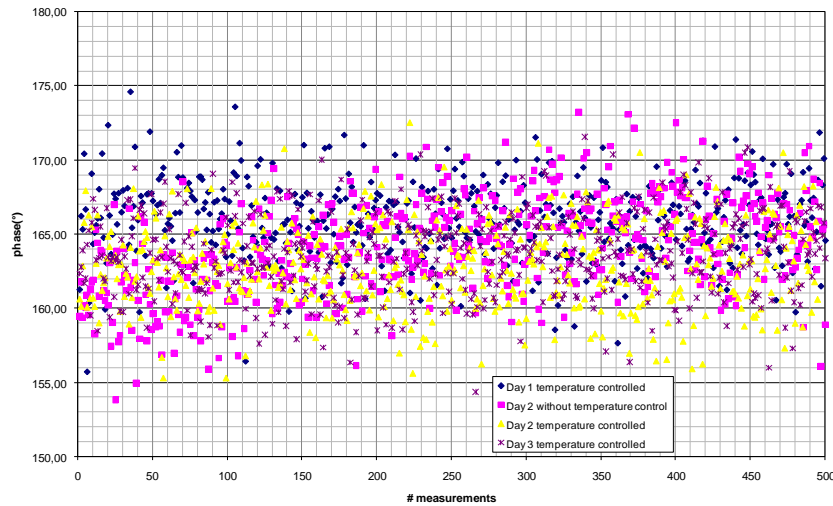


Figure 5.25 Phase measurements: upper(2f<sub>0</sub>) middle(3f<sub>0</sub>) lower(4f<sub>0</sub>).

Figure 5.26 Phase measurements:  $5f_0$ 

On the other hand, phase measurements reveals that:

-once again the worst case of phase variation occurs while HPR is reaching its steady state.

- there is nearly  $\pm 2^\circ$  of phase deviation in respect to the fundamental ( $f_0$ ), one can guarantee up to the fourth harmonic ( $4f_0$ ).

-the fifth harmonic ( $5f_0$ ) has got nearly  $\pm 10^\circ$  of phase deviation which could influence significantly both calibration and measurements.

However, one has to take into account that depending on the frequency range, the measurement results of the HPR's magnitude and phase deviations could be strongly affected by the instruments used to carry out the measurements (SO, MTA, etc) [30]. In fact an MTA at 10GHz ( $5f_0$ ) introduces a phase uncertainty around  $\pm 10^\circ$  which is the fifth harmonic phase variation. To avoid these undesired high phase measurement's uncertainty, a compact sampling oscilloscope (SO) seems the best tool.

---

**References**

- [1] Ferrero, A. Teppati, V. "A Novel Active Differential/Common-Mode Load for True Mixed-Mode Load-Pull Systems" Dept. of Electron. Eng., Polytechnic of Torino; Microwave Symposium Digest, 2006. IEEE MTT-S International 11-16 June 2006 1456-1459 San Francisco, CA.
- [2] Van der Heijden, M.P.; Hartskeerl, D.M.H.; Volokhine, I.; Teppati, V.; Ferrero, A. "Large-signal characterization of an 870 MHz inverse class-F cross-coupled push-pull PA using active mixed-mode load-pull" Radio Frequency Integrated Circuits (RFIC) Symposium, 2006 IEEE Volume , Issue , 11-13 June 2006 .
- [3] Mahmoudi, R., Spirito, M., Valk, P., and Tauritz, J. L., "A Novel Load and Source Tuning System for Balanced and Unbalanced WCDMA Power Amplifiers". *Digest of 54th ARFTG*, December 1999.
- [4] Product Note 75 DLPS, a Differential Load Pull System, Copyright 2003 Focus Microwaves Inc. All rights reserved May 2003.
- [5] M. Spirito M. P. van der Heijden M. de Kok L. C. N. de Vreede. A Calibration Procedure For On-Wafer Differential Load-Pull Measurements 61st ARFTG Conference Digest Measurement Accuracy Philadelphia, Pennsylvania June 13, 2003
- [6] D. E. Bockelman, "The theory, measurement, and application of mode specific scattering parameters with multiple modes of propagation," Ph.D. dissertation, Dept. Elect. Comput. Eng., Univ. Florida, 1997.
- [7]Dunsmore, J."New modeling results for non-linear differential amplifier behavior, including two-tone TOI" response Microwave Conference, 2005 European Volume 1, Issue , 4-6 Oct. 2005.
- [8] J.Dunsmore, "New Methods & Non-Linear Measurements for Active Differential Devices", Microwave Symposium Digest, 2003 IEEE MTT-S International ,Volume: 3 , 8-13 June 2003, pages:1655 – 1658.
- [9] Gian Luigi Madonna, *Member, IEEE*, and Andrea Ferrero, *Member, IEEE* "Simple Technique for Measuring Source Reflection Coefficient While Characterizing Active



Devices” Ieee Transactions On Microwave Theory And Techniques, Vol. 50, No. 2, February 2002.

[10] G.P. Bava, U. Pisani, V. Pozzolo, “Active Load Technique for Load-Pull Characterization at Microwave Frequencies” Electronic Letters 18th February 1982, Vol. 18, No. 4, pp. 178-180.

[11] [http://www.nardamicrowave.com/east/UserFiles/atten\\_notes.pdf](http://www.nardamicrowave.com/east/UserFiles/atten_notes.pdf)

[12] Micro Lambda, Inc. Product Technology YIG-tuned Filters Shrink Size to 1” Cubes Fremont, USA June 1994

[13] Teledyne Microwave. “Microwave YIG filters the complete microwave solution” USA California April 2006.

[14] G.P. Bava “dispensa corso microonde” Professore Ordinario DELEN -Dipartimento of Electronic III Facolta' Di Ingegneria industriale e dell'informazione Campi elettromagnetici .Charter 2 pag 18-23 .Didactic period 2006-2007.

[15] A. Ferrero, Active load or source impedance synthesis apparatus for measurement test set of microwave components and systems, United States Patent n. 6509743, 12 June 2000.

[16] Hewlett-Packard Company, *HP 8510C Network Analyzer: On Site Service Manual*, Santa Rosa, CA, Aug. 1991.

[17] Ing. Chiara Soragna-PAF, Prof. Andrea Ferrero-Polytechnic of Torino “MMS LINE Multiport S-parameter System” <http://www.pafmicro.com/products.htm>

[18]Agilent Technologies “Improving Network Analyzer Measurements of Frequency-translating Devices” Application Note 1287-7 Printed in U.S.A. April 2000

[19] Agilent Technologies, Inc. Agilent 8510 Network Analyzer Product Note 8510-7° “Microwave Component Measurements Amplitude and Phase Measurements of Frequency Translation Devices Using the Agilent 8510C Network Analyzer” Printed in USA, July 13, 2006

[20] Agilent Technologies “Signal Sources Basis” Application notes.

[21]Krakauer,S.S “Harmonic Generation, Rectification and Lifetime Evaluation with Step Recovery Diode” Proc.IRE, July 1962,pp.1665-1676.

[22] Hewlett-Packard company “Harmonic Generation Using Step Recovery Diodes and SRD Modules” AN 920.October 1984.

- 
- [23] Agilent U9391C Comb Generator from 10 MHz to 26.5 GHz Technical Overview Agilent Technologies, Inc. 2008 Printed in USA, July 18, 2008.
- [24] Volker Janssen, Roland Minihold, Christoph Rauscher . “Fundamentals of Spectrum Analysis” First edition 2001 Muchen-Germany.
- [25] Beck, B.: Understand the Effects of Retrace and Aging in OCXOs. *Microwaves & RF*, November 1998, p. 72.
- [26] Gaining advanced insight in the phase stability of comb generators using a Large-Signal Network Analyzer Guillaume Pailloncy, Marc Vanden Bossche *NMDG Engineering, Belgium*
- [27] Residual Phase Noise Measurements On Low Phase Noise Comb Generators, Picoseconds Pulse Labs, January 2005.
- [28] Tom Van den Broeck and Jan Verspecht,” Calibrated Vectorial Nonlinear-Network Analyzers,” 1994 IEEE MTT-S International Microwave Symposium Digest, Vol. 2, pp. 1069-1072, May 1994.
- [29] Agilent Technologies “Breakthrough Nonlinear Vector Network Analyzer Applications” 2008-07-17 .
- [30] Dylan Williams, Paul Hale, and Kate A. Remley “Sampling oscilloscope as microwave instruments” National Institute of Standards and Technology (NIST) August 2007 Boulder, Colorado, USA.

# **CHAPTER VI**

## **MEASUREMENT RESULTS**

---

## 6.1) MEASUREMENT RESULTS

The fundamental concepts of nonlinear differential amplifier parameters have been established in chapter II. The methods of measurement have also been thoroughly explored, and a specialized measurement system has been described. The error correction and measurement accuracy of such measurement system have been shown. Now, these tools of mixed-mode propagating theory and the measurement system can be applied to the analysis of some important RF devices, structures, and circuits. This chapter will focus on nonlinear differential power amplifiers, and the incident/reflected power waves based characterization approach will provide new insight into the performance of such components in both frequency and time domains. The simplified scheme of the test bench for harmonic load-source pull and time domain at the Polytechnic of Turin is depicted in figure 6.1.

As pointed out in previous chapters, before carrying out any measurement a suitable calibration procedure is required. S-parameter, Power, and Phase calibration procedures setup are shown in figures 6.2, 6.3 and 6.4 respectively. The experimental experience consisted of the characterization of two differential commercial amplifiers the TC22BP ( $AUT_1$ ) by Agilent and the ADC8351 ( $AUT_2$ ) by Analog Devices. The measurements involved a load-pull and a source-pull characterization. The common- and differential-mode load, both at the fundamental and harmonics were tuned. Source-pull measurements showed no significant results, this may be due to the good input/output isolation of the devices and test setup. In both cases the fundamental frequency was 2GHz and the time domain waveforms were reconstructed through frequency domain readings up to the fifth harmonic (10GHz).



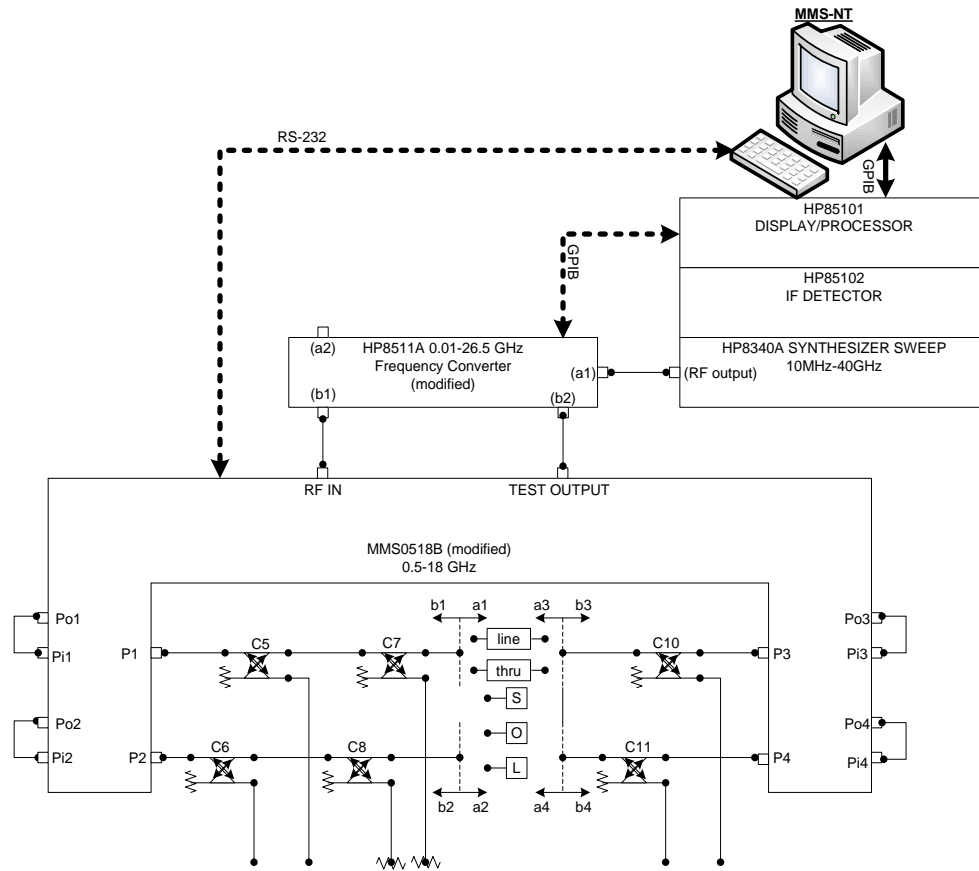


Figure 6.2 Test bench for differential harmonic load-source pull and time domain during S-parameter calibration procedure.

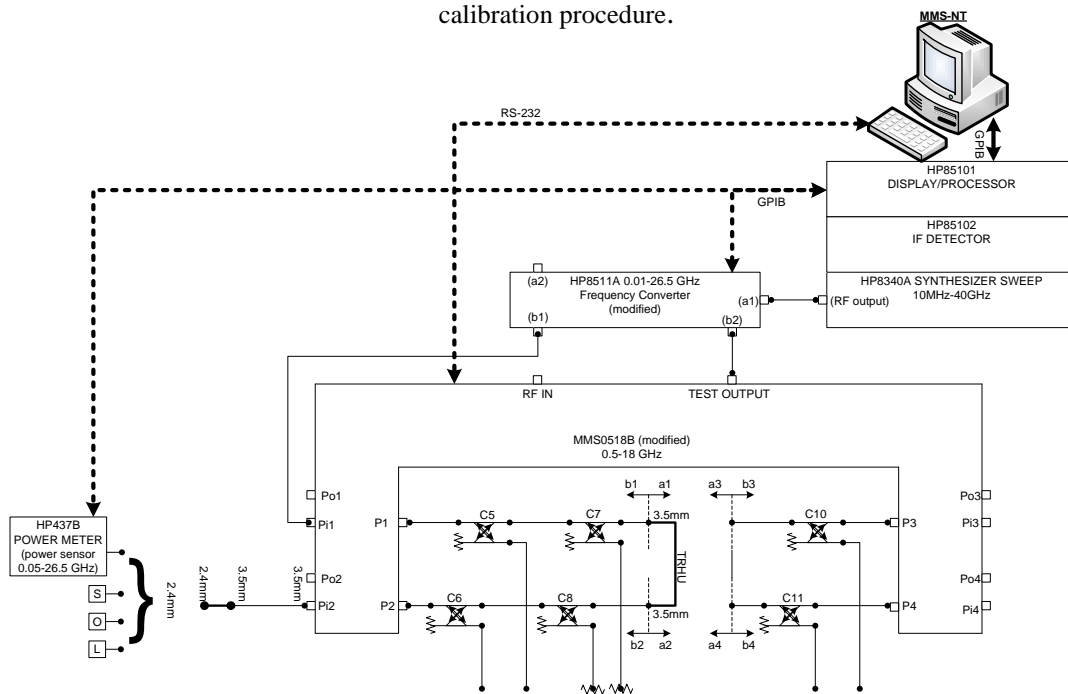


Figure 6.3 Test bench for differential harmonic load-source pull and time domain during Power calibration procedure.

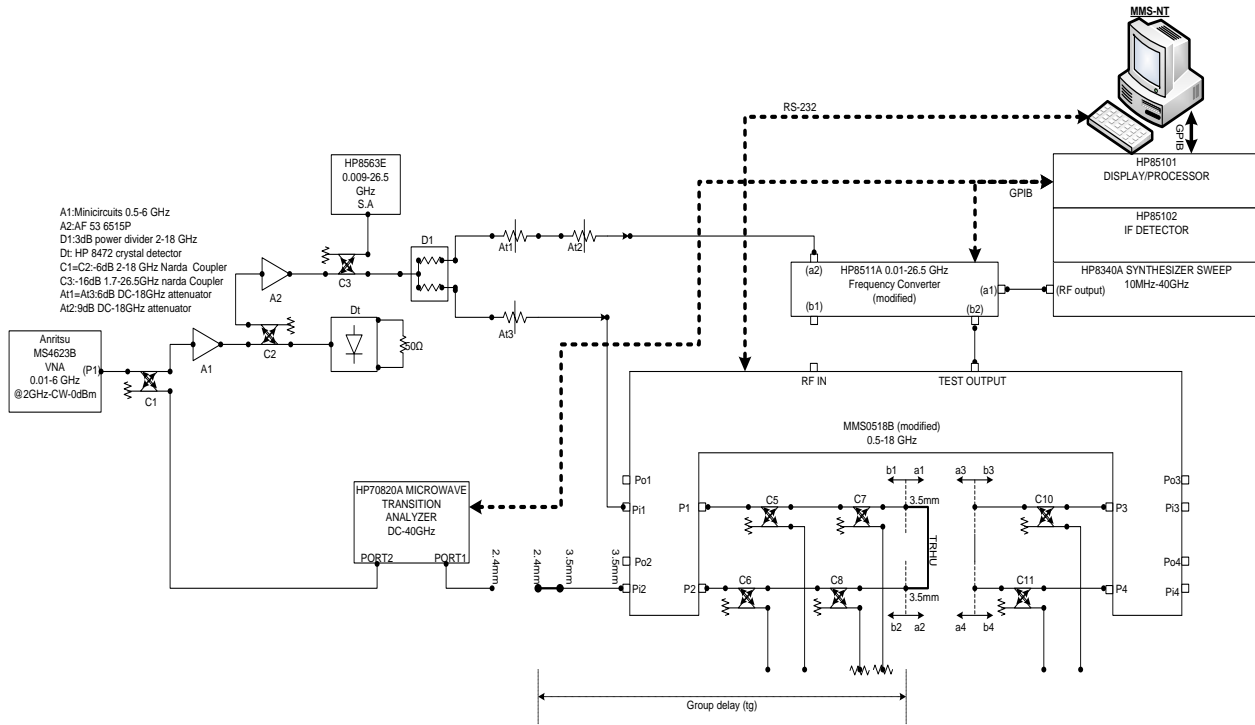
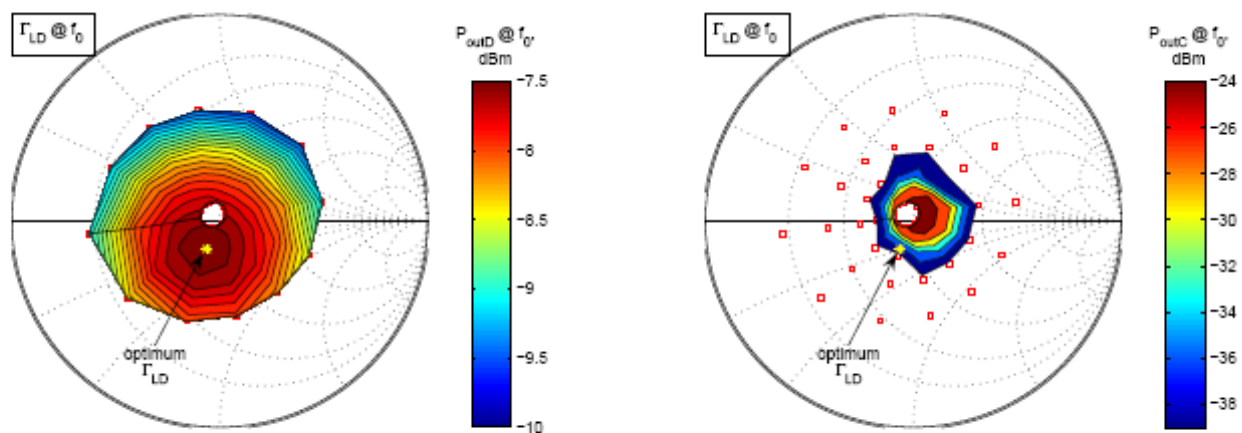


Figure 6.4: Test bench for differential harmonic load-source pull and time domain during Phase calibration procedure.

For (AUT<sub>1</sub>) a differential-mode load map at the fundamental (2GHz) was done (see figure 6.5). The optimum differential-mode load at the fundamental, in order to maximize the output power at 1 dB compression of the differential-mode gain ( $P_{OUTd-1dB@f_0}$ ) is reached slightly off the 100Ω load condition, and interestingly the common-mode content drops down when reaching the optimum load condition. Optimum is  $\Gamma_{Ld-OPT} = 0.154 - 115^\circ$ .

Then, for the same device (AUT<sub>1</sub>) a differential input power sweep ( $P_{IND@f_0}$ ) was performed (see figure 6.6 and 6.7). Power readings up to the fifth harmonic ( $5f_0$ ) were done. Both differential and common mode operating power gain and output power at the fundamental are shown in figures 6.8 and 6.9 The mixed mode output impedances at all frequencies of interest were fixed to  $Z_D=100\Omega$  and  $Z_C=25\Omega$ . Finally in order to verify the test bench time domain capabilities, from the previous power sweep a set of three points has been chosen. The time domain waveforms at the output of each propagating mode were measured up to the fifth harmonic (see figures 6.10-6.12).



(a) Differential-mode output power

(b) Common-mode output power

Figure 6.5: (AUT<sub>1</sub>) differential-mode load map at fundamental.



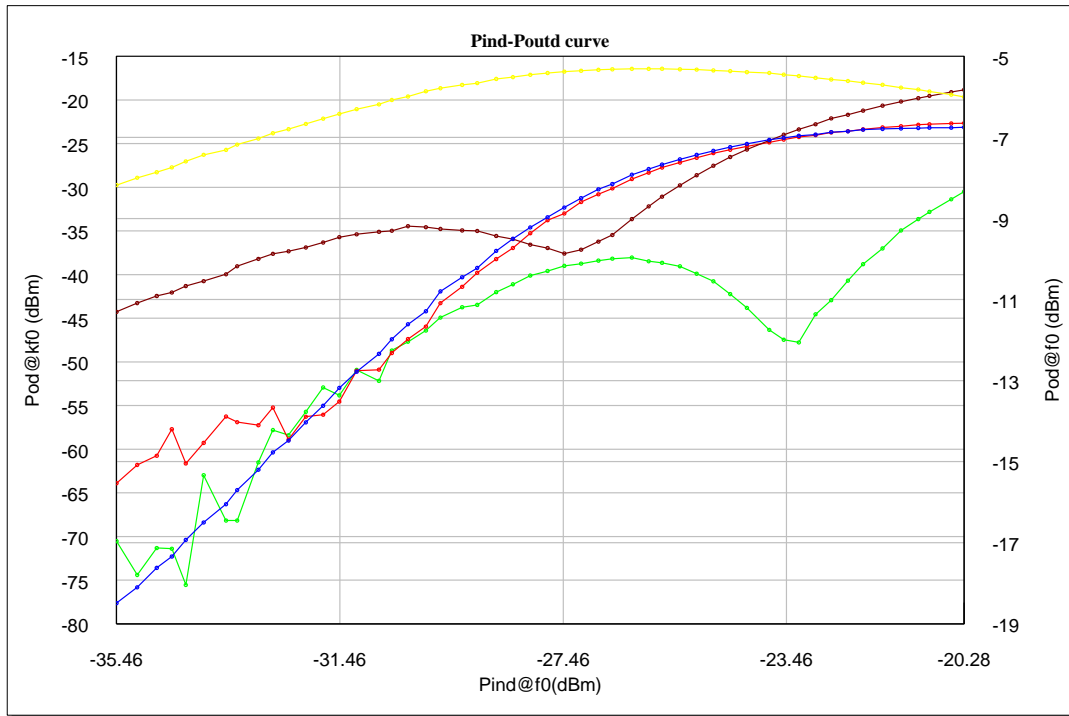


Figure 6.6: AUT<sub>1</sub> differential-mode output power at different frequencies of interest @  $Z_D=100\Omega$  and  $Z_C=25\Omega$ . blue( $f_0$ ), yellow ( $2f_0$ ), brown ( $3f_0$ ), red( $4f_0$ ) and green( $5f_0$ )

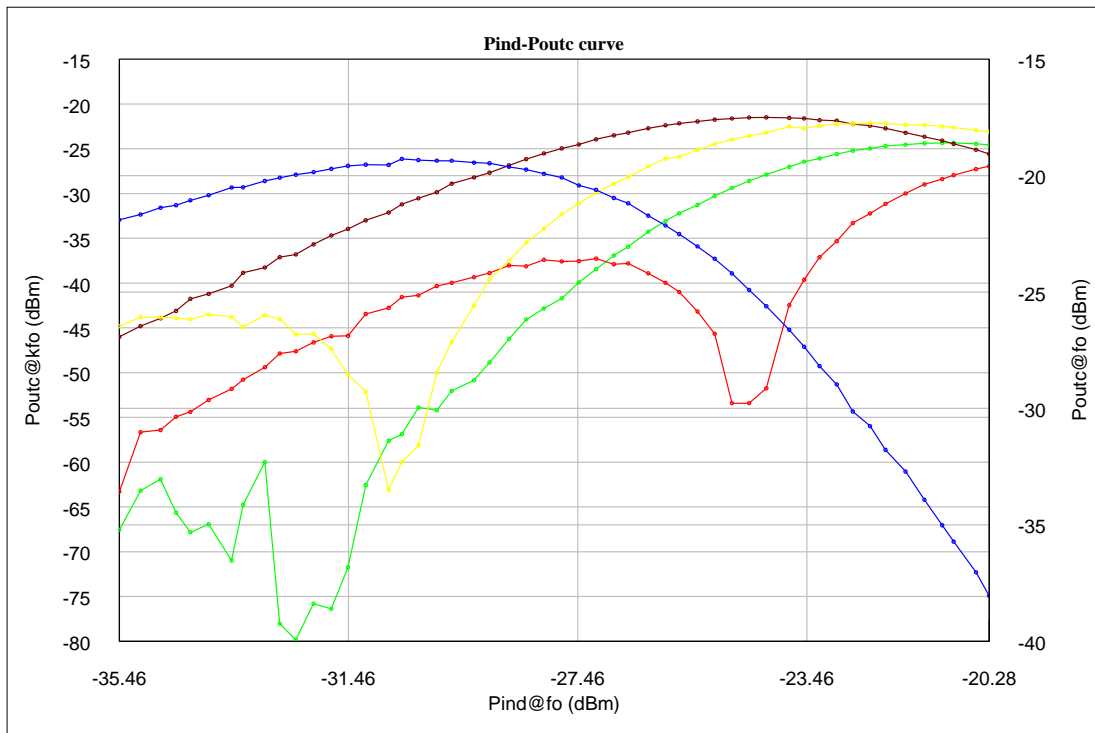


Figure 6.7: AUT<sub>1</sub> common-mode output power at different frequencies of interest @  $Z_D=100\Omega$  and  $Z_C=25\Omega$ . blue( $f_0$ ), yellow ( $2f_0$ ), brown ( $3f_0$ ), red( $4f_0$ ) and green( $5f_0$ ).

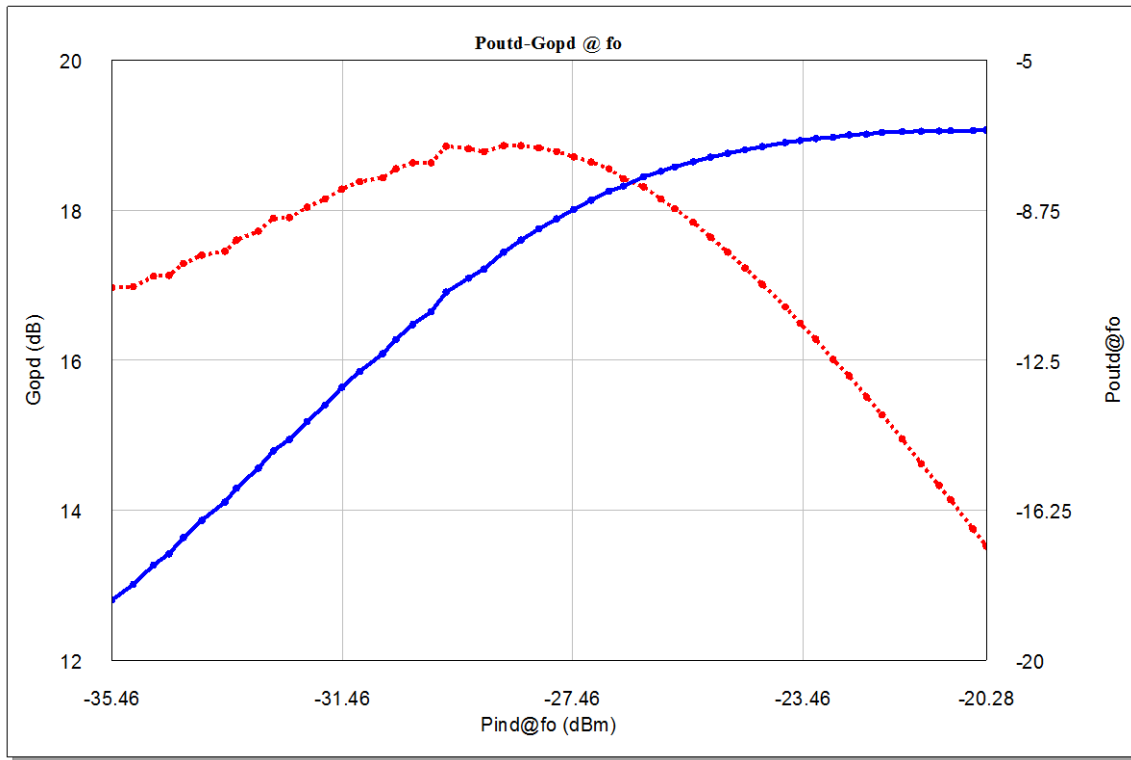


Figure 6.8: AUT<sub>1</sub> Differential-mode Output power (blue) and Operating gain (red) @  $f_0$   $Z_D=100\Omega$  and  $Z_C=25\Omega$ .

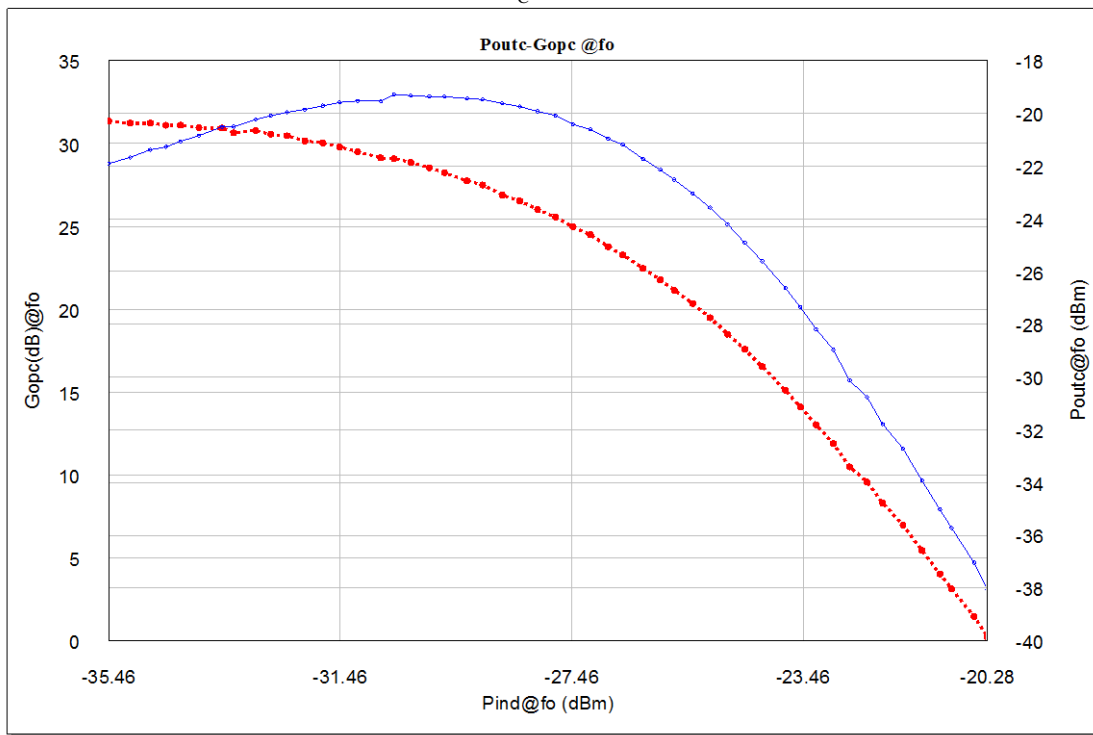


Figure 6.9: AUT<sub>1</sub> Common-mode Output power (blue) and Operating gain (red) @  $f_0$   $Z_D=100\Omega$  and  $Z_C=25\Omega$

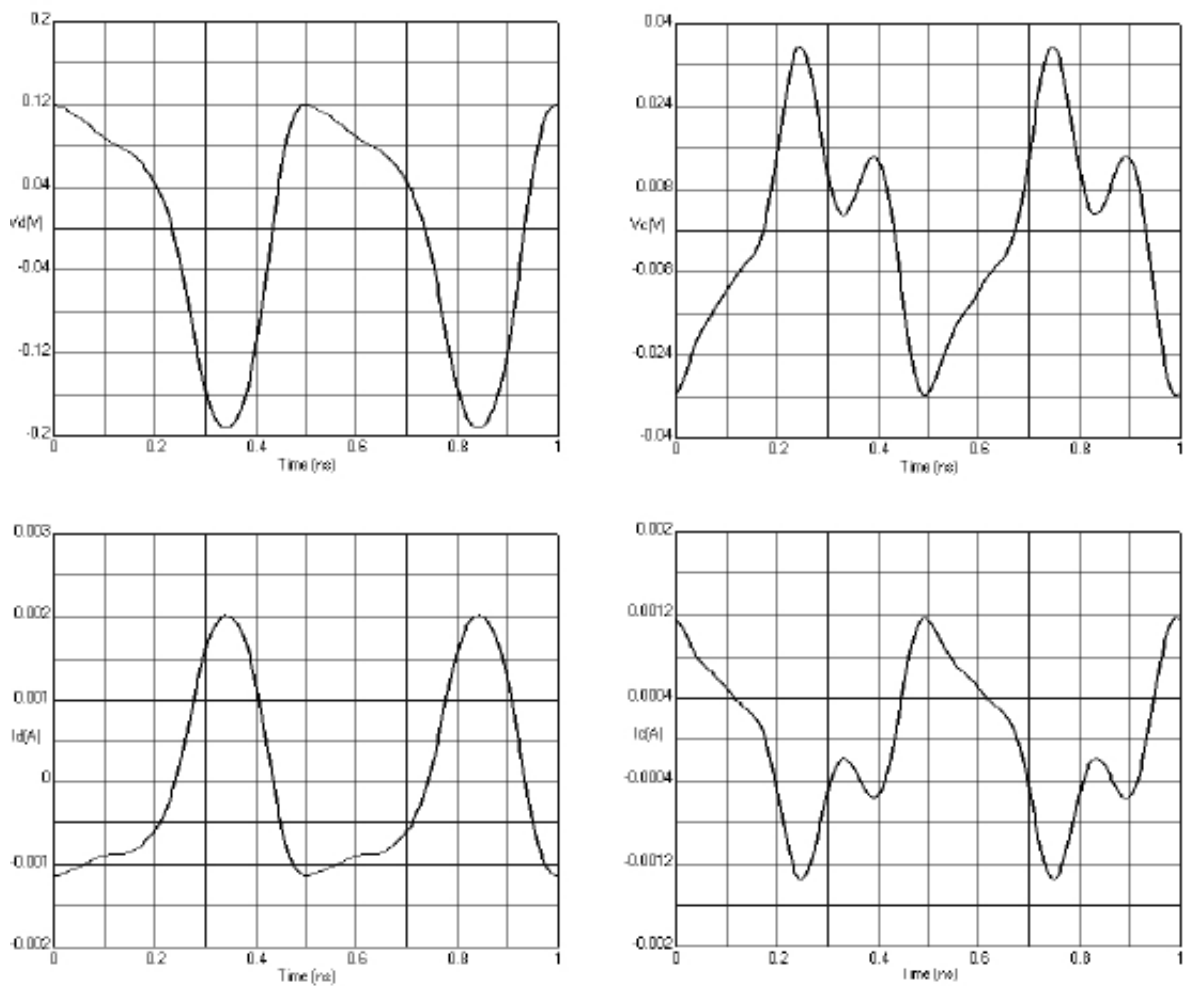


Figure 6.10:  $AUT_1$  output waveforms. Maximum differential gain point @  $G_{Pd} = 18.86$  dB,

$$P_{INd@f_0} = 28.66 \text{ dBm} \text{ and } P_{OUTd@f_0} = -9.80 \text{ dBm}$$

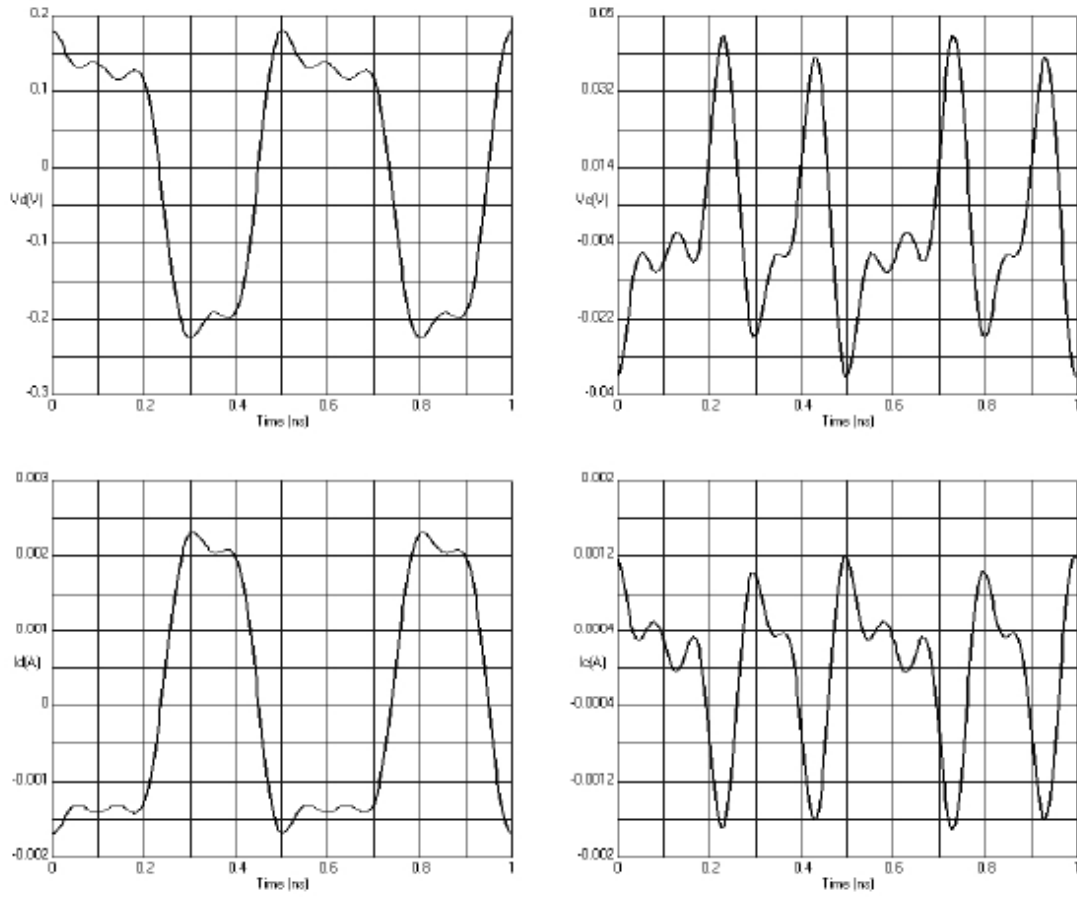


Figure 6.11:  $AUT_1$  output waveforms. 3 dB compression point @  $G_{Pd}$ .  $G_{Pd} = 15.78$  dB,  
 $P_{INd@f_0} = -22.66$  dBm and  $P_{OUTd@f_0} = -6.87$  dBm

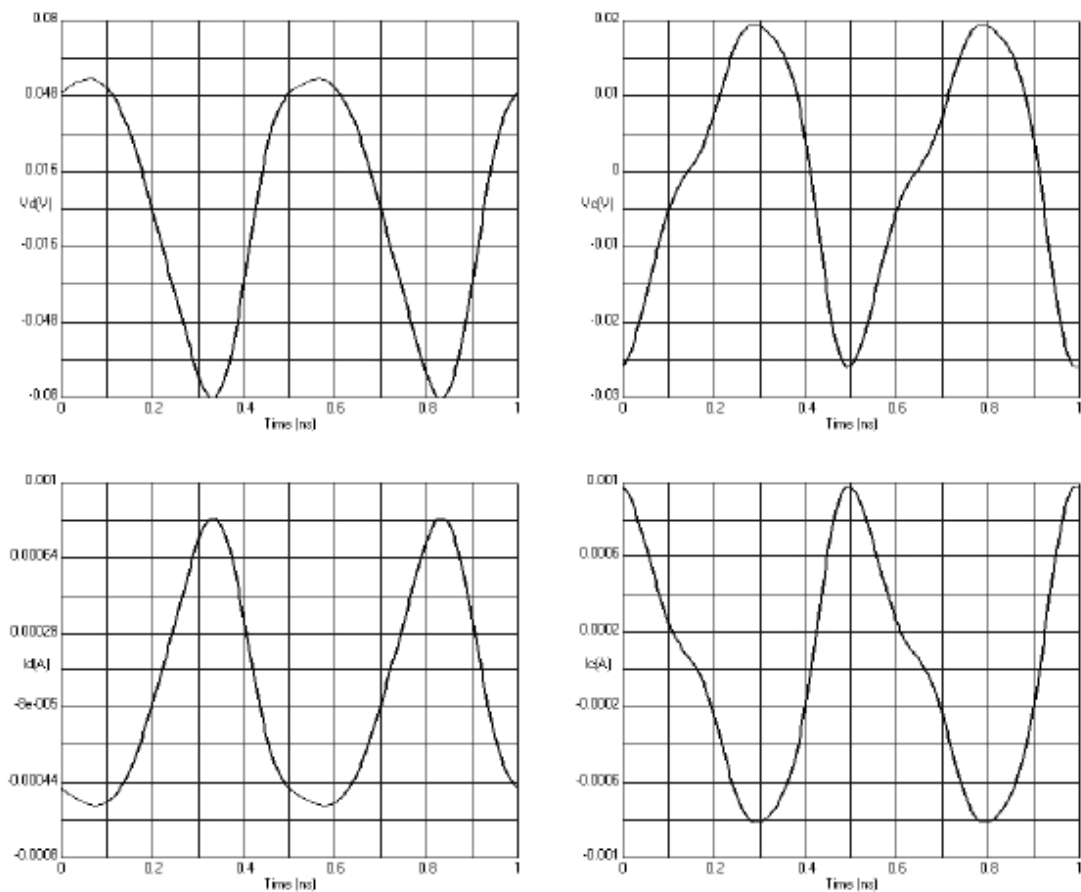
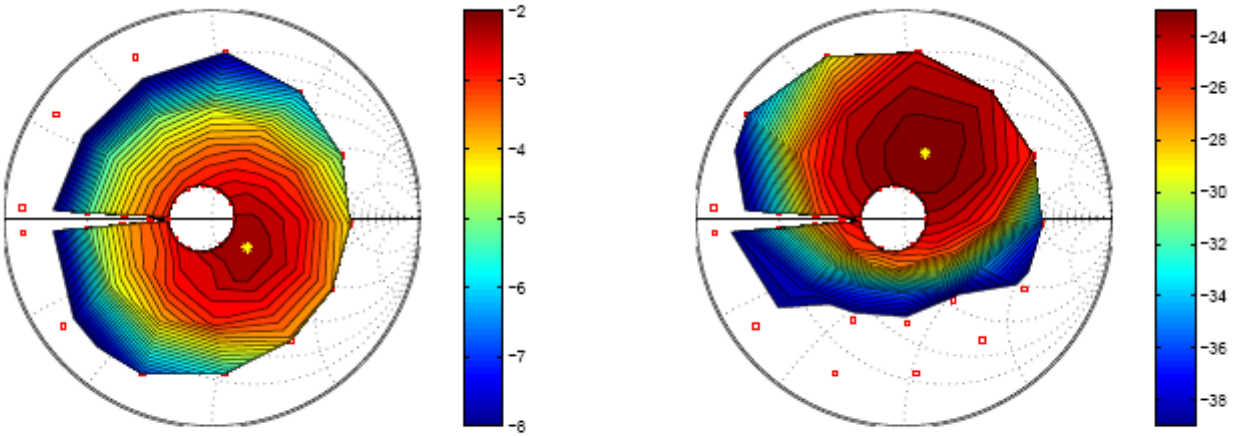


Figure 6.12:  $AUT_1$  output waveforms. 10 dB back-off from the 3 dB compression point.

@  $G_{Pd} = 17.40$  dB,  $P_{INd@f_0} = -33.90$  dBm and  $P_{OUTd@f_0} = -16.50$  dBm

In a similar way to (AUT<sub>1</sub>) on (AUT<sub>2</sub>) a differential mode load map was performed at the fundamental in order to maximize  $P_{OUTd-1dB@f_0}$ . Once again in this case the common mode output power was minimized (see figure 6.13). Optimum is  $\Gamma_{Ld-OPT} = 0.22\angle -40^\circ$ . Additionally a differential mode input power sweep was performed on the matched load for the differential- ( $Z_d = 100\Omega$ ) and common-mode ( $Z_c = 25\Omega$ ). Unfortunately, this device shows no interesting performances, because it is too linear and balanced. Even in compression, the differential waveforms look like pure sinusoids (see figure 6.14 and 6.15).



(a) Differential-mode output power

(b) Common-mode output power

Figure 6.13: AUT<sub>2</sub> differential-mode load map at fundamental. The output powers of each propagating mode @ $f_0$  at 1 dB compression of the differential-mode gain are shown.

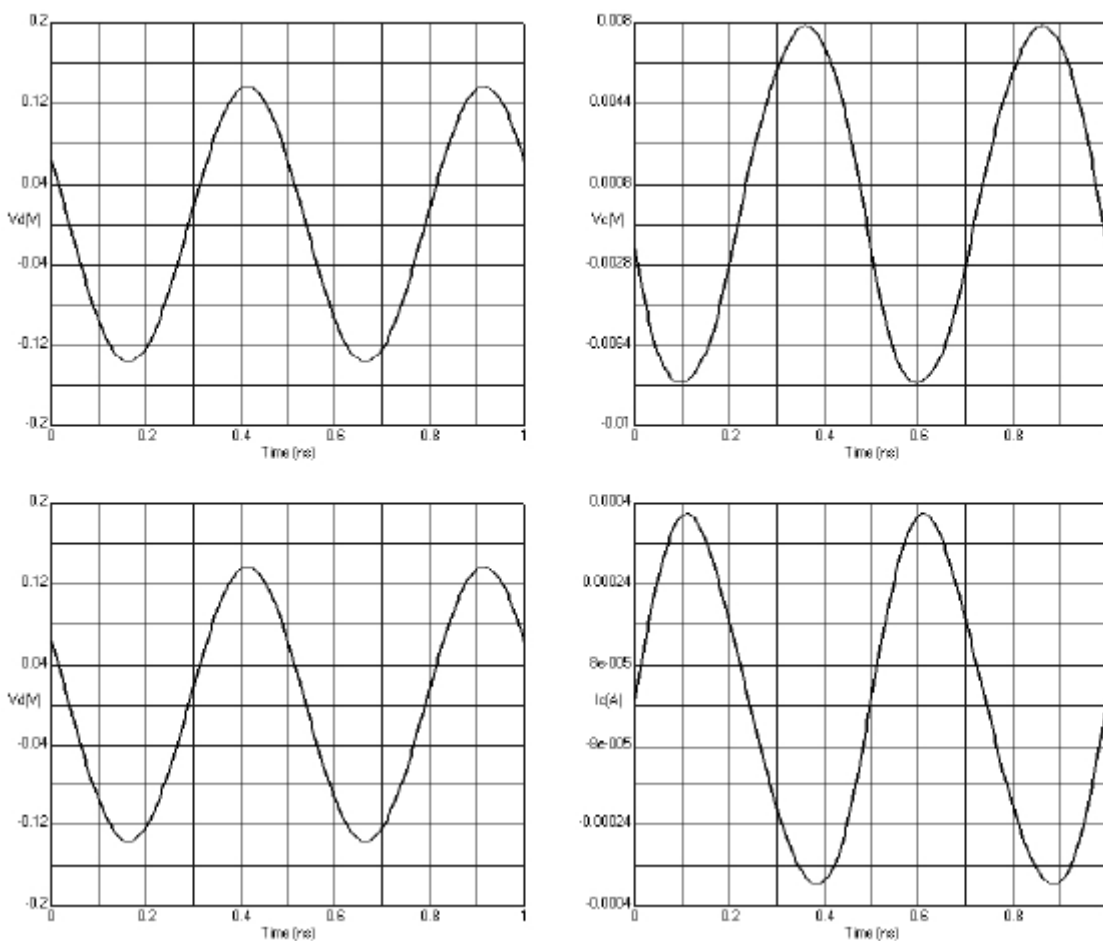


Figure 6.14:  $AUT_2$  output time domain waveforms in linearity, about 10 dB back-off from the 1 dB compression point. @  $G_{Pd} = 4.39$  dB,  $P_{INd@f_0} = -14.24$  dBm and  $P_{OUTd@f_0} = -9.86$  dBm

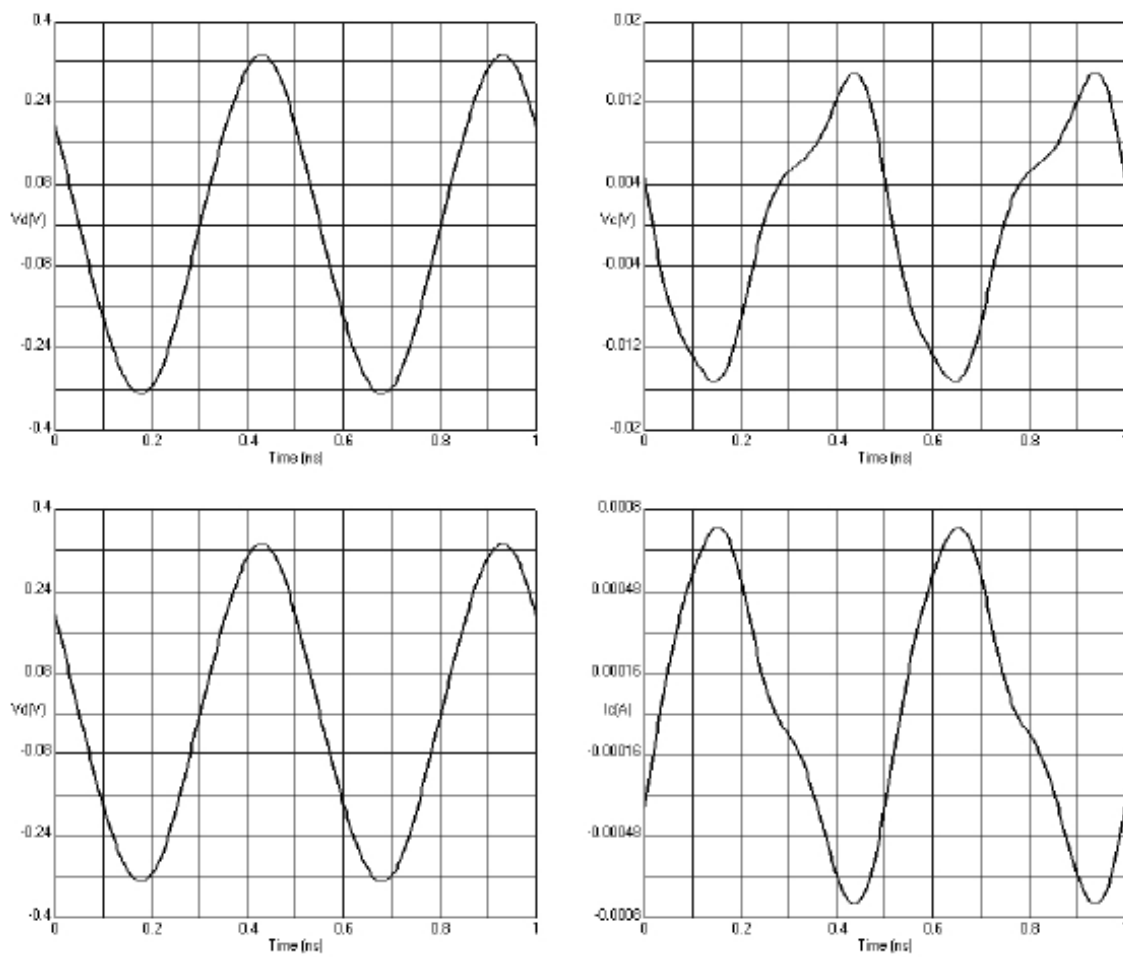


Figure 6.15:  $AUT_2$  Output time domain waveforms at 1 dB compression point of  $G_{Pd}$ . @  $G_{Pd} = 3.27$  dB,  
 $P_{INd@f_0} = -5.54$  dBm and  $P_{OUTd@f_0} = -2.27$  dBm



# *CONCLUSIONS*

This thesis work has described a way to accurately measure the differential- and common- mode incident and reflected power waves in VNA multiport systems, their magnitude ( $|.$ ) and their phases ( $\angle$ ). The main problem found was in the phase calibration procedure when mechanical constrains of the measurement environment were present. Undoubtedly the necessity of an amplitude-phase stable HPR signal is mandatory when time domain waveform measurements are needed. A group delay ( $t_g$ ) computation based approach was provided in chapter IV in order to solve the phase calibration problem when mechanical measurement environment constrains are present which clearly depend on the mechanical length of cables, coupler and connectors placed between the test port and auxiliary port. A brief comparison between this approach (developed a few years ago by the Department of Electronic Engineering at the Polytechnic of Turin) and other current approaches such as NVNA and LSNA technologies has been pointed out. Furthermore, the fact that mechanical measurement environment problems are present and that time domain waveforms are needed demands the use of non leaky error model, the simplest one, which may be unreliable in on-wafer measurement environments. The calibration methodology of a VNA multiport system described in this thesis work which provides time domain capabilities can be applied to both multiport on-wafer devices as well as multiport connected devices, it means, when gender connector problem are or are not present respectively. The usefulness of measuring accurately the phase and amplitude of the single-ended incident and reflected power waves in RF multiport systems has got huge importance into the RF device characterization field because it opens the possibility to see time domain waveforms with complete vector correction applied.

This usefulness has been exploited so as to characterize four port devices; specifically characterization of two differential commercial power amplifiers in nonlinear region of operation have been performed. Common- and differential-mode responses have been measured in both time and frequency domains under nonlinear region of operation.

Time domain waveforms up to the fifth harmonic have been measured under different m-mode harmonic impedances and differential input power sweeps. Common- and differential-mode output powers in respect to a differential input power sweep up to fifth harmonic were obtained.

There are many reasons why differential power amplifiers are subject of research interest, mainly because of the current growing preference in these kind of topologies in order to drive higher levels of circuit integration in the handset market, decreasing power supply voltage, reducing unwanted circuit-to-circuit coupling as well as increasing dynamic range. The ability to accurately measure, analyze, and design nonlinear differential circuits at RF will allow their wide spread use in IC applications.

Some important aspects of RF time domain techniques still need to be developed in the future, one issue is to be able to work with half or full leaky error models when gender connector problems are present, this will be useful in on-wafer measurement environments, meanwhile current RF time domain technologies (NVNA, LSNA, MMS-NT) only include non leaky error model.

Another issue is how to ensure and guarantee that the pre-characterized “harmonic phase reference standard” has stable long-term phase response.

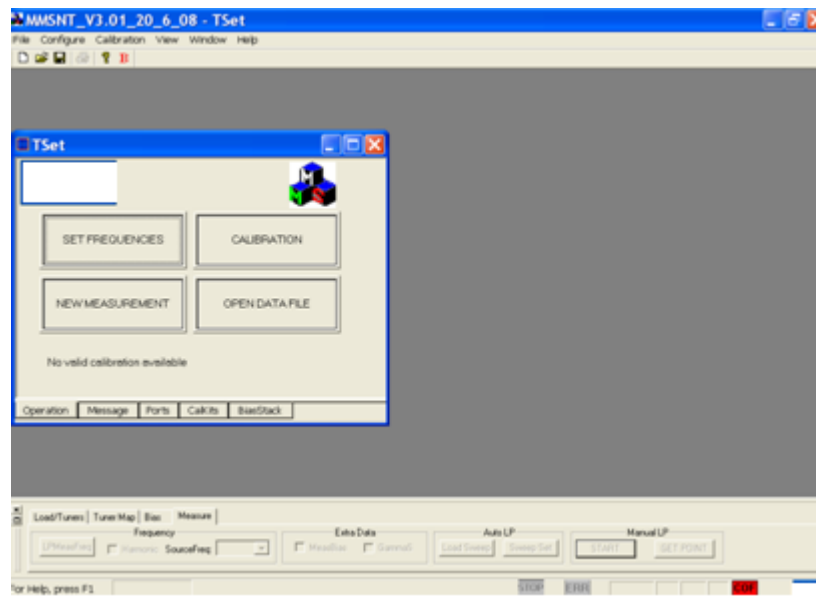
# *Appendix A*

## Calibration Procedure with MMS-NT software

## MMS-NT SCREEN ELEMENTS DESCRIPTION

This section describes briefly the Microwave Measurement Software MMS-NT, including the alternative navigation tools for mouse windows, toolbars, menus, dialogs, and common controls used during calibration and measurements.

The main window of MMS-NT provides all control elements to perform all settings required for calibration procedures: Menu bar, *TSet* Window.



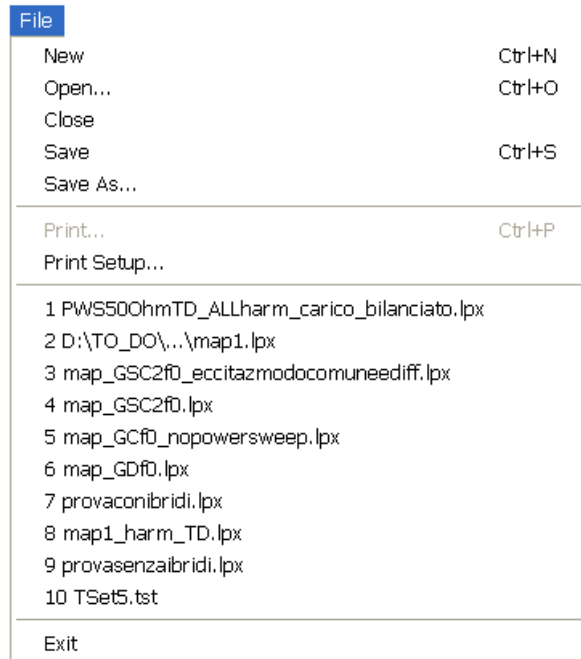
### 1) Menu Bar

All MMS-NT functions are arranged in drop-down menus. The menu bar is located across the top of the main window: Menus can be controlled with a mouse, like the menus in any Windows application. A left mouse click expands a menu or submenu. If a menu command has no submenu assigned, a left mouse click opens a dialog or directly activates the menu command.

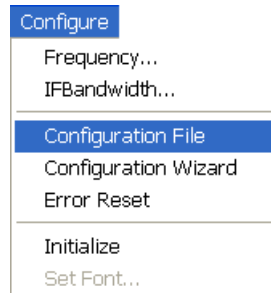
File Configure Calibration View Window Help

Overview of menu functions:

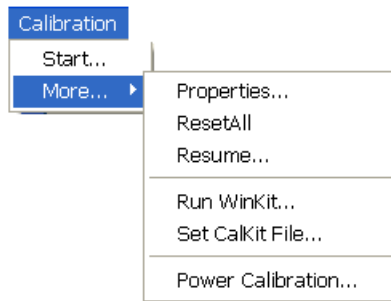
The *File* menu provides standard Windows functions to create, save, recall or print setups, and to shut down the application.



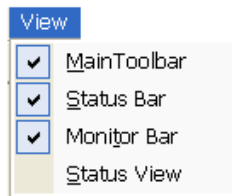
The *Configure* menu provides all settings and functions to create the frequency list, select and modify VNA's IF bandwidth, modify the *MMSNT.ini* configuration file (.ini), running the calibration wizard, rest the error message flag (**ERR**), and initialize all the measurements equipment in the test bench (VNA, switch unit, power meter, MTA/SO, etc).



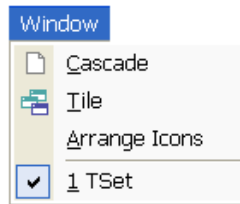
The *Calibration* menu provides all necessary functions to perform S-parameter, power and phase calibration procedures.



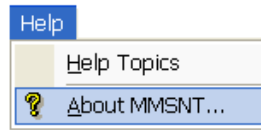
The *view* menu provides possibility of show or hides the Main toolbar, status and monitor bars and the status view.



The *Window* menu provides standard Windows™ functions to arrange different windows on the screen.

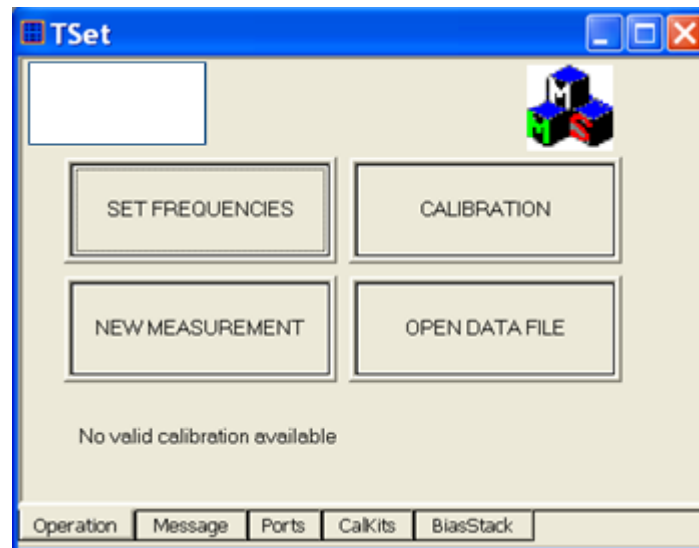


The *Help* menu provides assistance with MMS-NT and its current mode of operation (demo or measurement modes).




## 2) TSet Window


MMS-NT initially opens a test set file (.tst) labeled as “TSet” as default. It consists of five tab controls (*Operation*, *Message*, *Ports*, *CalKits* and *BiasStack*), used to manage calibration and measurements in the current test set file (.tst).





Overview of tab control functions:

The *Operation* tab control provides fast access to different options (also available in the *Configure* menu and in the *File* menu) by means of four buttons:

1)  Allows access to the *calibration frequencies editor*.

2)  Provides fast access to the *calibration measurement* windows only if an appropriate calibration has been done.

3)  Allows one to open a new load pull measurement file (.lpx).

- 4)  Allows one to open an already existent *TSet* file (.tst).

The *Message* tab control provides a resume of the current tasks carried out by MMS-NT.

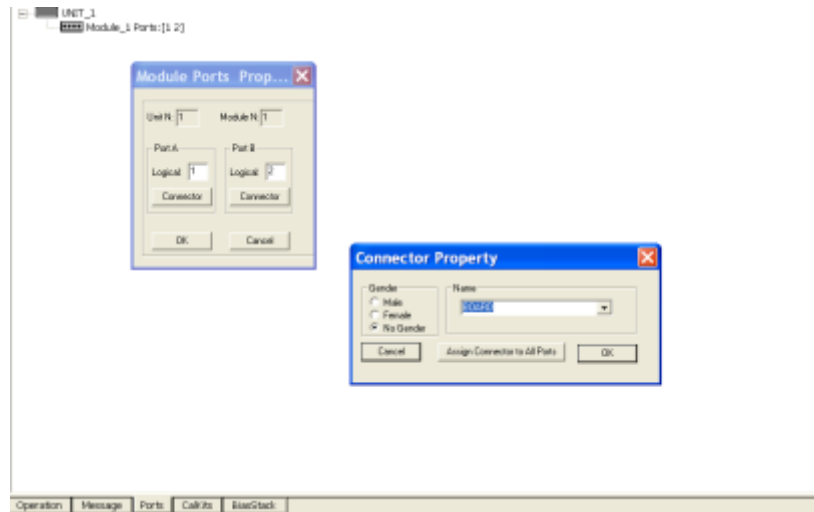
```

*****PAJ-----MMSNT-----LOGFILE
Date Mon Sep 22 09:05:33 2008

Mon Sep 22 09:05:33 2008: Initialize Application
Mon Sep 22 09:05:34 2008: Demo Mode Activated
Mon Sep 22 09:05:34 2008: Start Building TestSet
Mon Sep 22 09:05:34 2008: RTT load-pull
Mon Sep 22 09:05:34 2008: Auxiliary Device Activated
Mon Sep 22 09:05:34 2008: START BUILDING GENERAL DEVICES
Mon Sep 22 09:05:35 2008: ALL DEVICES SUCCESSFULLY BUILT
Mon Sep 22 09:05:35 2008: Open File for reading ASCII: C:\MMS_Configuration\MasterKit.tst
Mon Sep 22 09:05:35 2008: Loading CalKit File
Mon Sep 22 09:05:35 2008: Start Building Base Stack
Mon Sep 22 09:05:35 2008: Number Of Boxes: 1
Mon Sep 22 09:05:35 2008: Number Of Bank Of BOX 1 : 1
Mon Sep 22 09:05:35 2008: Dummy Switch Unit Driver Loaded
Mon Sep 22 09:05:35 2008: Initializing BOXStack
Mon Sep 22 09:05:35 2008: Initializing BOX
Mon Sep 22 09:05:35 2008: Initialize Device Addr:31
Mon Sep 22 09:05:35 2008: Initializing BOX Ended
Mon Sep 22 09:05:35 2008: Initializing BOXStack Ended
Mon Sep 22 09:05:35 2008: INITIALIZING GENERAL DEVICES
Mon Sep 22 09:05:35 2008: Initialize Device Addr:11
Mon Sep 22 09:05:35 2008: MTAR Dever Initialization Started
Mon Sep 22 09:05:35 2008: MTAR Dever Initialization Ended
Mon Sep 22 09:05:35 2008: Initialize Device Addr:31
Mon Sep 22 09:05:35 2008: PAF CRAGON: Dever Initialization Started
Mon Sep 22 09:05:49 2008: PAF CRAGON: Dever Initialization ended
Mon Sep 22 09:05:49 2008: ALL DEVICES SUCCESSFULLY INITIALIZED
Mon Sep 22 09:06:10 2008: -----EXCEPTION-----
Mon Sep 22 09:06:10 2008: C11002W Current CalKit does not contain the required standard
Check Standards connected between parts 1 and 2
Mon Sep 22 09:06:10 2008: -----EXCEPTION-----
Mon Sep 22 09:06:10 2008: C11002W Current CalKit does not contain the required standard
Check Standards connected between parts 1 and 2
Mon Sep 22 09:06:11 2008: -----EXCEPTION-----

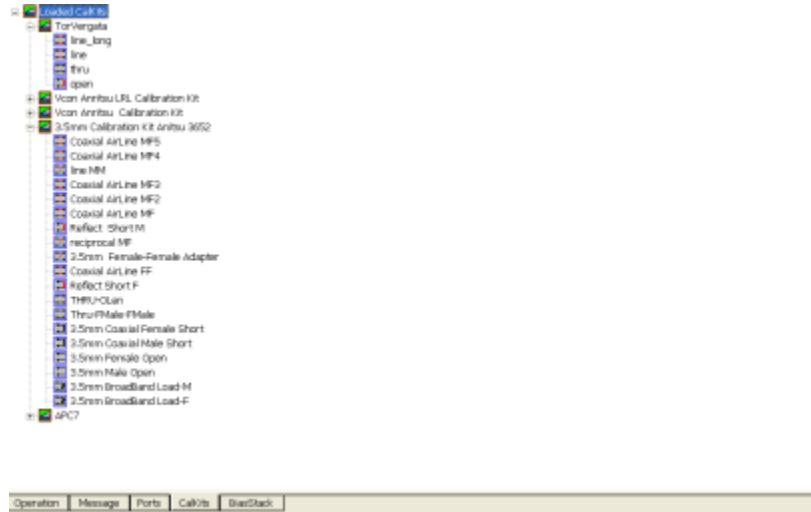
```

The *Ports* tab control allows one setting the gender connector type at each test port.

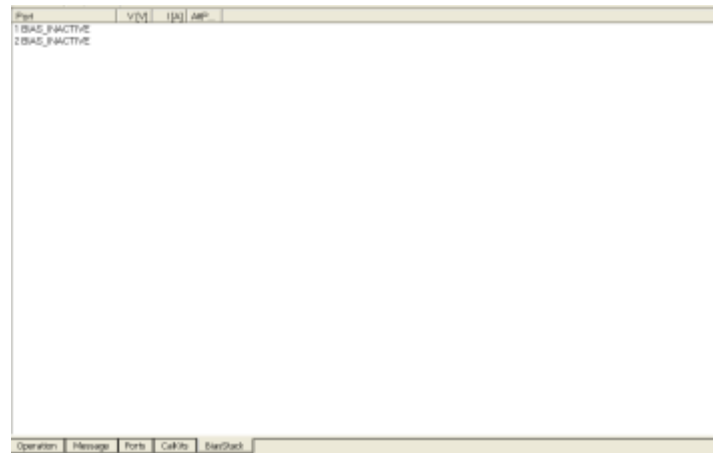




The *CalKits* tab control allows one to check the calibration standards kits available in the lab and specified in the current cal kit file (.std), which will be used by the current test set (.tst) during both S-parameter and power calibration procedures.



The *BiasStack* tab control allows one to activate and deactivate the bias of the DUT when needed.



## I)-S-PARAMETER CALIBRATION PROCEDURE

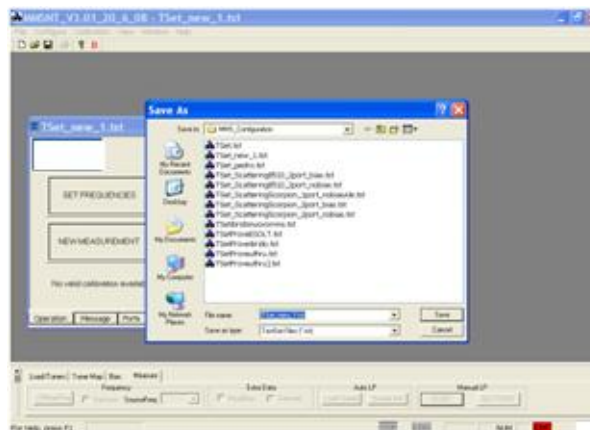
This section describes the basic steps and operational procedures for implementing an S-parameter calibration on a multiport VNA system by using MMS-NT. This process consists of three steps: 1) *TSet* file (.tst) configuration; 2) Calibration Standards Measurement 3) S-parameter Calibration Verification.

### 1) file (.tst) configuration

MMS-NT basically allows two ways to configure a test set file (.tst) properly, which will be used during and after an S-parameter calibration procedure. These two ways are: 1)the *TSet* window and the *Calibration* menu 2)Guided Calibration (*configuration wizard*). In both cases the test set file configuration consists of the following steps:

- 1.1)-Checking the current calibration standards file (.std)
- 1.2)- Setting hardware.
- 1.3)-Setting the frequencies of interest.
- 1.4)-Defining calibration methods.

Next, each step will be described using both methods simultaneously, first explaining it by using the MMS-NT *Configuration Wizard* and then by using the MMS-NT *TSet* window/*Calibration* menu. First of all, the user must open and save a new *TSet* file (.tst), where all changes done will be available to be recalled in future measurements if needed: *File>New>TSet>OK>File>Save as*.

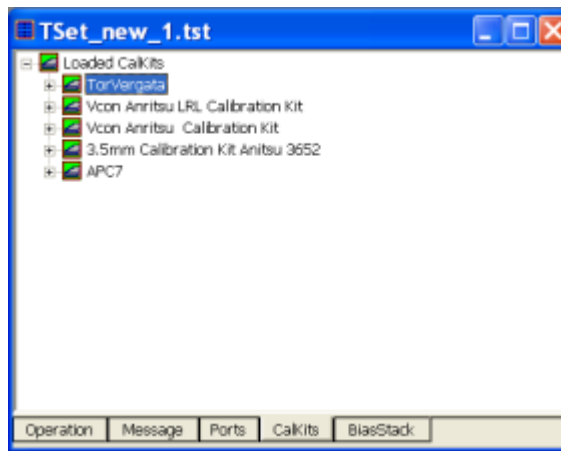


### 1.1) Checking the current calibration standards file (.std)

-Launch the *configuration wizard* tool from the menu bar: *configure >configuration wizard* :

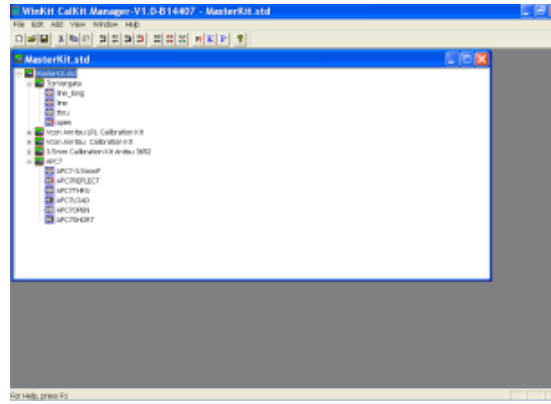


-From the *TSet* window simply pushing the *CalKits* tab control:



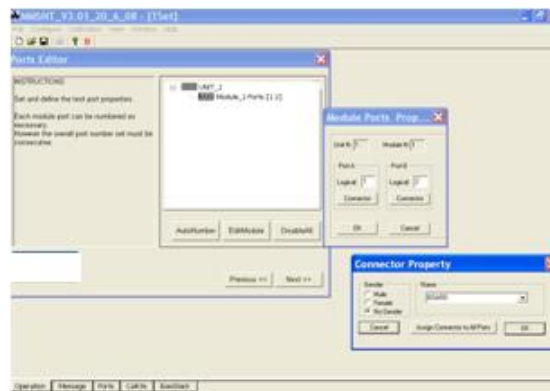
-In both cases, check to see if the mechanical calibration kits available in the labs are enough to solve the calibration problem, this depends on the calibration method (RSOL, SOLT, TRL, LRM, etc) to be used . In this sense, MMS-NT shows a tree node labeled as “*Loaded CalKits*” which contains all the calibration standards definitions available in the current calibration standards file (.std).

-If needed, from the menu bar launch the *WinKit* tool: *Calibration>More...>Run WinKit...* where it's possible to edit, modify, delete, reload, etc a new calibration kit file (.std) such as is available in commercial VNA system.

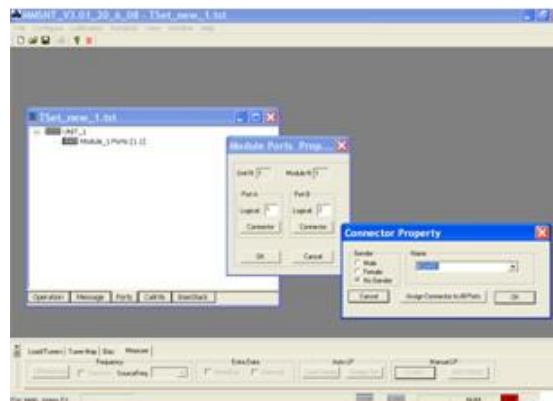


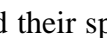

## 1.2) Setting Hardware

-From the *configuration wizard* simply press the *Next>>* button :

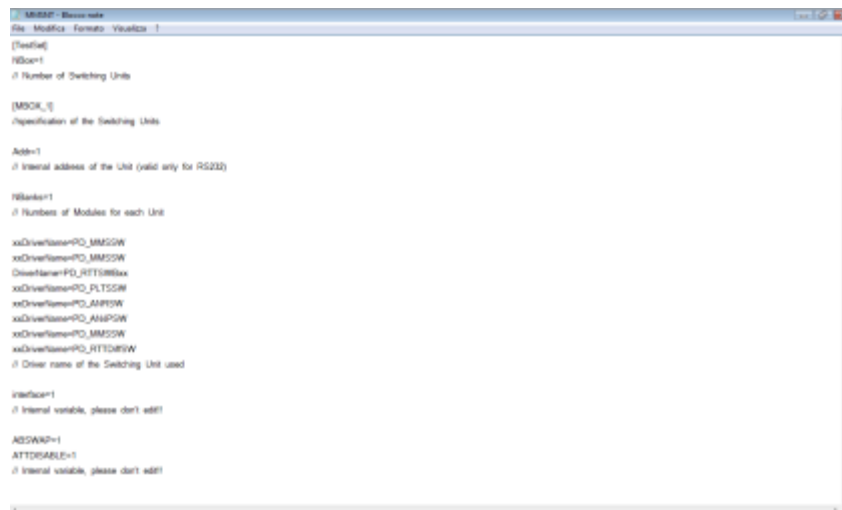


-From the *TSet* window pushing the *Ports* tab control:



-In both cases, one opens the *Ports Editor* tool which allows the user to specify the ports logical number and the type of port connectors. The number of physical ports available depends on the number of multiport test set units available in the test bench. According to how the user has defined all the multiport test set units in the *MMSNT.ini* configuration file (.ini), MMS-NT shows a tree node which contains the current's multiport test set units and their specified modules: each node (  ) corresponds to a physical multiport test set unit, which can include different port modules (  ). In this way, the user assigns to each physical port a logical number (1, 2, 3, etc) and its connector type, which can be placed in whichever port module of whichever test set unit was previously defined into the *MMSNT.ini* configuration file (.ini).

-If needed, open the *MMSNT.ini* configuration file (.ini) to look at the multiport test set units configuration: *Configure>Configuration File*.



```

MMSNT - Edit-ini
File  Modifica  Formato  Visualizza  ?
[TreeView]
NBox=1
; Number of Switching Units

[MBOX_1]
; specification of the Switching Units

Addr=1
; Internal address of the Unit (valid only for RS232)

NModules=1
; Numbers of Modules for each Unit

xxDriverName=PO_MM2GW
xxDriverName=PO_MM2GW
DriverName=PO_RFTSMBxx
xxDriverName=PO_PLTSGW
xxDriverName=PO_AHPSGW
xxDriverName=PO_MM2GW
xxDriverName=PO_RFTSMBGW
; Driver name of the Switching Unit used

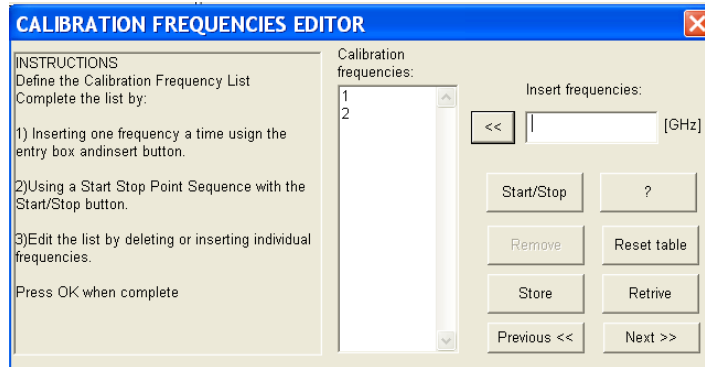
Interface=1
; Internal variable, please don't edit!

ADSWAP=1
ATTDSABLE=1
; Internal variable, please don't edit!

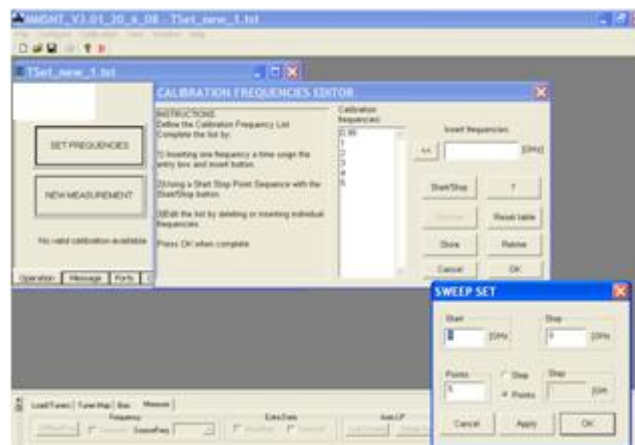
```

### 1.3) Setting the frequencies of interest

-From the *configuration wizard* tool simply press the *Next>>* button :



-From the *TSet* window pushing the *Operation* tab control and press the *SET FREQUENCIES* button :

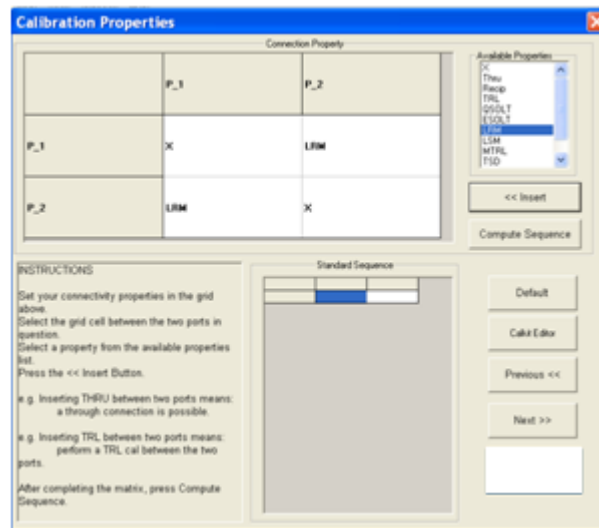


Both cases are conducive to the *Calibration Frequencies Editor* dialog, where the user must edit the frequency list which includes all frequencies of interest where one intends to get the DUT's S-parameters ( $f_0, 2f_0, \text{etc}$ ). If time domain measurements will be performed in the future and if auxiliary port will be needed, then, it's mandatory at this point to include an additional frequency point in the frequency list in order to compute the group delay ( $t_g$ ) of cables, through coupler's arm and connectors placed between the test port and the auxiliary port, where one connects the HPR signal and the time domain receiver (MTA/SO) respectively, during a phase calibration procedure. In MMS-NT there

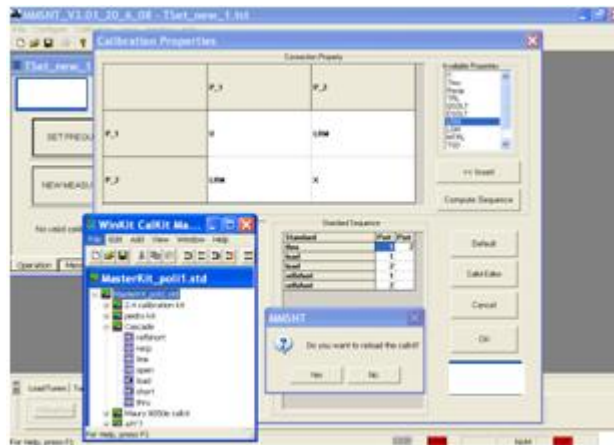
are different manners to introduce frequency points in the frequency list, such as those available in the CAD simulators: star/stop, point to point, etc.

#### 1.4) Defining calibration methods

-From the *configuration wizard* tool simply press the *Next>>* button :



-From the menu bar: Calibration>More...>Properties...



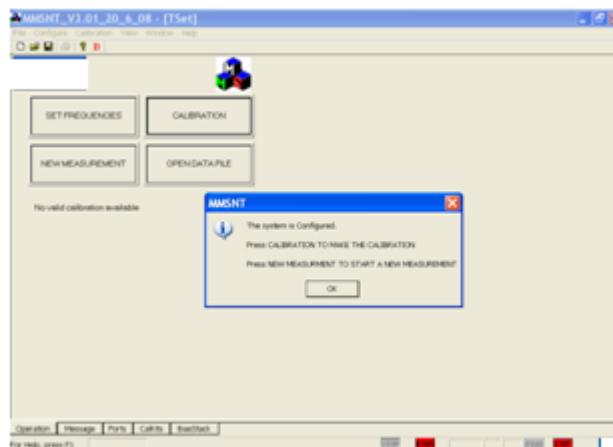
-Both approaches open the *Calibration Properties* dialog, which provides a wide range of sophisticated calibration methods (*LRM*, *TRL*, etc) to solve the calibration problem. MMS-NT uses a Non Leaky error model as a default error model to solve the S-parameter calibration problem. The user must set the desired calibration method (*connection property*) into a connection matrix as follows:

a-choose the calibration methods by using the mouse.

b-insert the calibration method into the connection matrix by pushing the <<*Insert* button.

Subsequently press the *Compute Sequence* button. MMS-NT will respond according to the types of calibration standards available and the test ports connectivity constrains to obtain a suitable sequence of calibration standards in order to accomplish the calibration methods previously chosen by the user.

If mechanical constrains are present and/or the amount of available standards is not enough to solve the calibration problem through the calibration methods previously chosen, MMS-NT will show an error message informing the user about current calibration kits available in the lab which are not enough to perform the calibration algorithm chosen previously. In this case, the user must get another calibration kit file (.std) by pushing the *Calkit Editor* button which lunches the *WinKit* tool where it will be possible to edit, modify, delete, reload, etc a new calibration kit file such as those available in commercial VNA systems. Otherwise, press the *Ok* button to finish the *TSet* file configuration. After that, the user can begin to connect and measure calibration standards.

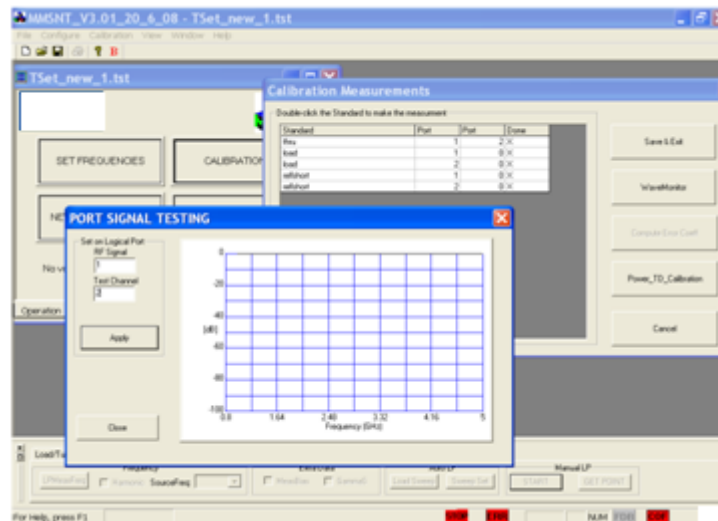



-Immediately after, save all changes done: *File>Save*.



## 2) Calibration Standards Measurements

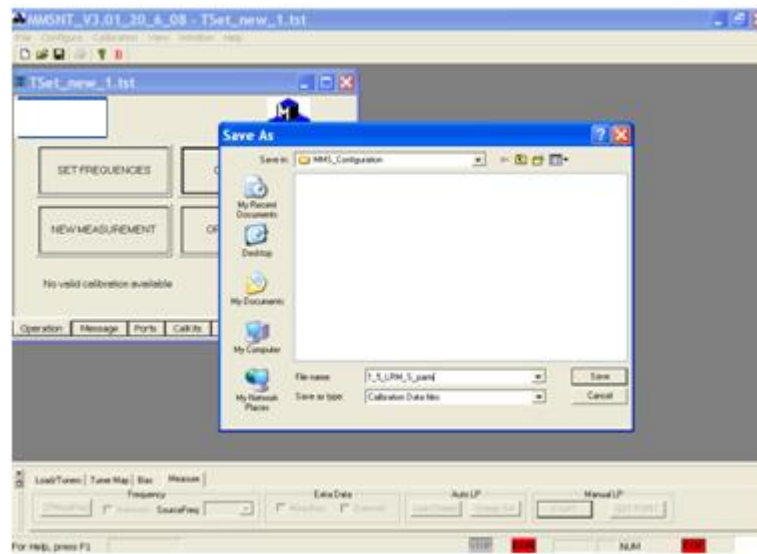
After a suitable *TSet* file (.tst) configuration, the next step is to perform the calibration standards measurements. From the *Operation* tab control launch the *Calibration Measurements* dialog by pushing the *CALIBRATION* button.



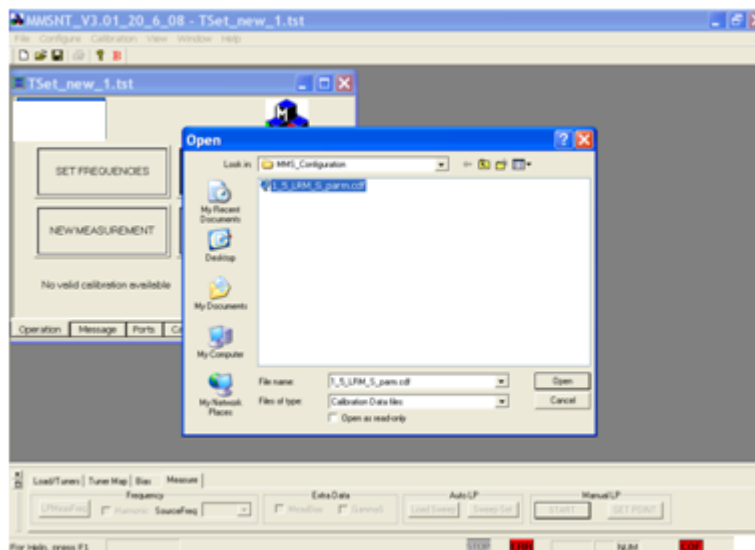
MMS-NT will show the user the calibration standard's sequence computed during the *TSet* file (.tst) configuration. The user must connect each calibration standard at a time and then click the empty box placed in the *Done* column beside the connected calibration standards label (*Short, Open, Load, Thru, line ,recipr, etc*), to initiate the measurement of the connected calibration standard. MMS-NT, by controlling the VNA, performs a calibration sweep at all frequencies included in the frequency list ( $f_0, 2f_0, etc$ ) and displays a progress bar . After the VNA completes the sweep a checkmark (X) appears into the empty box placed in the *Done* column beside the connected calibration standards label (*Short, Open, Load, Thru, line ,recipr, etc*). The user must remove the connected calibration standard and connect another one. This iterative process must be done for all calibration standards in the sequence computed by MMS-NT. Additionally, the user could see the calibration standard measurement progress when needed, by means of the *Port Signal Testing* window, by pushing the *WaveMonitor* button and choose an S-parameter of interest.

-After a correct calibration standard's measurement has been done, click the *Compute Error Coeff* button, MMS-NT will calculate the 4n-1 error terms included into the non leaky error model, which will be applied to correct futures S-parameter measurements.

-Finally, press the *Save&Exit* button to store the S-parameter calibration's error terms file (.cdf) and close the *Calibration Measurements* windows.

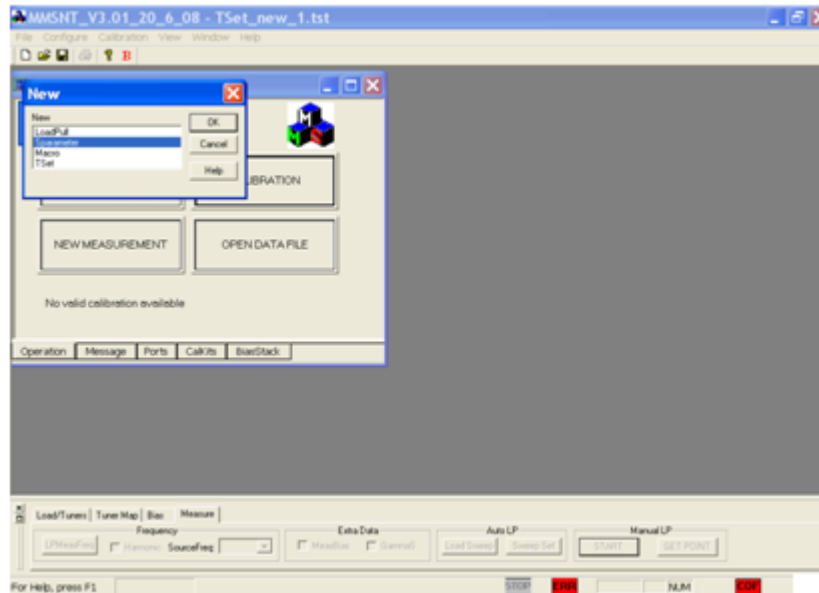


In this way, one can recall previous S-parameter calibration files (.cdf) to perform future measurements, whenever the measurement test bench is not modified.

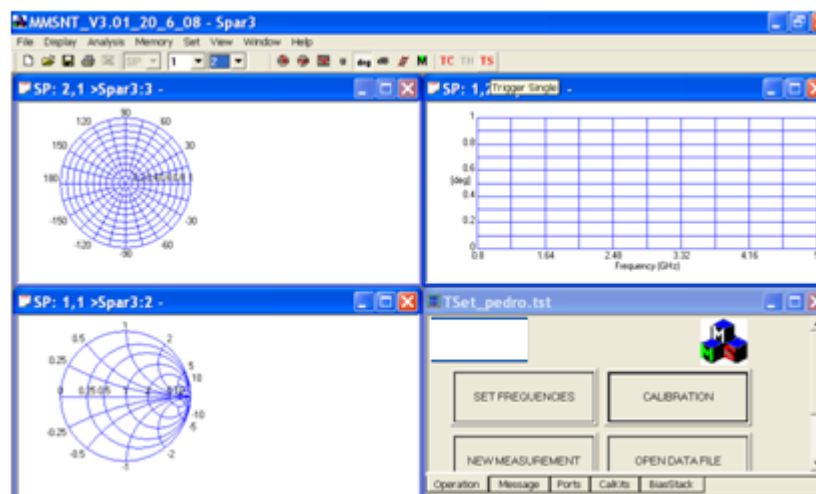





### 3) S-parameter Calibration Verification

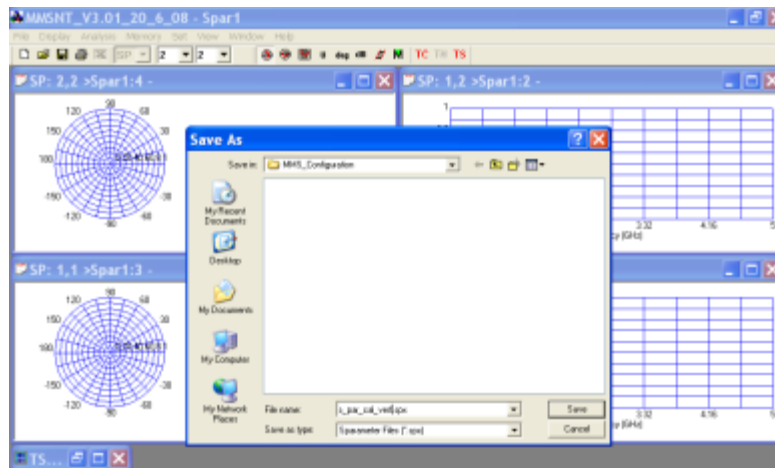
Once an S-parameter calibration has been done, and error correction has been applied, MMS-NT provides another file class: S-parameter file (.spx) (*File>New>Sparameter>OK*) in order to verify the calibration procedure performance and/or perform S-parameter measurements.



When performing S-parameter measurements, an S-parameter file (.spx) allows the user to add graphs with different data formats: polar, smith chart and rectangular such as in a CAD simulator: *View>Add View...*



-Connect a well known DUT between test ports and compare its ideal behavior with the S-parameter measurement obtained by means of MMS-NT in the S-parameter file graphs. There are two types of S-parameter measurements available in MMS-NT: 1) single trigger mode (activated by pushing **TS** button) 2) continuous trigger mode (activated by pressing **TC** button). The former launches only one measurement, displays it and stop itself automatically, whereas, the latter launches one measurement, displays it and continues with this cycle until **TC** button is deactivated. From the toolbar once an S-parameter measurement has been done, it's possible to access whichever S-parameter of interest ( **1** **2** ), change the representation format (    ), change units ( **U** **deg** **dB** ) add markers ( **M** ), etc, in the current graph.



The current S-parameter file (.spx) can be stored and used in future measurements whenever the frequencies of interest are the same.

## II) POWER CALIBRATION PROCEDURE

This section describes the basic steps and operational procedures for implementing a Power level calibration procedure on a multiport VNA system by using MMS-NT. This process consists of three or four steps depending on whether an auxiliary port is used or is not needed respectively.

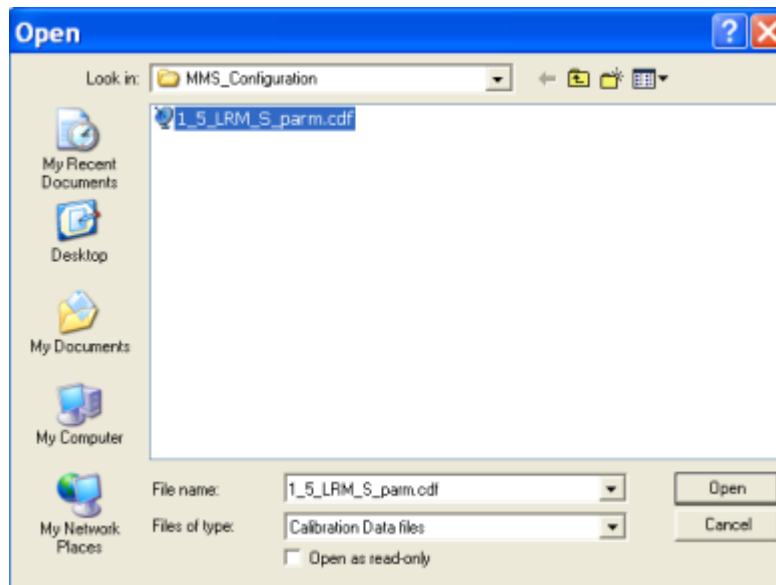
Without auxiliary port: 1)Loading S-parameter Calibration; 2) Power Measurements 3) Power Calibration Verification.

With auxiliary port: 1)Loading S-parameter Calibration; 2) S-O-L calibration 3) Power Measurements 4) Power Calibration Verification.

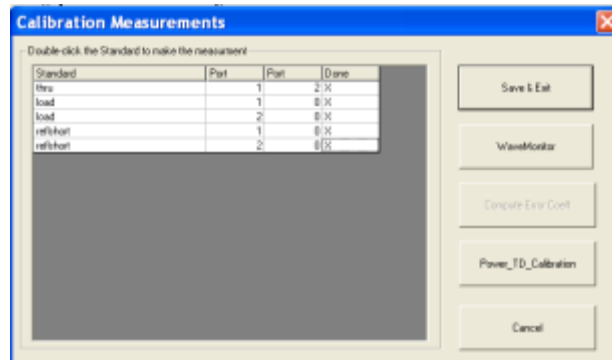
Next, due to both cases are conducive to the *Power Calibration* tool they will be explained simultaneously pointing out differences between them when needed.

### 1) Loading S-parameter Calibration

From the current *TSet* file (.ini) recall an already existent S-parameter calibration file (.cdf): *Calibration>More...Resume...*

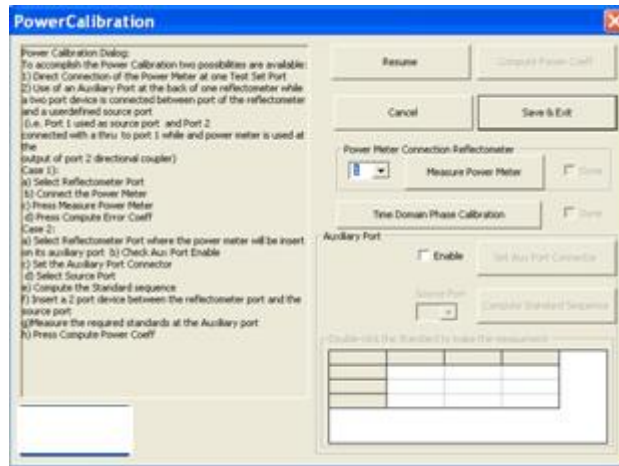


As mentioned in the S-parameter Calibration procedure section it's mandatory that whatever existent S-parameter calibration file (.cdf) matches the current *TSet* file (.tst) configuration when the former is recalled by a *TSet* file (.tst). In this way, the user has access to the  $4n-1$  error coefficients of the non leaky error model included in the current *TSet* file (.tst). The *Calibration Measurement* dialog shows all S-parameter calibration standard's measurements which have been done by a checkmark (X) in the checkbox labeled as "Done".

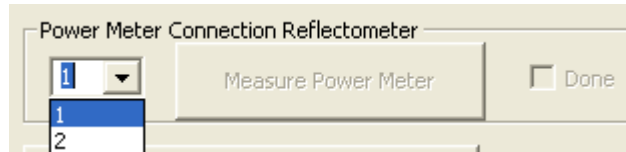


## 2) S-O-L calibration (only if auxiliary port is needed)

Similar to when performing an S-parameter calibration procedure, when the auxiliary port is needed, the user must check if the current Calibration Standards file (.std) loaded into the current *TSet* file (.tst) has got an appropriate calibration standards definition which allows one to carry out the S-O-L calibration at the auxiliary port (connector type, calibration standard type, etc). One can check it and/or make it possible by launching the *WinKit* tool (*Calibration*>*More...*>*Run WinKit...*) where it will be possible to edit, modify, delete, reload, etc a new calibration kit file such in a commercial VNA system. Once, the user has checked an appropriate calibration standard definition, launch the *Power Calibration* tool by pushing the *Power\_TD\_Calibration* button from the *Calibration Measurement* dialog:



-First of all, select the auxiliary port number from the *Power Meter Connection Reflectometer* group box by expanding the combo box control:



-Second, select the check box labeled as “Enable” to activate the use of auxiliary port in MMS-NT from the *Auxiliary Port* group box.

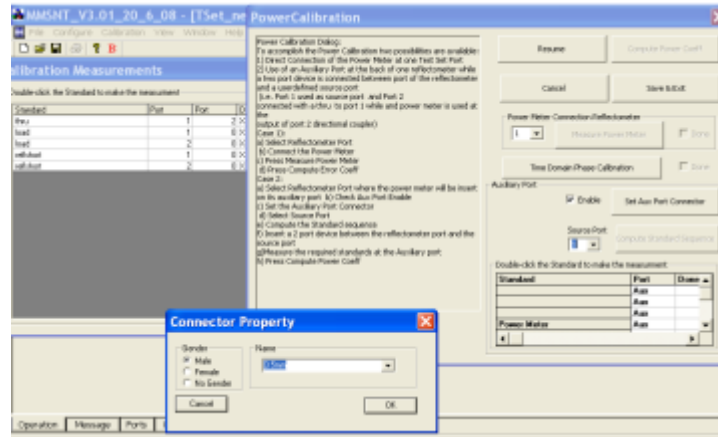
-Select the RF input port where the user intends to connect the Synthesized Sweep

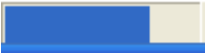
Generator by expanding the *Source Port* Combo box control .

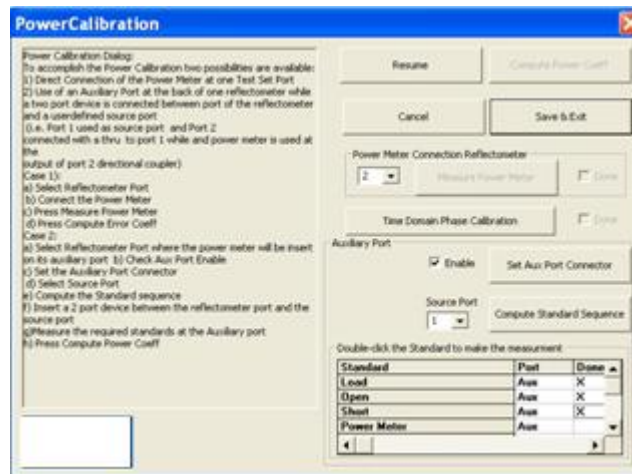
The user must specify the auxiliary port connector type by pressing the *Set Aux Port Connector* button to open the *Connector Property* dialog.

-Select the auxiliary port connector family among all the connector families (3.5mm, 2.4mm, APC7,ect) available in the current calibration standard file (.std) from the *Name* combo box.

-Select the auxiliary port gender type from the radio buttons labeled as “Male” , “Female”, etc. Push the *OK* button, to begin an S-O-L calibration at the auxiliary port previously chosen. As in an S-parameter calibration procedure the user must perform a calibration standards measurement.




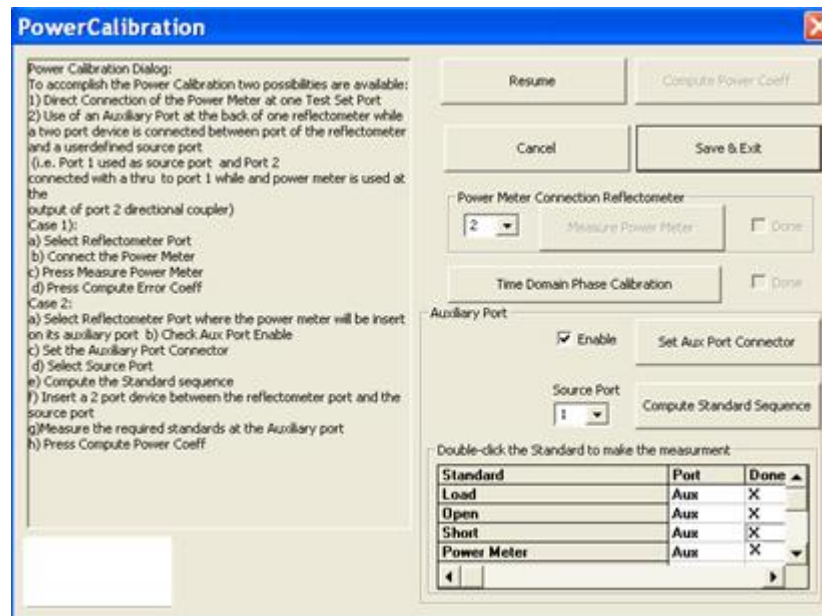
Next, press the *Compute Standard Sequence* button, MMS will show the prior known S-O-L calibration standard sequence on the *Double-click The Standard to made the measurement* group box. Connect each calibration standard one at a time and click the empty box placed in the *Done* column beside the connected calibration standard's label (*Short, Open, Load*) to initiate the measurement of the connected calibration standard. MMS-NT by controlling a commercial VNA system that performs a calibration sweep at all frequencies included in the frequency list ( $f_0, 2f_0, etc$ ) and displays a progress bar . After the VNA completes the sweep a checkmark (X) appears in the empty box placed in the *Done* column beside the connected calibration standards label (*Short, Open, Load*). The user must remove the connected calibration standard and connect another one. This iterative process must be done for the three calibration standards in the calibration sequence computed by MMS-NT.





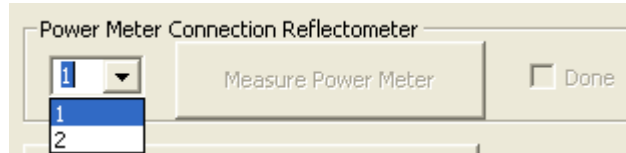
### 3.1) Power Measurements with auxiliary port


After suitable calibration standard measurements have been done (with the Synthesizer Sweep Generator connected to the RF input port previously chosen) the user must connect a power meter to the auxiliary port, while remembering to never change the auxiliary port connector type previously defined. In this sense, the user must match mechanically the power sensor connector type (at its reference plane) to the auxiliary port connector type previously chosen. Then, from the *Power Calibration* dialog launch the power measurements by pushing the empty box placed in the *Done* column beside the *Power Meter* label, which is placed into the *Auxiliary Port* group box, to initiate power measurements. MMS-NT by controlling both power meter and the Synthesizer Sweep Generator performs a calibration sweep at all frequencies included in the frequency list ( $f_0, 2f_0, \text{etc}$ ) and displays a progress bar . After both power meter and Synthesizer Sweep Generator have completed the sweep a checkmark (X) appears into the empty box placed in the *Done* column beside the *Power Meter* label, placed into the *Auxiliary Port* group box, indicating auxiliary port power measurements have been done.

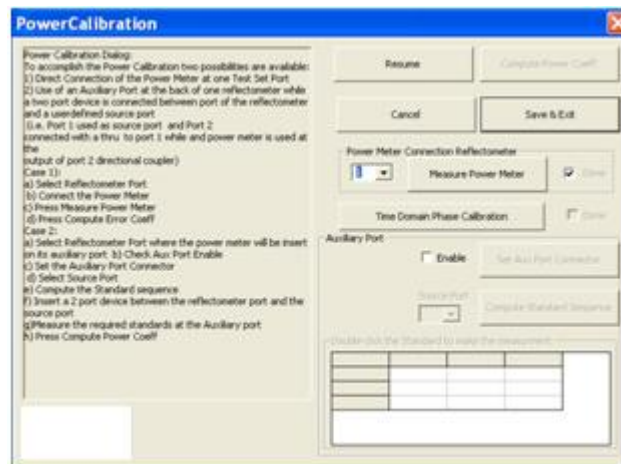


### 3.2) Power Measurements without auxiliary port

When the auxiliary port is not required the user simply launches the *Power Calibration* tool by pushing the *Power\_TD\_Calibration* button from the *Calibration Measurement* dialog, it sets the test port number from the *Power Meter Connection Reflectometer* group box by expanding the combo box:



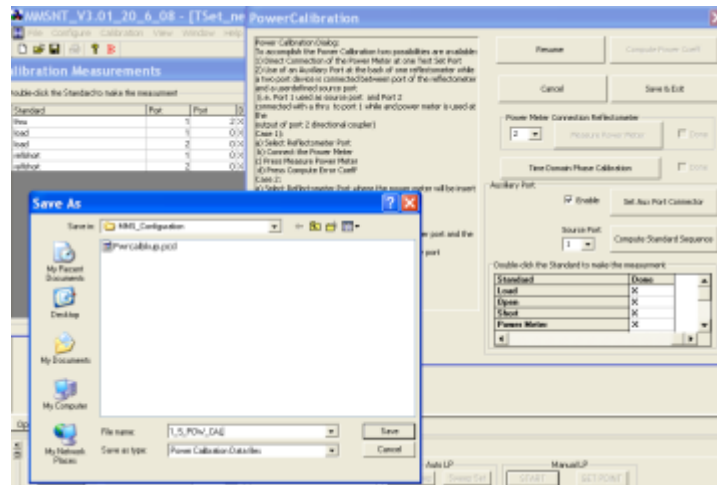
Next, from the *Power Calibration* dialog launch the test port power measurements by pushing the *Measure Power Meter* button placed in the *Power Meter Connection Reflectometer* group box. MMS-NT by controlling both power meter and Synthesizer Sweep Generator performs a calibration sweep at all frequencies included in the frequency list ( $f_0, 2f_0$ , etc) and displays a progress bar . After both power meter and Synthesizer Sweep Generator complete the sweep a checkmark () appears into the *Done* check box placed in the *Power Meter Connection Reflectometer* group box, indicating test port power measurements have been done.



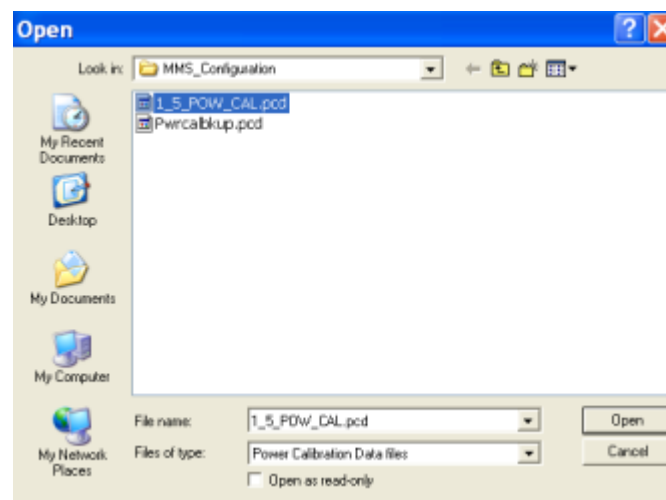
In both cases (with and without auxiliary port), after a right calibration standard's measurements and/or power measurements have been done, the user must click the

Compute Power Coeff button, MMS-NT will calculate  $|k_{ii-aux}|$  or  $|k_{11}|$  error terms (depending on whether the use of the auxiliary port is or is not required respectively), which will be applied to correct future power measurements.

-Finally, press the *Save&Exit* button to store the power calibration's error terms file (.pcd) and close the *Calibration Measurements* dialog.



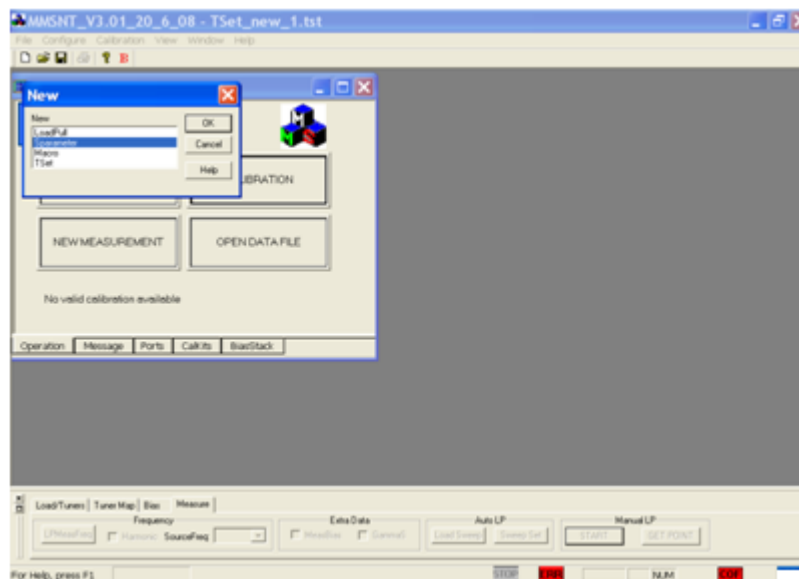
In this way, in future measurements one can recall any power calibration file (.pcd) whenever the measurement test bench is not modified.



## 4) Power Calibration Verification

### 4.1) Load Pull file (.lpx) overview

Once both S-parameter and power calibrations have been done, and error correction applied, MMS-NT allows the user to verify the calibration procedure's performance and/or perform the power-dependent DUT's performance measurements through another powerful file class: *LoadPull* file (.lpx). *File>New>LoadPull>OK* or by pressing the *NEW MEASUREMENT* button from the *OPERATION* tab control placed into the *TSet* window.



In terms of power dependent DUT's performances a *LoadPull* file (.lpx) basically allows the user to perform measurements at each frequency of interest previously defined in the frequency list ( $f_0$ ,  $2f_0$ , etc) through *RunView* files (.rvf) (*Display>RunView>Edit FormatFile*) which can be modified, reloaded, edited, etc. Furthermore, MMS-NT provides already existents *RunView* files (.rvf) such as *default\_2port\_better.rvf* which can be used as help to build customized *RunView* files (.rvf). Each *RunView* file (.rvf) is related to a *RunView* window. When a new *LoadPull* file (.lpx) is opened a *Run View* window appears beside a *Load Window* (in smith chart format) as default. All measurements previously defined into a *RunView* file (.rvf) will appear into the *RunView* window in tabular format:

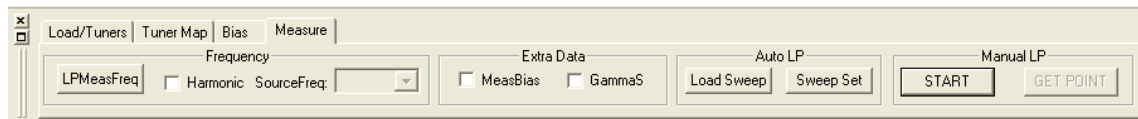


### **Manual Control**

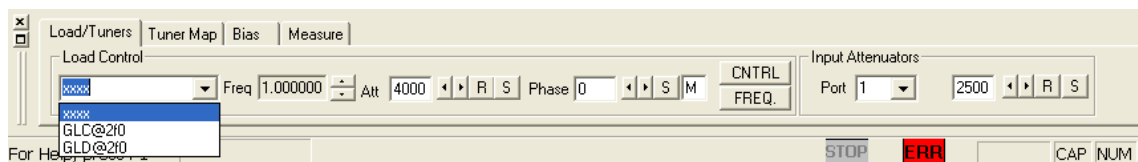
*LoadPull* files (.lpx) allow the user to perform both load ( $\Gamma_L, \Gamma_S$ ) and power sweeps ( $P_{in}$ ) at a given frequency of interest in a manual mode of operation. Both load and power sweeps can be managed in manual mode by means of the monitor bar as follows:

### **Manual Power Control**

a- press the *Measure* tab control, press the *START* button placed into the *ManualLP* group box to launch the *RunView* file's (.rvf) measurements.



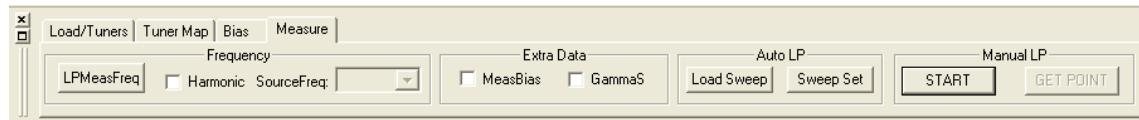
b- press the *Load/Tunes* tab control ,set power levels at the input ( $P_{in}$ ): -first set an input port number by expanding the *Port* combo box control (  ) placed into the *InputAttenuators* group box; then, -fix an input power level by decreasing the attenuation level of the input attenuator by pushing the horizontal spin buttons (  ) placed in the *InputAttenuators* group box. The lower the attenuation value the higher the input power level.



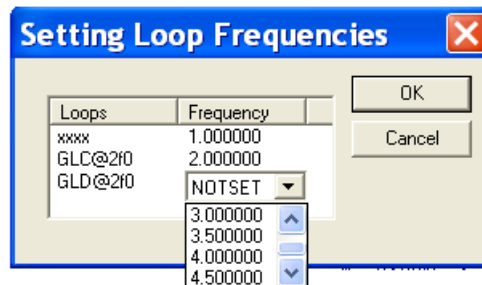
The input signal's frequency is fixed by the external CW or synthesized sweep generator connected to the digital attenuator controlled by MMS-NT.

### **Manual Load Control**

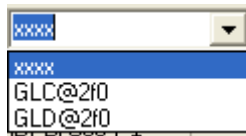
a- press the *Measure* tab control, press the *START* button placed into the *ManualLP* group box to launch the *RunView* file's (.rvf) measurements.



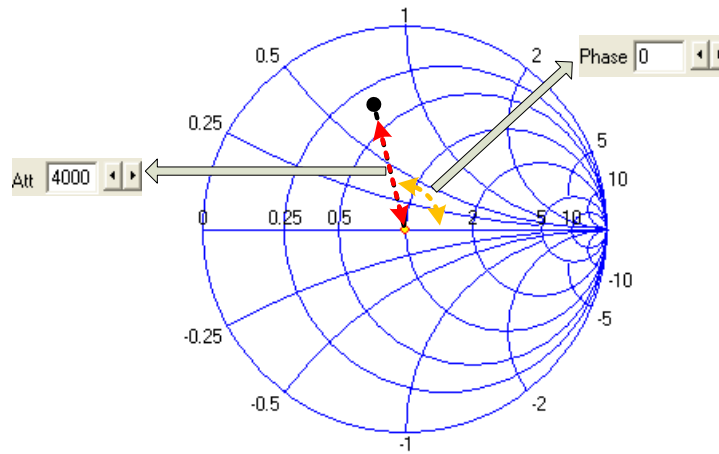
b-set the load ( $\Gamma_L, \Gamma_S$ ) values at a given frequency of interest ( $f_0, 2f_0, \text{etc}$ ) : -select an active loop unit among all those previously defined into the *MMSNT.ini* configuration file (.ini) and -set its YIG filter frequency of operation. This can be done in the *Setting Loop Frequencies* tool from the menu bar *Set>LoopFrequencies...*



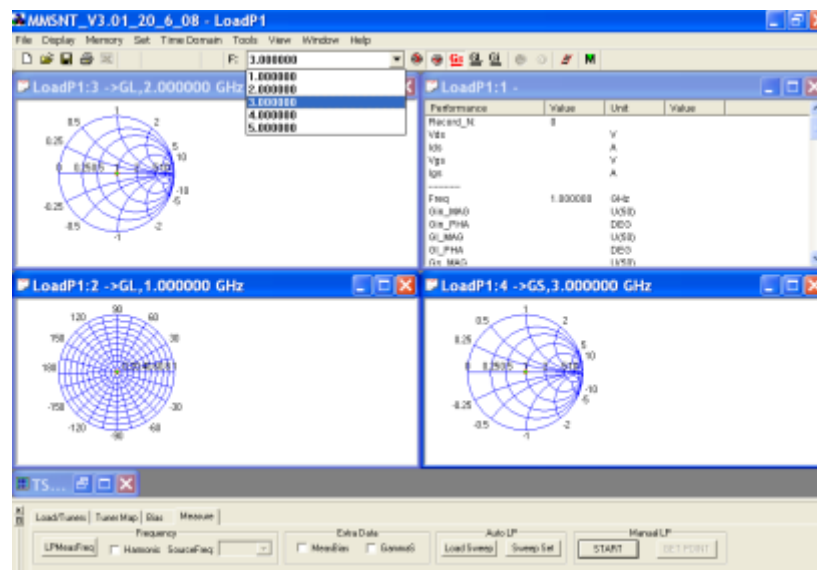
c-Once an active loop has been configured, the user can pull  $\Gamma_L$  or  $\Gamma_S$  onto the smith chart at a given frequency of interest manually as follows: fix an active loop to be used by expanding the combo box control placed into the *Load Control* group box.





d-The active loop's frequency of operation previously chosen will appear in the *Freq* box ( *Freq* 1.000000 ). Next, use the *Att* control and the *Phase* control ( *Att* 4000 *R S* *Phase* 0 *S* ) to vary both load's ( $\Gamma_L, \Gamma_S$ ) modulus ( $|\cdot|$ ) and angle ( $\angle$ ) respectively .


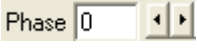
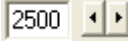



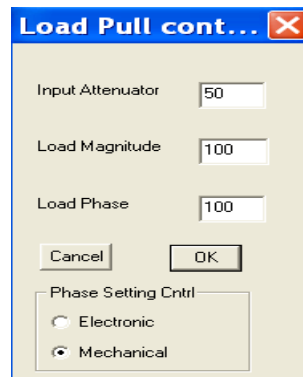
The user can see these reflection coefficients and/or power variations in real time in either tabular (Run View window) or graphic (*Load Window*) formats at whichever frequency of interest. For graph format the user can open other Load Windows (*Window>New Load Window*), select the reflection coefficient of interest ( **Gs** , **GL** , **Gi** ) and set the frequency of interest ( **F: 1.000000** ). For tabular format the Run View window shows automatically all reflection coefficients measurements previously defined into the current *RunView* file (.rvf) in real time at all frequencies of interest previously chosen from the *Frequency Setting* tool.





If needed, save more than one measurement point by pushing , this allows the user to see more than one measurement point at a time. Each measurement point is fixed in each graphic representation (smith chart, etc) and stored in an Excel file (.xls) which can be open by pressing .

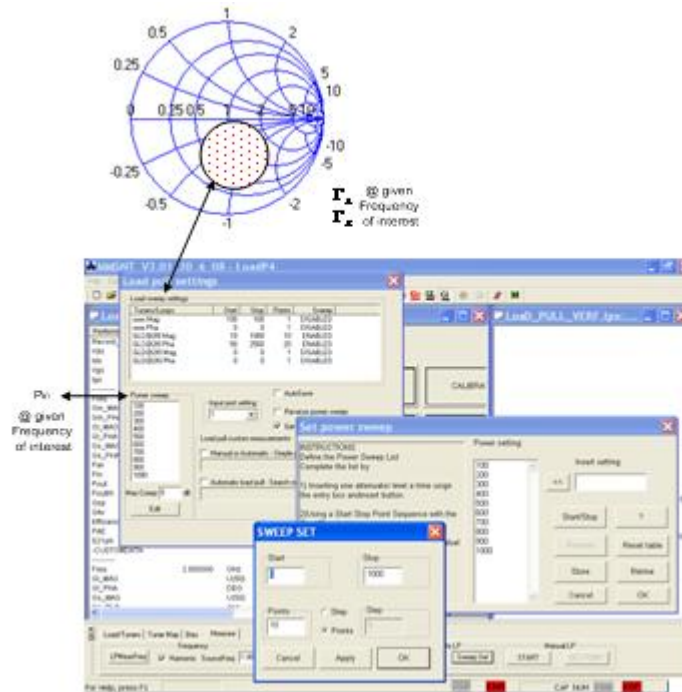
For both manual load and power control MMS-NT allows one to change the minimum step of modulus, phase and attenuation, introduced by ,  and  controls respectively. From the menu bar: *Set>Control Step...* or press  from the *Load Control* group box. The load phase control can be done electronically and mechanically. The former by taking advantage of the abrupt YIG filter phase response and/or digital phase shifter and the latter simply by using a plunger or tuning element which can be moved in parallel to the center conductor of a transmission line.



Both load and power manual control can be deactivated: from the *Measure* tab control, press the *STOP* button placed into the *ManualLP* group box

### Automatic Sweeps

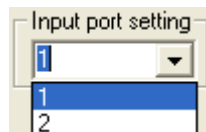
Both load and power sweeps can be managed also in automatic mode by means of the *Load pull settings* tool available from the *Monitor Bar* (press the *Measure* tab control, press **Sweep Set** placed into the *AutoLP* group box) or from the menu bar (*Set>Load Setting...*)



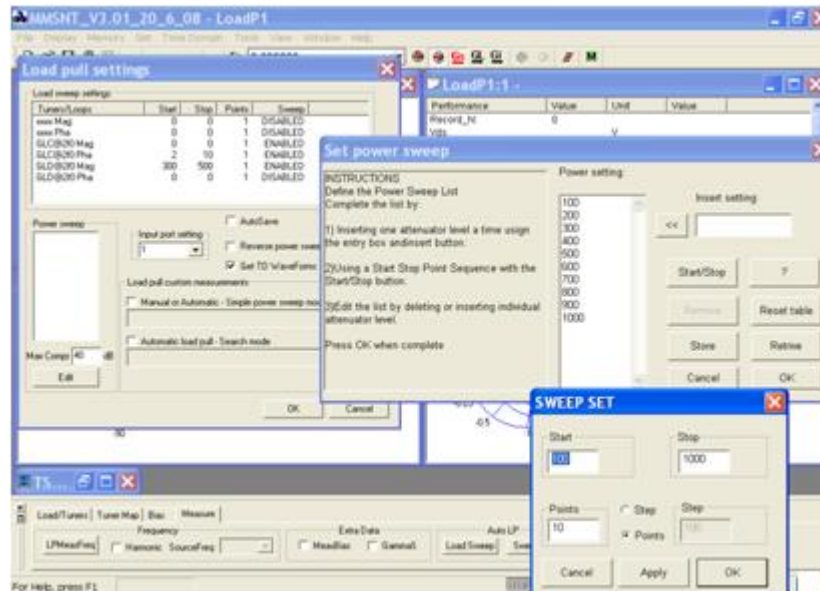
### Automatic Power Sweep

The process to edit, modify, load, etc a power sweep consists of the following steps:

a-Select the input port where the user intends to connect the input source, by using the *Input port setting* combo box:



b-Define the sweep power levels into the *Set power sweep* dialog: pressing the *Edit* button placed in the *Power Sweep* group box. MMS-NT allows different ways to introduce points of power into the sweep power list, such as those available in the CAD simulators: star/stop, point to point, etc. Press *OK* to save the current power sweep.

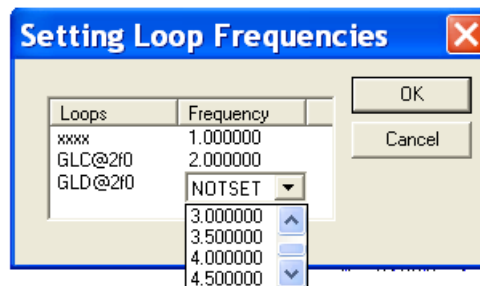


Once a power sweep has been defined, the user can launch it simply by pressing **Load Sweep** placed into the *AutoLP* group box.

### Automatic Load Sweep

The process to edit, modify, load, etc an automatic load sweep consists of the following steps:

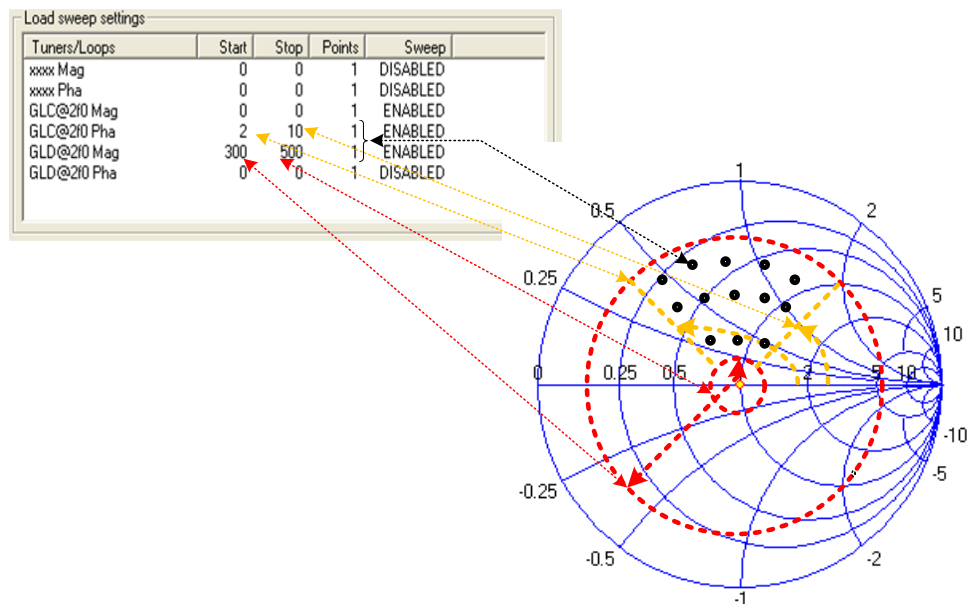
a- select an active loop unit among all those previously defined in the *MMSNT.ini* configuration file (.ini) and set its YIG filter frequency of operation. This can be done in the *Setting Loop Frequencies* tool from the menu bar *Set>LoopFrequencies...*




b- activate the *Mag* and *Pha* active loop attributes to vary both load's ( $\Gamma_L, \Gamma_S$ ) modulus ( $|\cdot|$ ) and angle ( $\angle$ ), by selecting the *ENABLE* text box control placed in the *Load sweep settings* group box.

Load sweep settings					
Tuners/Loops	Start	Stop	Points	Sweep	
xxxx Mag	0	0	1	DISABLED	
xxxx Pha	0	0	1	DISABLED	
GLC@2f0 Mag	0	0	1	ENABLED	
GLC@2f0 Pha	2	10	1	ENABLED	
GLD@2f0 Mag	300	500	1	ENABLED	
GLD@2f0 Pha	0	0	1	DISABLED	

c-Use the *Start* and *Stop* controls to introduce the maximum and minimum values of the modulus and phase required. Set also both phase and modulus' point numbers.



Press *OK* to save the current load sweep. Once a load sweep has been defined, the user can launch it by pressing **Load Sweep** placed into the *AutoLP* group box. Once both automatic load and/or power sweeps have finished, the user can look at the measurement data in either graphic or tabular formats. For graphic format the user can open **Load Windows** (*Window>New Load Window*), select the reflection coefficient of interest ( **GL**, **Gi**, **Gs** ), and set the frequency of interest ( **F: 1.000000** ). For

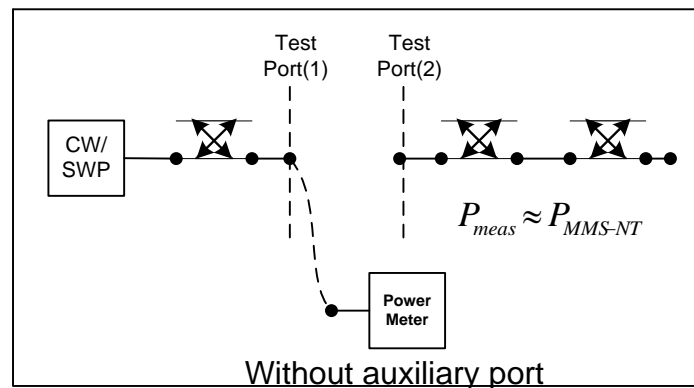
tabular format MMS-NT stores the last load sweep measurement data into an Excel file (.xls) which can be open by pushing .

Furthermore, MMS-NT provides powerful tools to plot Load pull contours, stability circles and VSWR circles in different data formats: polar, smith chart, rectangular such as in a CAD simulator: From the menu bar: *Tools...*

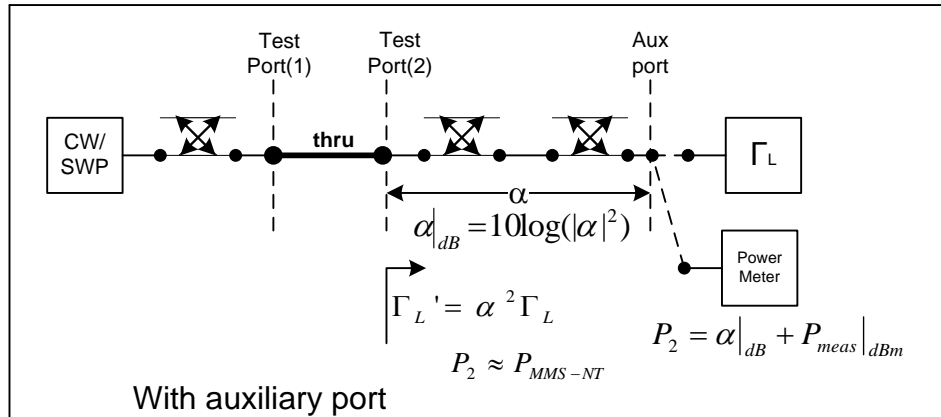


#### 4.2) Power calibration verification without/with auxiliary port

When gender connector problems aren't present the user can connect a power sensor directly whichever test port and launch a manual power control (as explained previously) in order to compare both power measurements: from MMS-NT into the Run View window and from the power sensor as shown in the next figure:



When gender connector problems are present the auxiliary port is needed, in this case the user can perform a manual power control (as explained previously) and apply a procedure similar to that depicted in the next figure to verify power calibration performance:



It means:

a-Connect two test port through a line or thru .

b-Connect a known reflection coefficient to the auxiliary port ( $\Gamma_L$ ) often a short or an open calibration standard, in order to compute the test port reflection coefficient ( $\Gamma_L'$ ) . This allows one to compute the attenuation ( $\alpha$ ) introduced by cables, couplers and connector placed between test and auxiliary ports.

c-Connect a power meter to the auxiliary port to obtain  $P_{meas}$  reading.

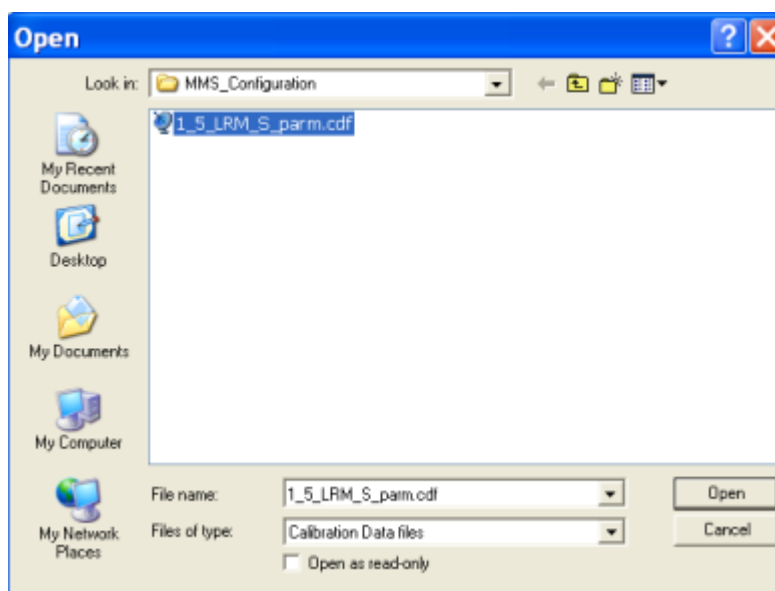
Once  $P_{meas}$  and  $\alpha$  are known at a given frequency of interest, the user can compare both test port output power ( $P_2$ ) values: from MMS-NT in the Run View window, and that computed through  $P_{meas}$  and  $\alpha$ .

### III) PHASE CALIBRATION PROCEDURE

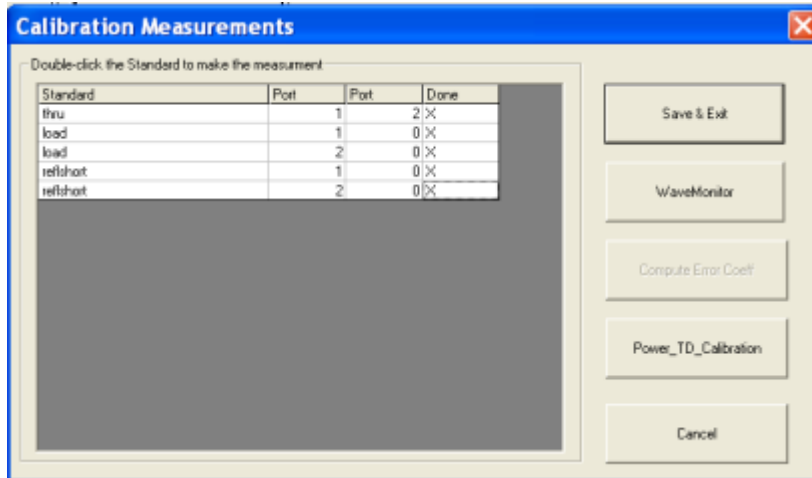
This section describes the basic steps and operational procedures for implementing a Phase calibration procedure on a multiport VNA system by using MMS-NT. This is based on four steps independently on whether the auxiliary port is or is not needed: 1) Loading S-parameter calibration ; 2) Perform a Power Calibration ; 3) Phase Measurements ; 4) Phase Calibration Verification.

#### 1) Loading S-parameter Calibration

From the current *TSet* file (.ini) recall an already existent S-parameter calibration file (.cdf): Calibration>More...Resume...



As mentioned in the S-parameter Calibration procedure section: when whatever already existent S-parameter calibration file (.cdf) is recalled by a *TSet* file (.tst), the former must match the current *TSet* file (.tst) configuration. In this way, the user has access to the  $4n-1$  error coefficients from the non leaky error model included in the current *TSet* file (.tst). The *Calibration Measurement* dialog with a checkmark (X) on the checkbox labeled as “Done” shows all S-parameter calibration standards measurements have been done.

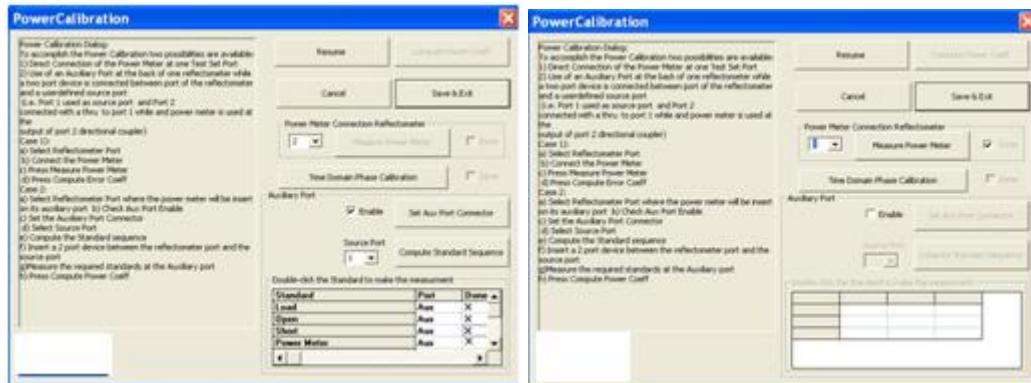


### 2) Perform a Power Calibration

Depending on whether the auxiliary port is or is not needed the user can perform a proper power calibration procedure following the steps given in **II) Power Calibration Procedure** section.

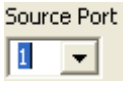
### 3) Phase Measurements

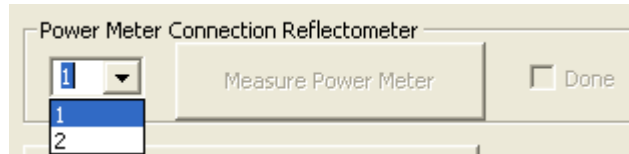
In both cases with or without the auxiliary port, after suitable power measurements the user is in front of the *Power Calibration* tool environment:



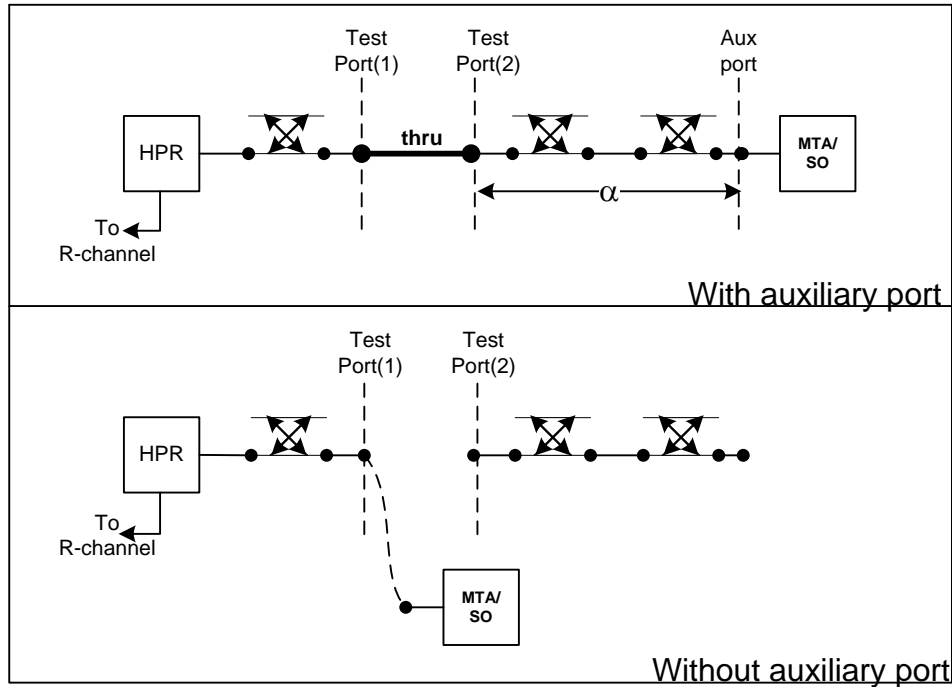



Since, a phase calibration requires an amplitude-phase stable signal outgoing from an HPR, the user must connect an HPR signal into the RF input port where the synthesized sweeper generator was connected during power calibration procedure. If the auxiliary port is needed do not to change the RF input port number previously selected, from the

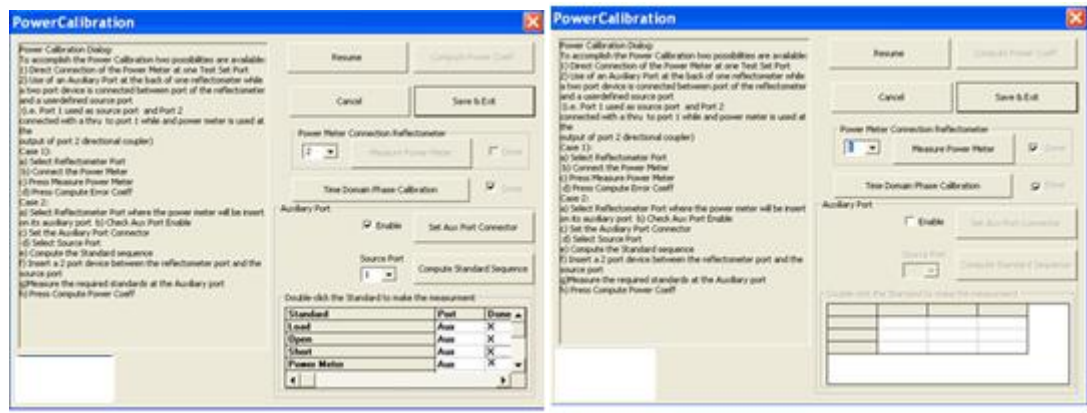
*Auxiliary Port* group box in the *Source Port* Combo box control . Furthermore, the user must not to change the auxiliary or test port number previously chosen from the *Power Meter Connection Reflectometer* group box:



Next, in order to carry out phase measurements, connect a time domain receiver (MTA/SO) to the auxiliary port or the test port (defined previously in the power calibration procedure) depending on whether the auxiliary port is or not needed respectively. Additionally connect the HPR signal into the VNA reference channel in order to guarantee its appropriate phase locking.

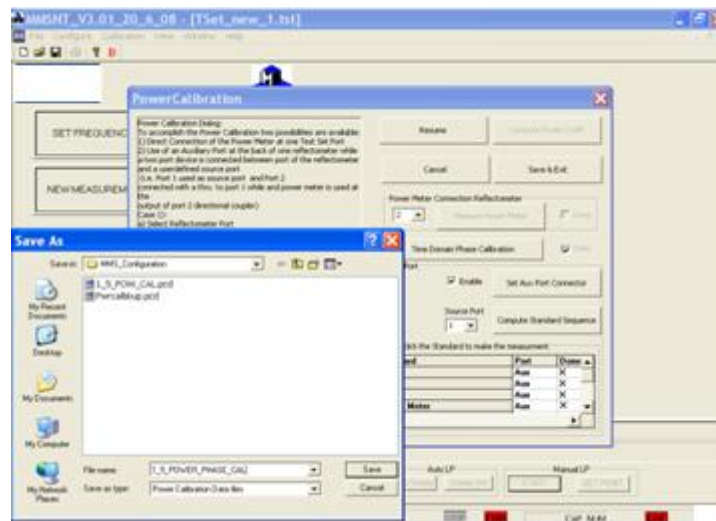


After that, launch the phase measurements by pushing the *Time Domain Calibration* button. MMS-NT by controlling both VNA and the time domain receiver (MTA/SO) performs a calibration sweep at all frequencies included in the frequency list ( $f_0, 2f_0, \text{etc}$ ) and displays a progress bar . After both VNA and the time domain receiver complete the sweep a *Done* check box (beside the *Time Domain Calibration* button) indicates auxiliary or test port phase measurements have been done.



In both cases (with or without auxiliary port), after correct power and phase calibration procedures has been done, press the *Compute Power Coeff* button. MMS-NT will calculate  $k_{11}$  error term (its modulus and its angle).  $k_{11}$  values will be applied to correct future powers and/or time domain waveform measurements.

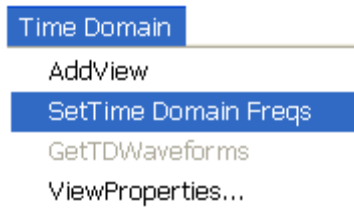
Finally, press the *Save & Exit* button to store the power and phase calibration's error terms file (.pcd) and close the *Calibration Measurements* windows.



So, in future measurements one can recall whatever power-phase calibration file (.pcd) whenever the measurement test bench is not modified.

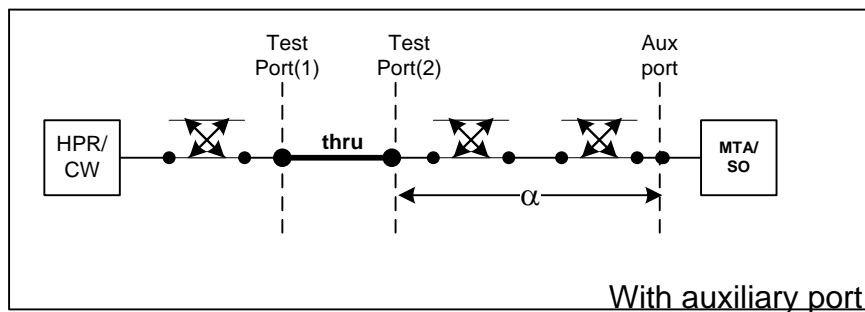
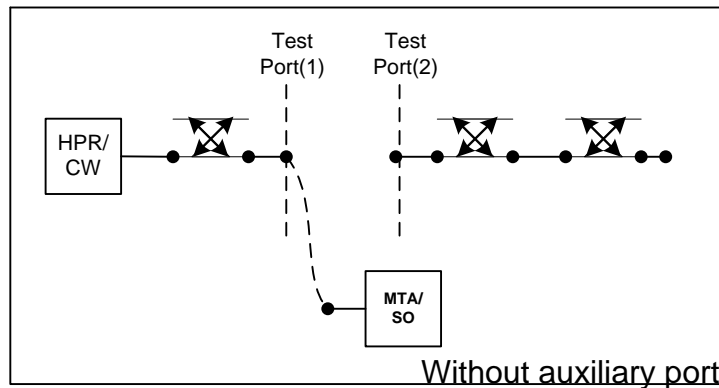
#### 4) Phase Calibration Verification

Phase calibration verification and/or time domain waveform measurements can be done easily by using a *LoadPull* file (.lpx): *New >LoadPull>OK*, or by pressing the *NEW MEASUREMENT* button from the *OPERATION* tab control placed into the *TSet* window. All time domain waveform measurements are managed by means of the *Time Domain* menu (add graphs, change graph properties, etc) placed in the menu bar.



-Inject an RF signal probe into an RF input port such as during a power or phase calibration procedures. This task can be done by connecting an HPR or a CW generator. Then, connect a time domain receiver (MTA/SO) to the auxiliary port or to a test port, depending on whether the auxiliary port is or is not required, in a similar way to when

performing a phase calibration procedure. Additionally connect an HPR to the VNA R-channel in order to guarantee its appropriate phase locking (not shown in figure).

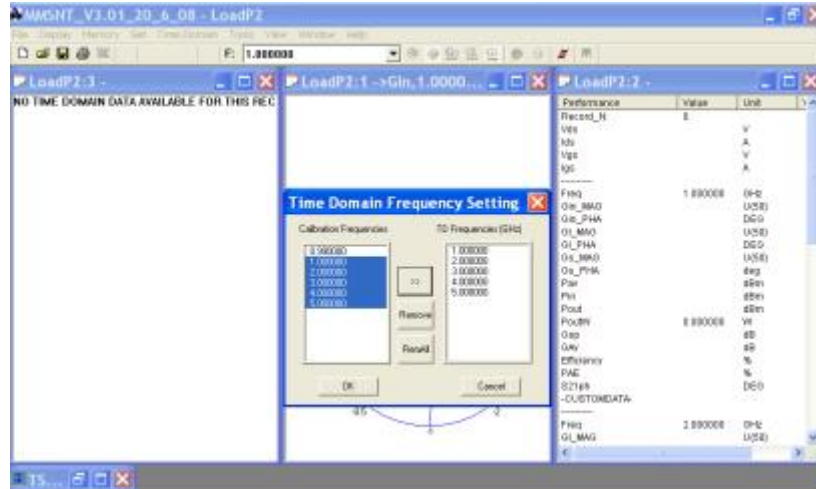


In order to verify the current phase calibration performance, the target is to compare the time domain waveform measurements obtained by means of MMS-NT and the time domain receiver (MTA/SO). Obviously, when the auxiliary port is required the cables, coupler and connectors' attenuation ( $\alpha$ ) will affect amplitude comparisons, however, this can be accounted for through  $\alpha$  values previously computed during the power calibration verification procedure.

When an RF signal probe, the VNA and the time domain receiver (MTA/SO) have been properly connected, one creates a time domain measurement in the current load pull file (.lpx) through the following steps:

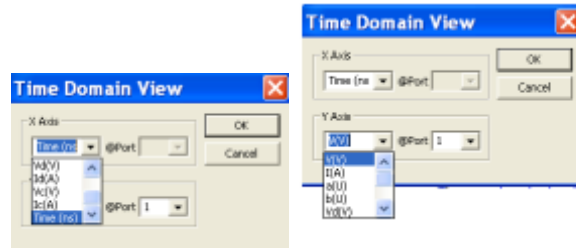
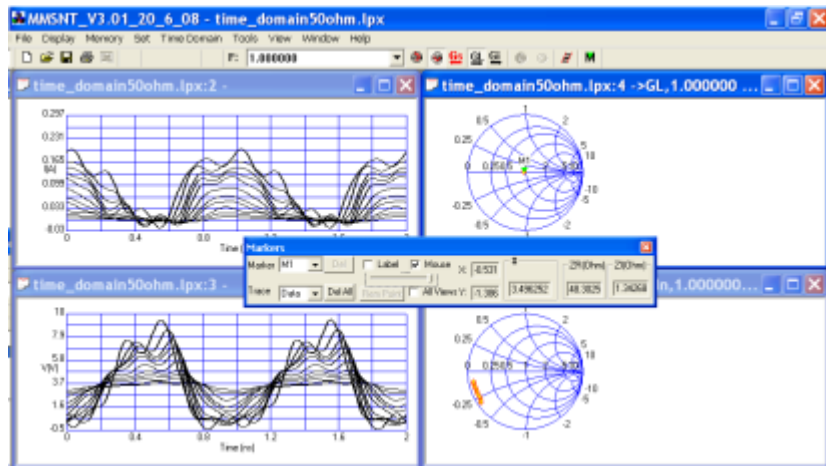
a-Select *Time Domain>Add View...* to open a time domain measurement view window. Open more than one view if needed and define the time domain waveform at each graph ( $V_1(t)$ ,  $I_2(t)$ , etc): *Time Domain>View Properties...*

b-Define all frequencies of interest to represent the time domain waveform (among all calibration frequencies): *Time Domain>Set Time Domain Freqs* .Press OK to save changes



c-Launch a manual/automatic power sweep (as explained in the power calibration verification section). Be careful with the power level setting in order to not damage the time domain receiver sampler (MTA/SO).

d-Launch the time domain waveform measurements previously configured: *Time Domain>Get TD Waveforms*. MMS-NT will acquire the power waves in the frequency domain from the VNA system and it will perform an IDFT (Inverse Discrete Fourier Transform) in order to obtain their time domain waveforms which will be shown in graphic format into a time domain view window. The user can change the current time domain view window properties through the *Time Domain View* dialog clicking on it such as in a CAD simulator.



In this way, one can compare time domain waveforms parameters such as: pick value, pick to pick value, etc between both MMS-NT and time domain receiver measurements (MTA/SO) in order to check the current phase calibration procedure performance.

